SPIN POLARIZED TUNNELING SPECTROSCOPY OF INTERCALATED $Bi_2Sr_2CaCu_2O_{8+\delta}$ SUPERCONDUCTOR

A Thesis Submitted to
the Graduate School of Engineering and Science of
İzmir Institute of Technology
in Partial Fulfillment of the Requirements for the Degree of

MASTER OF SCIENCE

in Material Science

by
Mehtap ÖZDEMİR

June 2006
İZMİR

We approve the thesis of **Mehtap ÖZDEMİR**

Date of Signature

14 June 2006

…………………………………………
Assoc. Professor Lütfi ÖZYÜZER
Supervisor
Department of Physics
İzmir Institute of Technology

14 June 2006

…………………………………………
Professor Doğan ABUKAY
Department of Physics
İzmir Institute of Technology

14 June 2006

…………………………………………
Assoc. Professor Salih OKUR
Department of Physics
İzmir Institute of Technology

14 June 2006

…………………………………………
Professor Kemal KOCABAŞ
Department of Physics Engineering
Dokuz Eylül University

14 June 2006

…………………………………………
Assist. Professor Muhittin AYGÜN
Department of Physics Education
Dokuz Eylül University

14 June 2006

…………………………………………
Prof. Muhsin ÇİFTÇİOĞLU
Head of Department
İzmir Institute of Technology

…………………………………………
Assoc. Prof. Semahat ÖZDEMİR
Head of the Graduate School

ACKNOWLEDGEMENT

ABSTRACT

SPIN POLARIZED TUNNELING SPECTROSCOPY OF INTERCALATED $Bi_2Sr_2CaCu_2O_{8+\delta}$ SUPERCONDUCTOR

There has been continuing interest in decades in heterostructure tunnel junctions that combine ferromagnetic material (F), insulator (I) and superconductor (S). This junction has been known to a good probe to analyze the physical properties of ferromagnetic and superconducting materials. In order to understand the influence of the spin injection on the c-axis tunneling characteristics of a Bi-2212 single crystal as a function of temperature and magnetic field, two sets of samples have been prepared; in one set, the surface of $HgBr_2$ intercalated Bi-2212 crystals have been deposited with merely Au while the other set has ferromagnetic multilayer (Au/Co/Au) on top of the crystal. The micron sized mesa arrays have been patterned using photolithography and ion beam etching techniques. The surface topography and height of the mesa were investigated using atomic force microscopy. Tunneling characteristics were examined by means of the novel technique, point contact tunneling (PCT), and experiment were performed wide range of temperatures from 4.2 K to 300 K and that of magnetic field from 0 G to 2600 G. The results of spin polarized tunneling measurements compared with spin degenerate tunneling. Magnetic field dependence hysteretic I-V curves with multiple branches were examined to show the suppression of the superconductivity with spin polarized current. The distinct temperature dependence of depression in tunneling conductance near Fermi level was discussed for spin degenerate and polarized currents above T_c. The zero bias conductance and resistivity versus temperature plots were investigated to show the existence of the pseudogap in tunneling spectroscopy of investigated samples.

ÖZET

İNTERKALASYONLU $Bi_2Sr_2CaCu_2O_{8+\delta}$ ÜSTÜNİLETKENLERİNİN SPİN POLARİZE TÜNELLEME SPEKTROSKOPİSİ

Ferromagnetic, yalıtkan ve üstüniletken malzemelerden oluşan tünel eklemleri üzerinde son on yıldan beri süregelen bir ilgi vardır. Bu eklemler ferromagnetic malzeme ve ustun iletkenlerin fiziksel özelliklerini belirmek için iyi bir probe olarak bilinirler. Bi–2212 tek kristaline c ekseni boyunca enjekte edilen spin etkisini incelemek için iki grup örnek hazırlandı. İlk grup ta Bi–2212 tek kristali sadece altın film le kaplanırken, ikinci gruptaki kristaller Au/Co/Au üç katmanlı filmle kaplandı. Fotolithografi ve Ar iyon aşındırması teknikleri kullanılarak mikron boyutta mesa yapıları üretildi. Elde edilen mesaların yüzey topografileri ve kalınlıkları atomik kuvvet mikroskobu yardımıyla belirlendi. Elde edilen eklemlerin akim-gerilim karakteristikleri ve tünelleme iletkenlikleri, yüzeylerinden nokta kontak alınarak geniş bir sıcaklık (4.2 K–300 K) ve magnetic alan (0 G–2600 G) aralığında ölçüldü. Spin polarize akim sürülerek elde edilen sonuçlar spin dejenere akim sürülerek elde edilen sonuçlarla karsılaştırıldı. Manyetic alana bağımlı I-V eğrilerinden üstüniletkenliğin spin polarize akımla bastırıldığı belirlendi. Fermi seviyesi civarında sıcaklığa bağlı tünelleme karakteristikleri incelenerek, kritik sıcaklığın üzerinde hala bir enerji aralığının olduğu yani sanki enerji aralığı olduğu belirlendi.

TABLE OF CONTENTS

LIST OF FIGURES

LIST OF TABLES

CHAPTER I

INTRODUCTION

Since the discovery of high temperature superconductors (HTS) in 1986 by Bednorz and Mueller, cuprates have puzzled scientists. There is no consensus on the mechanism of high temperature superconductors which is different from the conventional superconductors but its exact mechanism has not been established yet. It is necessary to investigate the peculiar properties of high temperature superconductors in a detailed and accurate manner to clarify this mechanism.

In the BCS quantum-mechanical theory of conventional superconductors, the electron flux consists of bound pairs of electrons. An attractive force between electrons causes the pairing. The electrons are bound in Cooper pairs by an electron-phonon interaction. The wave function of the electrons is spherical, indicating that a pair has an equal chance of moving in any direction. This pairing is said to have s-wave symmetry. On the other hand, in high temperature superconductor, lattice vibrations alone are not strong enough to maintain electron pairing at elevated temperatures. To prove the high critical temperatures of HTS, pairing mechanisms of magnetic origin have been proposed. The magnetic exchange energies are about four times the phonon energies. In this case, a wave function of the electron pairing would have been d-wave symmetry. The d-state appears as a four lobes lying in a plane, like a four-leaf clover.

While the HTS superconductors show many of the well-known properties of conventional superconductors, such as Josephson tunneling, vortex structure, type II behavior and Meissner effect. They also have properties that are unusual for BCS-like materials, for instance, their high critical temperature, their linear dc resistivity in the normal state and their extremely small coherence length. In addition, HTS are characterized by a large spatial anisotropy, which is due to their layered crystal structure. These layers consist of Cu-O planes, separated from each other by insulators. It is believed that superconductivity and charge transport are mostly confined in the Cu-O planes. This structural anisotropy translates into anisotropy of most physical properties. Researchers have performed a number of experiments to prove d-wave pairing. The results pointed to the presence of d-wave symmetry, but they couldn't rule

out an additional contribution from s-wave pairing. Especially, the crystal geometry requires that the electron pairing be either s-wave or d-wave.

The electronic properties of the HTS can be investigated by several techniques, such as electron tunneling, angular resolved photoemission spectroscopy (ARPS), and Raman spectroscopy. Among to these techniques electron tunneling (both quasiparticle and Josephson tunneling) is a powerful technique to probe the excitation spectrum, the superfluid density and the pair wave function phase of high temperature superconductors. c-axis and a-b plane quasiparticle tunneling illustrates the extreme anisotropy of these superconductors and shows that surfaces are very different with possible bound states due to the broken symmetry at the a-b interface. Intrinsic c-axis tunneling attempts to address the relationship between the superconducting gap and the pseudo gap (Schuller, 2002). The principal goal of this thesis is to measure these properties by driving spin polarized current along the c-axis of intercalated $Bi_2Sr_2CaCu_2O_{8+\delta}$. In a high-$T_c$ superconducting thin film, the injection of spin polarized quasiparticles could suppress the superconductivity by breaking the spin-neutral Cooper pairs. Detailed knowledge of how the pair potential responds to such spin perturbations, especially at coherence length scales, would thus important information on the pairing mechanism (Ngai, 2004).

1.1. High Temperature Superconductivity

After the discovery of the superconductivity in mercury at 4 K by Kamerlingh Onnes in 1911, the search for the new superconductors led to a slow increase in the highest known transition temperature T_c over the decades. After years, in 1986, the path to higher transition temperature was opened by the discovery of superconductivity in ceramic $La_{2-X}Ba_XCuO_4$ with T_c=36 K (Bednorz and Muller). The following year, the liquid nitrogen temperature barrier (77 K) was broken with the discovery of $YBa_2Cu_3O_{7-\delta}$, superconducting at 90 K (Wu et al., 1987). Shortly thereafter, still higher T_c were found in the $Bi_2Sr_2Ca_2Cu_3O_\delta$ with T_c=110 K (Chu et al., 1988) and $Tl_2Ba_2Ca_2Cu_3O_\delta$ with T_c=130 K. After that, Tc above the 130K for the Hg series of compounds $HgBa_2Ca_\delta Cu_{\delta+1}O_{2\delta+4}$ with δ =1, 2, 3 have been reported by many researches (Chu et al., 1993; Iqbal et al., 1994; Schilling et al, 1994). The transition temperature of Hg compounds increases with pressure (Gao et al., 1994). The record transition temperature value of $HgBa_2Ca_2Cu_3O_8$ is 160-165 K.

In all of these systems, copper oxide planes form a common structural element, which is thought to dominate the superconducting properties. The crystallographic unit cell contains varying number of CuO_2 planes, depending on the choice of stoichiometry. In addition, these compounds contain CuO chains, which are thought to serve as charge reservoirs to control the electron density in the planes. The structure of these oxides is classified as of the perovskite type. Perovskites are crystalline ceramics that their name derive from a specific mineral known as perovskite $CaTiO_3$ due to their crystalline structure. Perovskite structure has a cubic unit cell with titanium atoms at the corners, oxygen atoms at the midpoints of the edges, and a calcium atom in the center. Each titanium atom is octahedrally coordinated with six oxygen atoms, with a calcium atom in the center. All HTS consist of a stack of some basic perovskite cells along the c-axis with vacancy of some oxygen sites, which eliminates the electronic neutralization and let the material show superconducting properties.

There are two types of superconductors, Type-I and Type-II. A Type-I superconductor (Fig. 1.1) expels the externally applied magnetic field from its interior when the material is cooled below the critical temperature, T_c. The superconductor becomes perfectly diamagnetic. This perfect diamagnetic property of superconductors is the most fundamental macroscopic property of a superconductor and is referred to as the Meissner Effect. When the magnetic field is increased to a given point the superconductor returns to the normal resistive state.

Transition of Type-II superconductors from a superconducting state to normal state occurs as gradually. There are two critical fields for type-II superconductors; the lower H_{c1} and the upper H_{c2} (Fig. 1.2). If applied fields smaller than H_{c1}, it is completely expelled from material. Above the H_{c1} the magnetic field partially penetrates into the material up to H_{c2}. Between the H_{c1} and H_{c2} the superconductor said to be in the mixed state and magnetic flux in form of tubes called as vortices. Above H_{c2} vortices overlap and the field inside the superconductor becomes strong everywhere so the material returns to the normal state. In this case the layered structure of the materials plays an important role. Such as, for Bi-2212, H_{c1} and H_{c2} values 200 G and 60 T respectively.

Type I Superconductor

Induced Magnetic Field

Normal State

Superconducting State

H_c

Applied Magnetic Field

Superconductor

The Meissner Efect
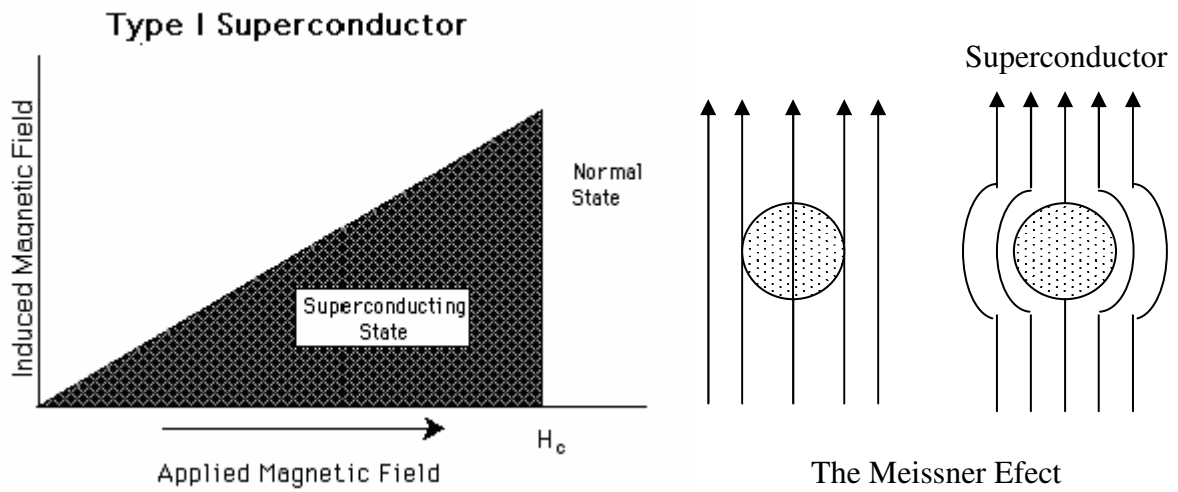
Figure 1.1. The transition behavior of type-I superconductors under externally magnetic field

Type II Superconductor

Induced Magnetic Field

Superconducting State

Mixed State

Normal State

H_{c1} H_c H_{c2}

Applied Magnetic Field

$B < B_{c1}$
Meissner Efect

$B_{c1} < B < B_{c2}$
Mixed State

$B > B_{c2}$
Normal State
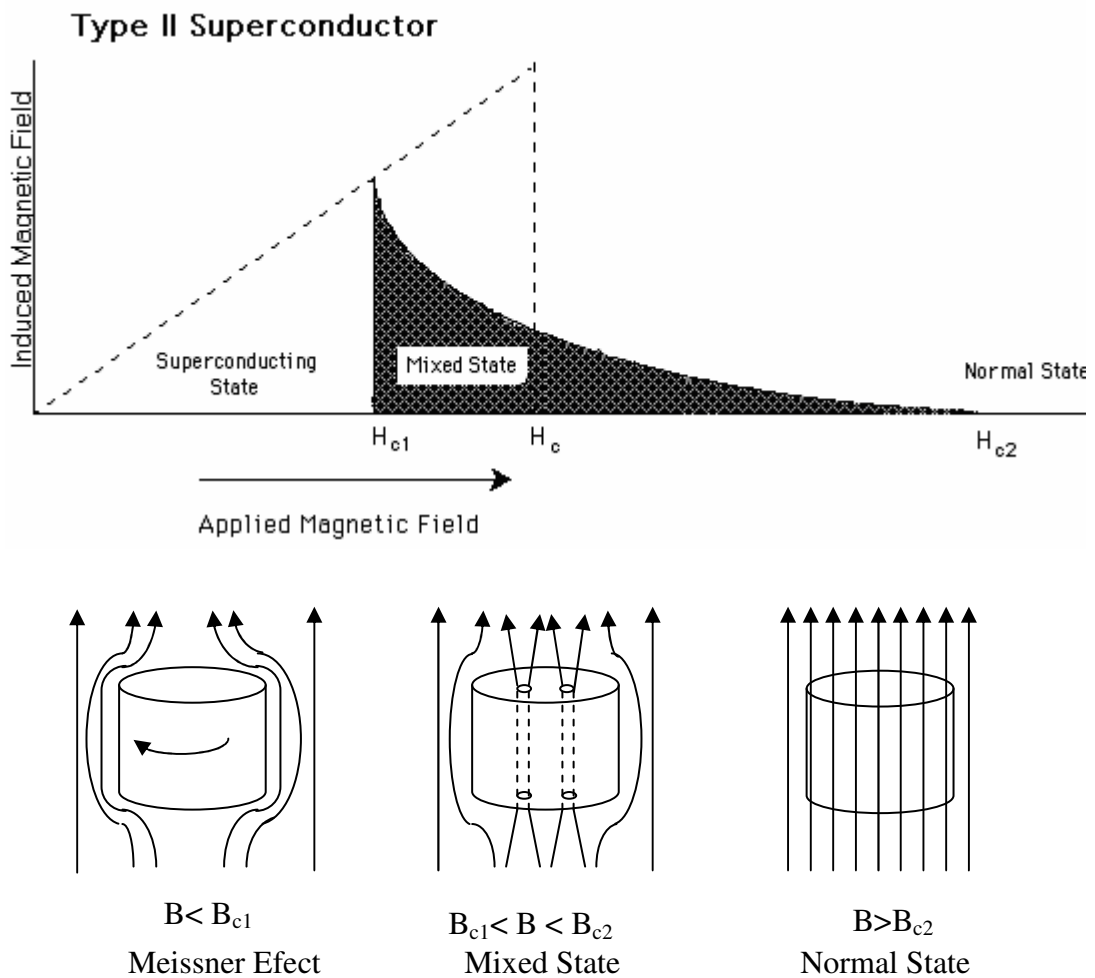
Figure 1.2. The transition behavior of type-II superconductors under externally magnetic field

4

All HTS are extremely type-II superconductors. Ginzburg-Landau Theory can explain their magnetic properties. Magnetic properties include two important parameters that influence energy minimization; London penetration depth λ and coherence length ξ. London penetration depth is the characteristic length of the fall off of a magnetic field due to surface currents. Coherence length is a measure of the shortest distance over which superconductivity may be established. The ratio of London penetration depth to coherence length is known as the Ginzburg-Landau parameter $\kappa=\lambda/\xi$. If this value is greater than $\sqrt{2}$, complete flux exclusion is no longer favorable and flux is allowed to penetrate the superconductor so vortex occurs.

In addition, there are unusual properties of copper oxide superconductors apart from having relatively higher critical temperatures. The crystal structure of the copper oxides determines these properties. The multi-layered structures of HTS make them highly anisotropic. This kind of structure has two fundamental axes; the ab-axis that includes copper oxide sheets providing superconductivity and c-axis, which is perpendicular to the copper oxide sheets. According to these axes, characteristic physical parameters for example energy gap, resistivity, London penetration depth, coherence length, critical fields show anisotropic behaviors. This means that crystal directions are more favorable for superconductivity than others. Copper oxide superconductors indicate the gap anisotropy, which means that excitations in the ab-plane have different energy gap than excitations along the c-axis. The resistivity of cuprate superconductors greater along the c-axis than parallel to the ab plane; such as for Bi-2212, $\rho_c/\rho_{ab}=10^5$. (Buckel, 2004) The London penetration depth is also anisotropic. It is much larger for a magnetic field orientation parallel to the layers, for instance λ_{ab}=200-300 nm, λ_c=15-150 μm for Bi-2212 (Buckel, 2004). The coherence length is very small for copper oxide superconductors for Bi-2212 ξ_{ab} and ξ_c is 2 nm and 0.1 nm respectively (Buckel, 2004).

Up to now, the measurements gave information on the absolute value of the pair wave function. In addition, phase-sensitive experiments were achieved that directly detect the sign chance of the wave function. These experiments confirm that $d_{x^2-y^2}$ state is realized in the cuprates.

The existence of the energy gap between the ground state and the quasiparticle excitations of the systems had been suggested earlier by Daunt and Mendelssohn to explain the absence of thermoelectric effects (1946). The specific heat measurements of

superconductors were done by Corak et al. These measurements indicated that the electronic specific heat well below T_c shows exponential variation, which corresponds to an energy gap. After that, in 1957 Bardeen, Cooper, and Schrieffer (BCS) produced theory of superconductivity. This theory demonstrated the existence of a temperature dependent gap in the excitation spectrum of the superconductor. One of the key predictions of this theory is that energy gap is a minimum energy to break a Cooper pair. In 1961, I.Giaever pointed out the possibility of determining the energy gap by means of tunneling experiments.

1.2. Tunneling Spectroscopy

Tunneling is a fundamental phenomenon in quantum mechanics. Tunneling, or barrier penetration, is a process that electrons can pass from one superconductor to the other although a non-conducting layer exists between the two metals. This process plays an important role in the field ionization of atomic hydrogen, field emission from a free electron metal, alpha decay of atomic nuclei, metal-insulator-metal junctions.

The first experiments on superconducting tunneling were point out by Giaever in 1960 by measuring current-voltage characteristics of a superconductor-insulator-normal metal (SIN) sandwich junction. He showed the existence of the energy gap which is responsible for reducing the electron flow through the junction by not accepting electrons with small excitation energies. And also he was able to show that the tunneling current was controlled primarily by the density of states in the superconductor (Ozyuzer 1999a)

After that, Giaever's experiments go on and they were extended to investigate superconductivity aspects. The temperature dependence and magnetic field dependence of energy gap was widely studied with the aid of tunneling.For this reason different types of tunneling junctions such as NIN, SIN, SIS (N:normal metal, S:superconductor, I:insulator) were created.

Two types of tunneling occur in the SIS junction; single particle (quasiparticle) tunneling and Cooper pair tunneling. There are two type of process to consider quasiparticles. A pair may be broken, creating a hole excitations on the side where the pair was and injecting the electron into the other side (Duzer and Turner 1999). The second type is that excited electron transfers from one side to the other side. The second tunneling is the Cooper pair tunneling. Because of the Cooper pairs, the two

superconductors are coupled to each other, and a weak supercurrent, the Josephson current, can flow across the barrier. In 1962, Brian D. Josephson predicted this current theoretically for the first time. He predicted that if there is a sufficiently thin insulating layer (less than 1 nm) between the superconducting layers Cooper pairs can tunnel through thin non superconducting barrier. This tunneling of Cooper pairs is now known as Josephson tunneling. There are four modes of pair tunneling: (1) the dc Josephson effect, the absence of an applied electric or magnetic field, (2) the dc Josephson effect, relating to the current with an applied voltage, (3) the inverse ac Josephson effect, whereby dc voltages are induced across an unbiased junction by incident radiation or an impressed rf current, (4) macroscopic quantum interference effects, involving a tunnel current with an oscillatory dependence on the applied magnetic flux (Poole, Farach and Crewick, 1995). These Josephson effects can be observed across any sufficiently localized weak link within a suitable superconducting circuit such as SIS junction, SNS or proximity junction, point contact junction and thin film microbridge. The Josephson current shows amazing properties, which are connected with the phase of microscopic wave function in the superconducting state. SIS junctions can be categorized in two general groups: conventional Josephson Junctions (CJJ) and intrinsic Josephson junctions (IJJ) (Kurter 2005). A single CJJ can be easily obtained by separating two superconductors with a sufficiently thin insulating layer. On the other hand, IJJs are ordered periodically in HTS in natural way.

IJJs are the most attracting aspects among the other junctions in that the junctions are uniform because they are intrinsic. The coupling difficulty caused by impedance mismatch should be less severe than with a single junction since the junctions are periodically bound to each other. IJJ is formed in single high temperature superconductors, crystals of CuO_2 and insulating layers between them. Perfect stacks are more easily obtained in c-axis high quality thin films than in a-axis or single crystal whiskers. On the other hand, the IJJ fabrication method using c-axis thin films and single crystals needs intricate process and limits the junction size in mesa type structures. This structure will be explained in Chapter III. IJJ has two kinds of Josephson plazma one is the longitudinal plasma vertical to layers(c axis direction), another is the transverse plasma along layers (a-b plane)(Tachiki, 2002). Tunneling measurements on a small-sized stack, including only a few intrinsic junctions, provide valuable information on the nature of the inherent superconducting gap and the pairing mechanism of unusual symmetry in the materials.

IJJ has a potential for an important industrial technology; the super-high-speed computer, the storage elements, high capacity and high-speed optical communication conversion devices in the highly networked information society.

IJJ consists of monocrystalline and it is possible to use almost permanently. Because IJJ device has a special character, a generation of the Terahertz electromagnetic wave is possible. For this reason, IJJ device is utilized as the next generation device such as the Teraherz electromagnetic wave generator. So the large capacity and super-high-speed next-generation computer, which is higher speed of three orders of magnitude and three order low power consumption compared with a present high-speed computer, can be developed.

1.3. Spin Injection into a Superconductor

Spin injection is a technique to introduce spin disequilibrium into some electronic materials to alter their underlying electronic correlations. The investigation of spin-polarized transport and spin-polarized tunneling in superconductors can provide useful information on spin-dependent electronic properties and spin relaxation. And also a tunnel junction contains a ferromagnetic material and a superconductor, ferromagnetic/insulating/superconductor (FIS) junction, has been known to be a good probe to analyze the physical properties of both ferromagnetic and superconducting materials (Ishibashi,2001). Experiments on spin-polarized tunneling in superconductors were carried out in the seventies by Tedrow and Merservey. In HTS thin film, such as superconductivity is suppressed by the injection of spin polarized current. This phenomenon has been observed in FIS tunnel junction, and is believed to be due to magnetic pair breaking in the superconducting cuprate by spin polarized quasiparticles injected from the ferromagnetic manganite. Magnetic pair breaking is an important phenomenon in the field of superconductivity. The combination of this mechanism holds great potential in device applications and it is involved the rapid tuning of superconductivity by a small current (Wei, 2002). These devices are spin switches, spin transistors and spin-dependent logic elements.

1.4. Organization of the Thesis

The thesis is organized as follows: Chapter 2 introduces the theoretical background of the tunneling spectroscopy. In Chapter 3, experimental procedure, the mesa fabrication, and the point contact-tunneling technique will be described. In addition to this, single crystal Bi-2212 will be presented. Chapter 4, present tunneling results obtained by PCT measurements on various Bi-2212 single crystal. Finally, in chapter 5 the results will be summarized and the thesis will be concluded.

The aim of this thesis is investigate the effect of the spin polarized current injection along the c-axis direction of Bi-2212 single crystal, using mesas of stacked intrinsic Josephson junctions prepared on the crystal surface. For this reason, the spin polarized current was injected to the mesa from a ferromagnetic Co electrode. Because of the extremely small size mesa areas, PCT was used to obtain tunneling spectroscopy. The measurements configuration allowed us to compare the tunneling characteristics between the spin-polarized and spin-degenerate bias configurations for an identical stack of IJJs.

CHAPTER 2

THEORETICAL BACKGROUND

2.1. Tunneling Effects

Tunneling is a quantum mechanical phenomenon. According to classical mechanics, a particle can pass through a potential barrier only if the kinetic energy of the particle E is larger than the energy of barrier E_b, otherwise it would be reflected. In reality, this is not correct because of the wave-like behavior of electrons. Tunneling effect occurs and the electrons can pass through a barrier. The tunneling of electrons through a potential barrier is schematically illustrated in Figure 2.1

$$\Psi_1(x) = Ae^{ikx} + Be^{-ikx} \qquad \Psi_2(x) = Ce^{kx} + De^{-kx} \qquad \Psi_3(x) = Ee^{ikx}$$
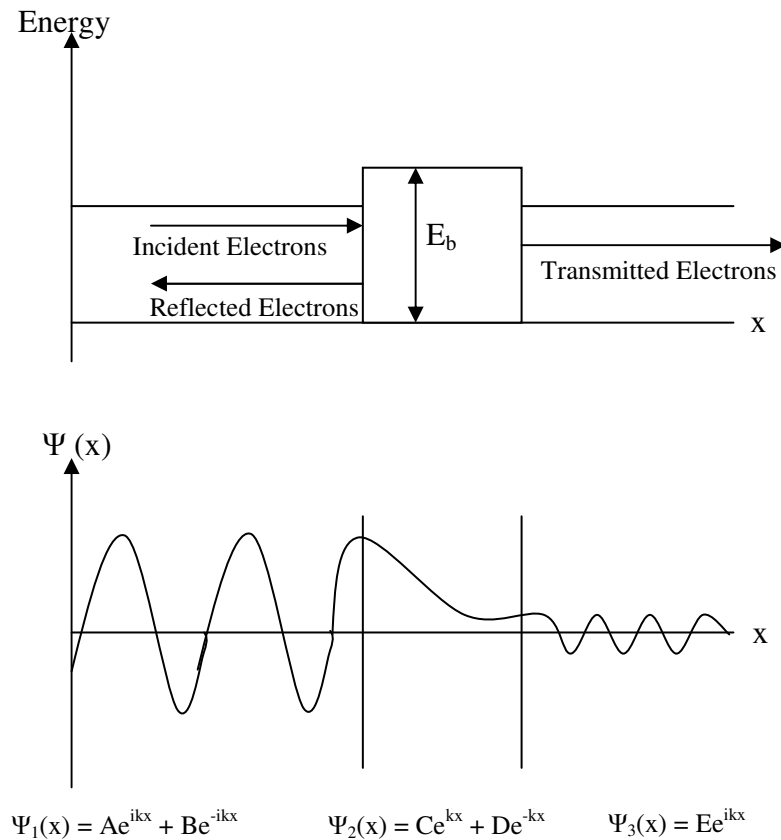
Figure 2.1 (a) Schematic representation of electron tunneling through a sufficiently thin potential barrier (b) the electron wave functions

Momentum of an electron is p = *mv* and the wavelength of an electron is

$$\lambda_e = \frac{h}{p}$$ (2.1)

where *h* is Planck's constant. Within the barrier wave function is

$$\Psi_2(x) = Ce^{kx} + De^{-kx}$$ (2.2)

where C and D depend on boundary conditions while

$$k' = [2m(E_b - E)]^{1/2} / \hbar$$ (2.3)

the wave function $\Psi_2(x)$ decays nearly exponentially within the potential barrier.

2.1.1 Tunneling Junctions

In order to determine the energy gap of a superconductor, tunneling is one of the most sensitive probes among the some techniques such as specific heat, thermal conductivity, nuclear relaxation, ultrasonic attenuation and electromagnetic absorption. Tunneling experiments firstly were done by Giaever to determine the energy gap in 1960 using a tunneling junction. The method is based on the observation of tunneling current across a thin insulating layer between two metals (normal or superconducting) to be studied. Figure 2.2 shows the experimental set-up for the measurement of tunneling current. Probability of tunneling depends on the energetic height and on the thickness of the barrier (Buckel, 2004). And also for tunneling, the electron must find an unoccupied state on the other side. Otherwise the passage of the electron is impossible.
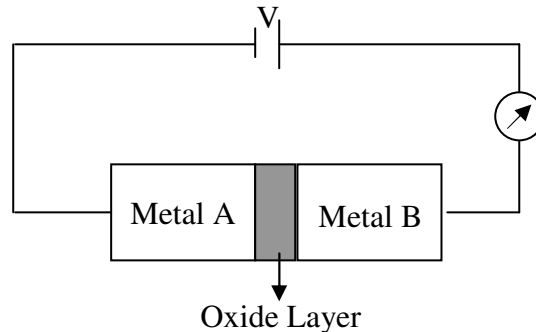
Figure 2.2. Tunneling of two metals separated by a thin oxide layer

If both of metals are normal metal, when they are brought together, Fermi levels of them become equal because electrons can be exchanged between two metals. For this level the net exchange of particles is exactly zero. When a small potential V is applied to the junction, applying voltage leads to a difference eV of the Fermi levels of the two metals and electrons can flow from the one side to another.

In addition to normal metal-insulator-normal metal (NIN) tunneling junction, there are also superconductor-insulator-normal metal (SIN) and superconductor-insulator-superconductor (SIS) tunneling junctions.

2.1.2 Superconductor-Insulator-Superconductor (SIS) Tunneling Junctions

A superconducting tunnel junction is formed when two superconductors are separated by a very thin insulating layer approximately 1nm. This arrangement is called as a Josephson junction. There are two different representations of the energy levels of superconductors that are semiconductor and Bose condensation representations.
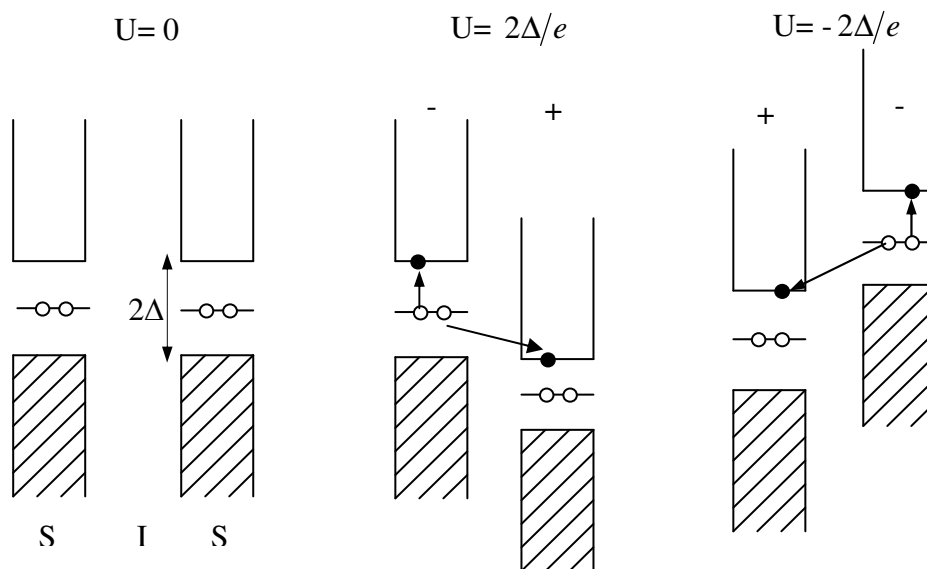
Figure 2.3. Bose condensation representation of single electron tunneling between two superconductors .

Bose condensation representation of the S-I-S tunneling process is shown in Figure 2.3. Strong tunneling occurs at an applied voltage $U \geq |2\Delta/e|$. This voltage is high enough to allow the empty states above the gap of the first superconductor, and the filled energy states below the gap of the second superconductor to overlap so pair-breaking process becomes possible. When the applied voltage exceeds $|2\Delta/e|$, the tunneling current rapidly increases. Because of thermally excited electrons for T>0 even at voltage well below $|2\Delta/e|$ a weak tunneling current is obtained as shown in Figure 2.3
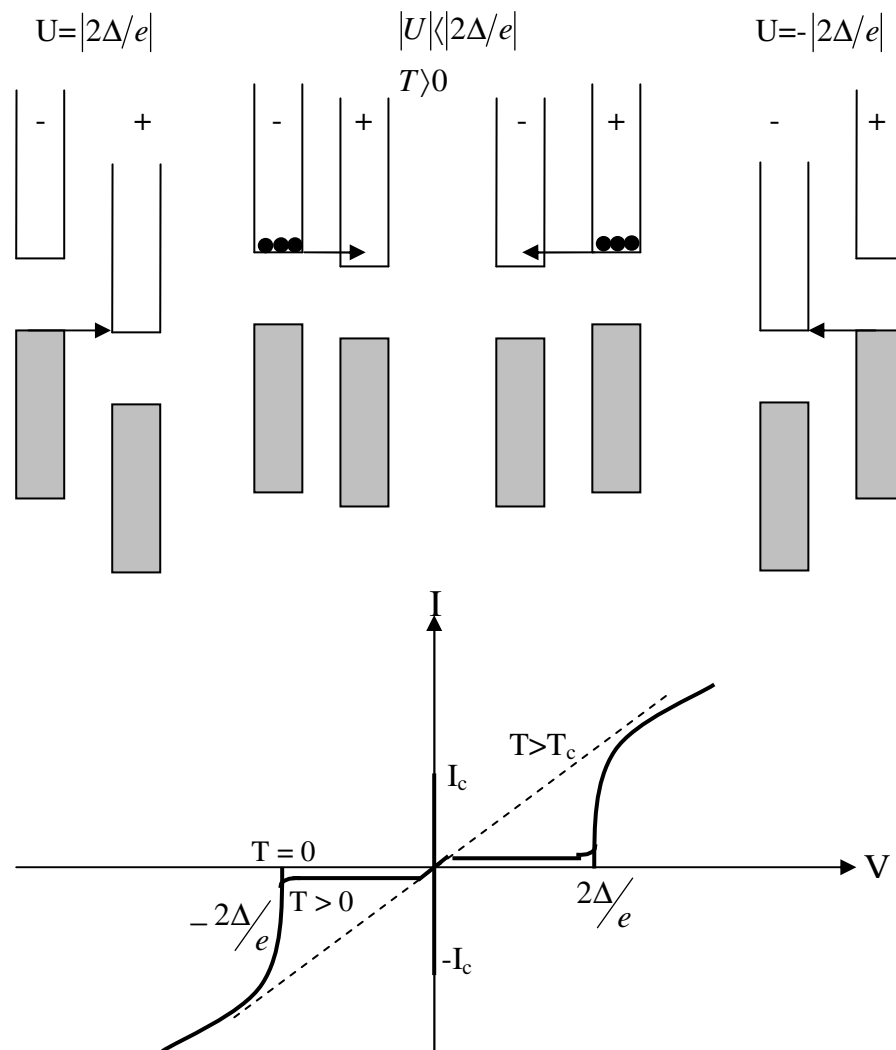
Figure 2.4 (a) The semiconductor representation of the S-I-S tunnel junction (b) I-V characteristic of the S-I-S tunnel junction

Differ from the other junction types SIS junctions show supercurrent tunneling because of Cooper pair transfer between two superconductors which is called

Josephson current. In 1962, B. D. Josephson predicted that for U=0 across the insulating layer Cooper pairs can tunnel through the barrier. The Josephson current due to Cooper pair tunneling at zero voltage across the insulating layer is shown Figure 2.4. The Josephson current flows without resistance below the critical current I_c of the S-I-S junction. When the current reach to the I_c, voltage and current jump to values voltage characteristic for single electron tunneling.
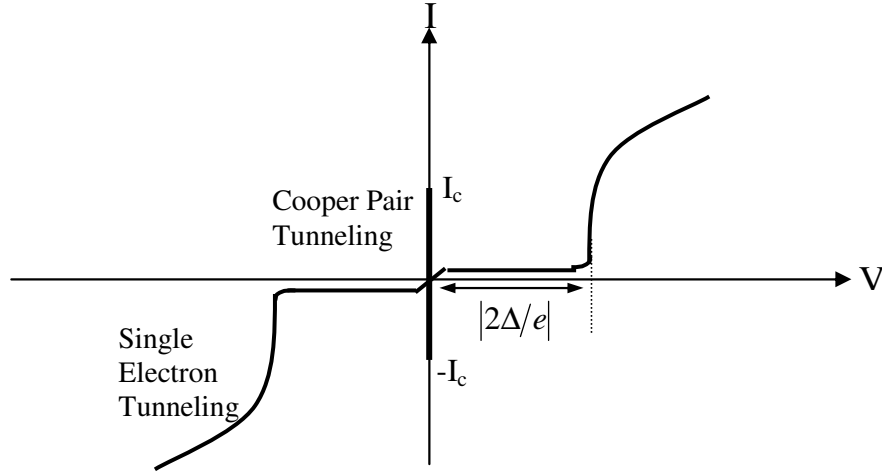
Figure 2.5 I-V characteristics of the S-I-S junction including Josephson current

The flow of the particles across the barrier is proportional to the probability for tunneling process to occur. This probability depends on the height and width of the barrier and called as transmission coefficient. Within the small energy range near the Fermi energy, this probability can be treated as a constant which is denoted by D. The number of electrons tunneling per unit time at energy E from left to right is proportional to the number of occupied states $N_I(E)f(E)$ on the left side and the number of unoccupied states on the right side (Buckel, 2004). While $f(E)$ is the probability of occupied states at energy E, $1-f(E)$ is the probability of finding an unoccupied states. If a voltage drops U across barrier, the electrons tunnel from a state with energy E on the left side into state with energy $E+eU$ on the right side. So at the voltage U their number is

$$N_{II}(E+eU)\left[1-f(E+eU)\right]$$ (2.4)

14

If we measure the electron energy from the Fermi energy: $\varepsilon = E - E_F$. So in a small energy interval $d\varepsilon$ at the energy ε, the tunneling current from left to the right is

$$dI_{I \to II} \propto D N_I(\varepsilon) f(\varepsilon) N_{II}(\varepsilon + eU)[1 - f(\varepsilon + eU)]d\varepsilon \qquad (2.5)$$

The total tunneling current $I_{I \to II}$ is obtained by integration over all energies that is

$$I_{I \to II} \propto D \int_{-\infty}^{\infty} N_I(\varepsilon) f(\varepsilon) N_{II}(\varepsilon + eU)[1 - f(\varepsilon + eU)]d\varepsilon \qquad (2.6)$$

Similarly the tunneling current $I_{II \to I}$ from left to right can be obtained

$$I_{II \to I} \propto D \int_{-\infty}^{\infty} N_{II}(\varepsilon + eU) f(\varepsilon + eU) N_I(\varepsilon)[1 - f(\varepsilon)]d\varepsilon \qquad (2.7)$$

The net tunneling current is

$$I = I_{I \to II} - I_{II \to I} \propto D \int_{-\infty}^{\infty} N_I(\varepsilon) N_{II}(\varepsilon + eU)[f(\varepsilon) - f(\varepsilon + eU)]d\varepsilon \qquad (2.8)$$

where $F(\varepsilon) = [1 + \exp(\varepsilon/k_B T)]^{-1}$ is the Fermi function with $\varepsilon = E - E_F$.

2.2. Spin Polarized Current Tunneling into a Superconductor

Spin injection into superconductors can be performed by passing electrical current through a ferromagnetic material before the tunneling across a thin insulating barrier into a superconductor. In resent years, the injection of spin polarized current in ferromagnetic-insulator-superconductor (F-I-S) junction has attracted significant effect on experimental interest. This technique utilizes the excellent lattice match among various perovskite materials for epitaxial film growth of the heterostructures. So, investigating the characteristic spin and charge relaxation and transport processes in the perovskite F-I-S devices can be unique vehicle for probing nonequilibrium superconductivity and possibly the pairing mechanism in the cuprates (Fu, 2002). However, strong suppression the superconducting critical current and significant modification to the quasiparticle density of states (DOS) is observed in superconductor

15

by injection of spin polarized current from ferromagnetic films. Consequently, the experimental findings are attributed to the dynamic pair-breaking effects of spin polarized quasiparticle as a result of excess magnetic moments and quasiparticle redistribution.

In spite of the fact that there are experimental reports about spin injection in cuprates, many important issues are yet to be resolved. Theoretically, microscopic interactions of spin polarized quasiparticle with the Cooper pairs is still unknown. Nonetheless, the intrinsic anisotropy in the cuprate superconducting order parameter because of the $d_{x^2-y^2}$ wave pairing symmetry and the weakly interacting layered structure are expected to be relevant to the spin and charge transport (Fu, 2002).

The schematic of quasiparticle injection into a cuprate superconductor is shown in Figure 2.5. On the left side, itinerant electrons in the ferromagnetic material (F) manganite layer is represented by filled circles, with the parallel –aligned arrows indicating their near- %100 spin polarization at the Fermi level (horizontal line). The right side shows the quasiparticle spectrum for the superconducting (S) cuprate with d-wave pairing symmetry, where the filled circles represent injected quasiparticle and the open oval represents a d-wave cooper pair. The insulating layer is represented by trapedizoidal injection barrier, indicating a bias voltage applied between the F and S layers.
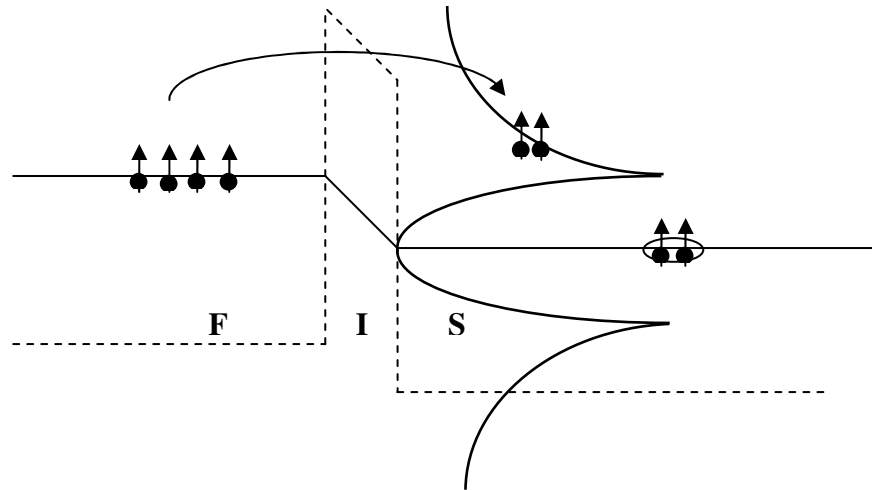
Figure 2.6. Schematic of spin polarized quasiparticle injection from ferromagnetic
material into a superconductor
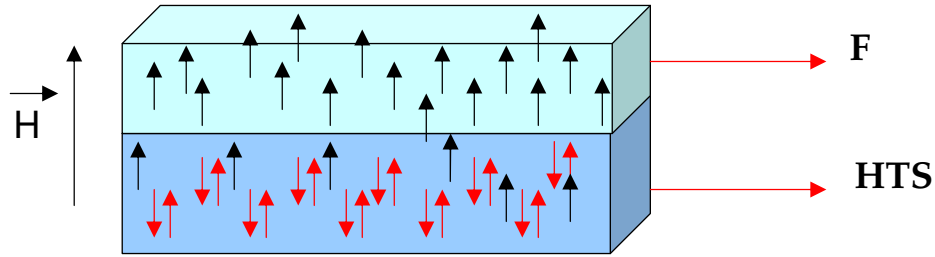
Figure 2.7. Schematic representation of spin polarized tunneling with applied magnetic field

When the spin polarized quasiparticle are injected from F to S to recombine into the spin singlet pairs, the quasiparticle first randomize their spins, making a spin relaxation .This spin relaxation process occurs slower than the charge relaxation. So, the quasiparticle recombination process is being effective because of ''spin bottlenecking''. Consequently, this spin polarized nonequilibrium quasiparticle distribution cause pair breaking via two different mechanisms: (1) raising the effective, nonequilibrium quasiparticle temperature, thus weakening the pairing interaction and (2) breaking the time reversal symmetry of the *d*-wave pairs.

When a magnetic field H is applied to heterostructure (F-I-S) along the c-axis, the field H can result from a combination of externally applied field and self-field of ferromagnet, which can be substantial near the ferromagnet. At the superconductor, the direction of the externally applied field may be opposite that of the self-field of the ferromagnet, resulting in a decrease in H as the external field is increased (Jiang, 2003) Because of the magnetic field, most spin of the electrons are directed with same way as applied magnetic field so spin polarized current increase. This current causes the more pair breaking effect while superconductivity is destroyed.

Consequently, the spin polarized tunneling current which is driven from a ferromagnetic material (FM) into a superconductor (SC) creates a non-equilibrium spin polarization in SC because of spin polarized electrons so superconductivity is strongly suppressed.

CHAPTER 3

EXPERIMENTAL

In this chapter, the experimental facilities used while conducting this study will be explained. In the first part, crystal structure and inherent properties of high temperature superconductor, $Bi_2Sr_2CaCu_2O_{8+\delta}$ (Bi-2212) will be presented in details. The second part of this chapter is associated with thin film preparation and micronsized mesa fabrication on Bi-2212 single crystals. In the final part, point contact tunneling characterization technique will be explained.

3.1. $Bi_2Sr_2CaCu_2O_{8+\delta}$ (Bi-2212)

The experiments were performed on $HgBr_2$ intercalated Bi-2212 ($T_c= 74K$) single crystal. These samples were prepared by D.G. Hinks at Argonne National Laboratory using a floating zone technique to grow pristine crystals.

$Bi_2Sr_2CaCu_2O_{8+\delta}$ (Bi-2212) is the most examined High-T_c superconductor by surface sensitive probes, since (i) growing of high quality mm-sized single crystal without any macroscopic defects or dislocations is relatively easy (ii) varying doping level by annealing in argon or oxygen is easy and (iii) the single crystal can be cleaved easily between the Bi-O layers to expose chemically inert and atomically flat surfaces over very large areas. These properties make Bi-2212 suitable for surface sensitive experiments such as scanning tunneling microscopy (STM), Raman and ARPES.

Like all HTS, Bi-2212 has an inherent structure consisting of stack of superconducting layers (CuO planes) and insulating layers (BiO and SrO layers) along the c axis. Therefore, Bi-2212 is the best material for fabricating IJJs. This layered structure present anisotropic characteristics in the directions parallel and perpendicular to the c-axis. There are two developed models to explain the mechanism of this structure: Multilayer model and proximity model (Yurgens et al.1996) shown in Figure 3.1
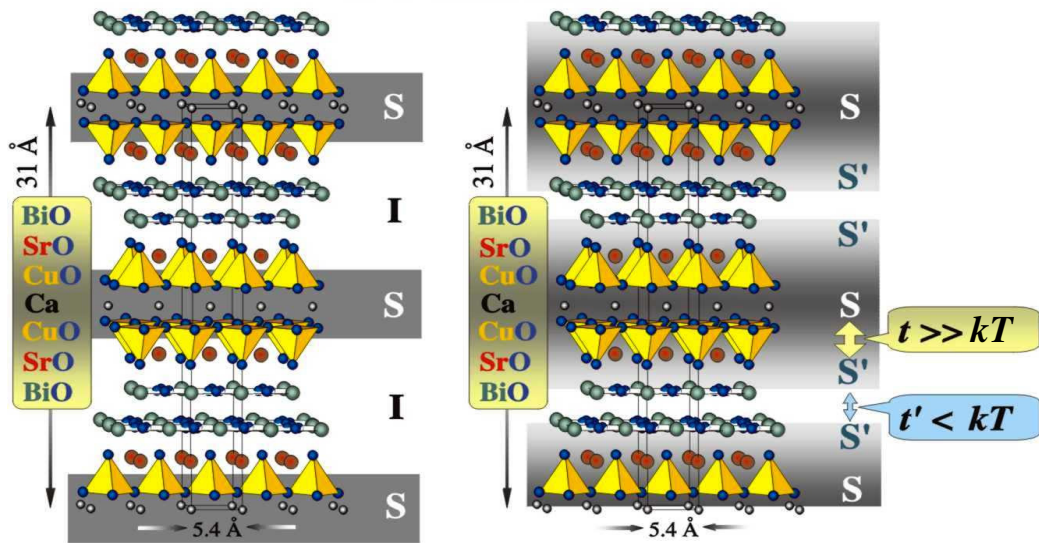
Figure 3.1 The crystal structure of Bi-2212.The left image corresponds to basic multilayer model the right image shows the proximity model   .

According to the multilayer model Bi-2212 high-Tc material can be conceived of as a stack of Josephson junctions along the crystal c-axis. In a simplified picture, Josephson coupling in this compound is believed to occur between superconducting double CuO layers of thickness 3 Ǻ separated by intermediate BiO and SrO layers of thickness d=12 Ǻ. CuO layers corresponds to the important building blocks in which the high temperature superconductivity takes place. On the other hand, BiO and SrO layers between the CuO planes not only stabilize the crystal structure, but also act as the charge reservoir, supplying the charge carriers to the copper oxide, which then combine into the Cooper pairs. As mentioned above, the superconducting coherence length of Bi-2212 in the c-axis is approximately 0.1 Ǻ, which is relatively very small if compared with the distance between two adjacent CuO_2 layers in the Bi-2212 unit cell. This point makes Josephson tunneling of Cooper pairs hard across the insulating layer (Yurgens et al.1996).

According to the proximity model not only CuO_2 layers but also Bi-O planes contribute to superconductivity of HTS. There is a strong coupling between the Cu-O and Bi-O layers (S-S') with weak Josephson coupling between neighboring Bi-O layers (S'-S') because Bi-O layers exhibit superconducting properties rather than insulating character.

To fabricate such junction stacks is very easy but large number of junctions in one stack is undesirable because to investigate tunneling characteristics of an individual junction from this stack is hard. While obtaining I-V data, Joule heating or quasiparticle injection, which can degrade or even damage the junctions, are the most encountered problems. There are several methods to eliminate these problems. One method of minimizing heating is to use stacks of intrinsic junctions (mesas) with small dimensions in order to reduce I_c. Another is to use a short pulse of current. The technique allows the intrinsic conductivity to be obtained from dc measurements. However, much of the interest of these measurements is in the behavior close to the energy gap, and high bias currents are required. The resulting dissipation, and consequent heating, is sufficiently large that dc measurements cannot be used to explore this region, and short pulse measurements are necessary (Thomas, 2002). One another method is to intercalate the Bi-2212 single crystal with inert guest molecules such as $HgBr_2$, HgI_2 or I_2 molecules to reduce the coupling between CuO_2 layers. Insertion of inert $HgBr_2$ molecules between adjacent BiO layers results in a significant stretching of Bi-2212 crystals in the c-axis direction without affecting the superconducting critical temperature T_c much Figure 3.2 (Yurgens, 1999) Due to intercalation the intrinsic tunneling barriers are becoming wider which results in a drastic decrease of the c-axis critical current density. Therefore, Joule heating can be significantly suppressed.
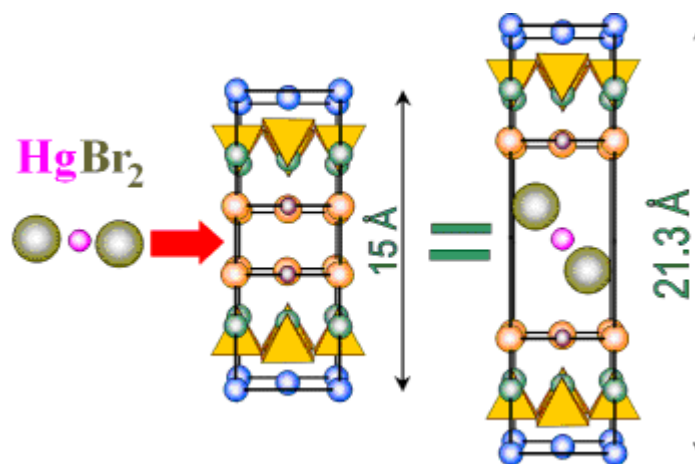

Figure.3.2. Intercalation of the inert $HgBr_2$-molecules into Bi-2212 single crystals

Intercalation reactions are carried out by vapor transport reaction method between host and guest in a vacuum-sealed Pyrex tube at 230 ^{0}C for 16 hours. After the

intercalation process, it can be realized that the lattice expansion is around 12.6 Å by using X-ray analysis (Yurgens et al.1999).

All of these methods exhibit dip and hump features, which is an indication of less heating, as seen by STM/S and point contact tunneling (PCT). These features are related to the fundamental pairing mechanism of HTS.

Bi-2212 superconductor is a type II superconductor; which means that its Ginzburg-Landau parameter $\kappa=\lambda/\xi$. is greater than $\sqrt{2}$. Associated with this parameter, it has large penetration depth λ_{ab}=200-300 nm, λ_c=15-150 μm (Buckel 2004) and extremely short coherence length ξ_{ab} and ξ_c is 2 nm and 0,1 nm respectively. (Buckel, 2004)

3.2. Experimental Procedure

3.2. 1. Mesa Preparation

Since IJJs were discovered in 1992 mesa structures have been widely used to understand the mechanism of superconductivity of HTS and to investigate fundamental properties such as energy gap or density of states near the Fermi level.

Before the mesa preparation, firstly deposition rate and etching rate of Au and Co is determined using the Argon ions. While deposition rate of Au is 30 nm per minute under conditions that 20 W, 402 V and 45 mA, that of Co is 6.5 nm per minute under conditions 20 W, 346 V, and 48 mA and etching rate of them 8 nm and 2 nm per minute respectively using Ar ions under conditions 21 W, 700 V, 30 mA.

Although there are some differences for methods of mesa preparation, the general features remain same. For mesa fabrication, firstly crystal of Bi-2212 having a smooth surface was glued onto an alumina substrate by an epoxy. In order to get fresh and flat regions, the crystal was then cleaved with an aid of adhesive tape and was immediately placed into sputter system to thin film deposition. The photography and schematic representation of sputter system in our laboratory is shown in Figure 3.3 and Figure 3.4 respectively. A 15 nm thick Au film was deposited on the cleaved crystal surface to protect it from the ensuing sample preparation processes. The superconducting properties of the films have been found to suffer severe degradation when the Co layer was directly sputtered onto the high T_c film (Ishibashi, 2001). After that Co metal of 80 nm thickness was deposited as a spin injector and then 156 nm

thick Au was deposited onto the cleaved crystal to protect the surface from chemicals such as photoresist, developer and water during the photolithography and also to get electrical contacts for characterization. Deposition conditions are shown in Table 1. Photolithography was then applied to replicate different sized mask patterns, such as squares with the edge dimensions of 12 µm on the crystals. Configuration of mask shown in Figure 3.5 and the photograph of mask is shown in Figure 3.6. For this purpose we used, Shipley Microposit 1813 positive photoresist to get the exact image on the photomask. Both positive and negative photoresists consist of photosensitive organic materials, usually including a resin, photosentizer and a special solvent.

For the photolithography process, photoresist was used to produce patterns on the substrates as a thin coating, typically by spin coating over the Bi-2212 and then heated to remove the casting solvent. The photoresist film was subsequently exposed to UV light through a mask to replicate $12x12$ μm^2 sized patterns. The exposed resist film is then developed typically by immersion in a developer solvent (0.2 M NaOH) for 25 seconds to generate three-dimensional relief images. The exposure may render the resist film more soluble in the developer. After the mask pattern was transferred into the substrate by etching and related processes, the resist film that remains as a protective mask. The resist film protects the underlying substrate while the bared areas are being etched. The remaining photoresist film is finally stripped using acetone, leaving an image of the desired pattern in the substrate. Finally, Ar ion beam etching was used to etch down the unprotected regions on the surface and proper mesa structures consisting of many IJJ and multilayer thin film were obtained. The steps of mesa fabrication process are given in Figure 3.7. For etching process, samples were placed into the chamber with an angle of 45^0 between the directions of Ar ion beam and etched by Ar ions with the energy of 700 eV at 22 W for 74 minutes. Even after ion beam milling, some remaining of photoresist is still available on mesa, i.e. a skin like coating may stay on top of the gold film. Such cases can require oxygen plasma etching process. The basic configuration of the Ar ion beam system is shown in Figure 3.8 (a) the photograph in Figure 3.8 (b) exhibits the system in our laboratory.

Figure 3.3. The photograph of sputter system in our laboratory
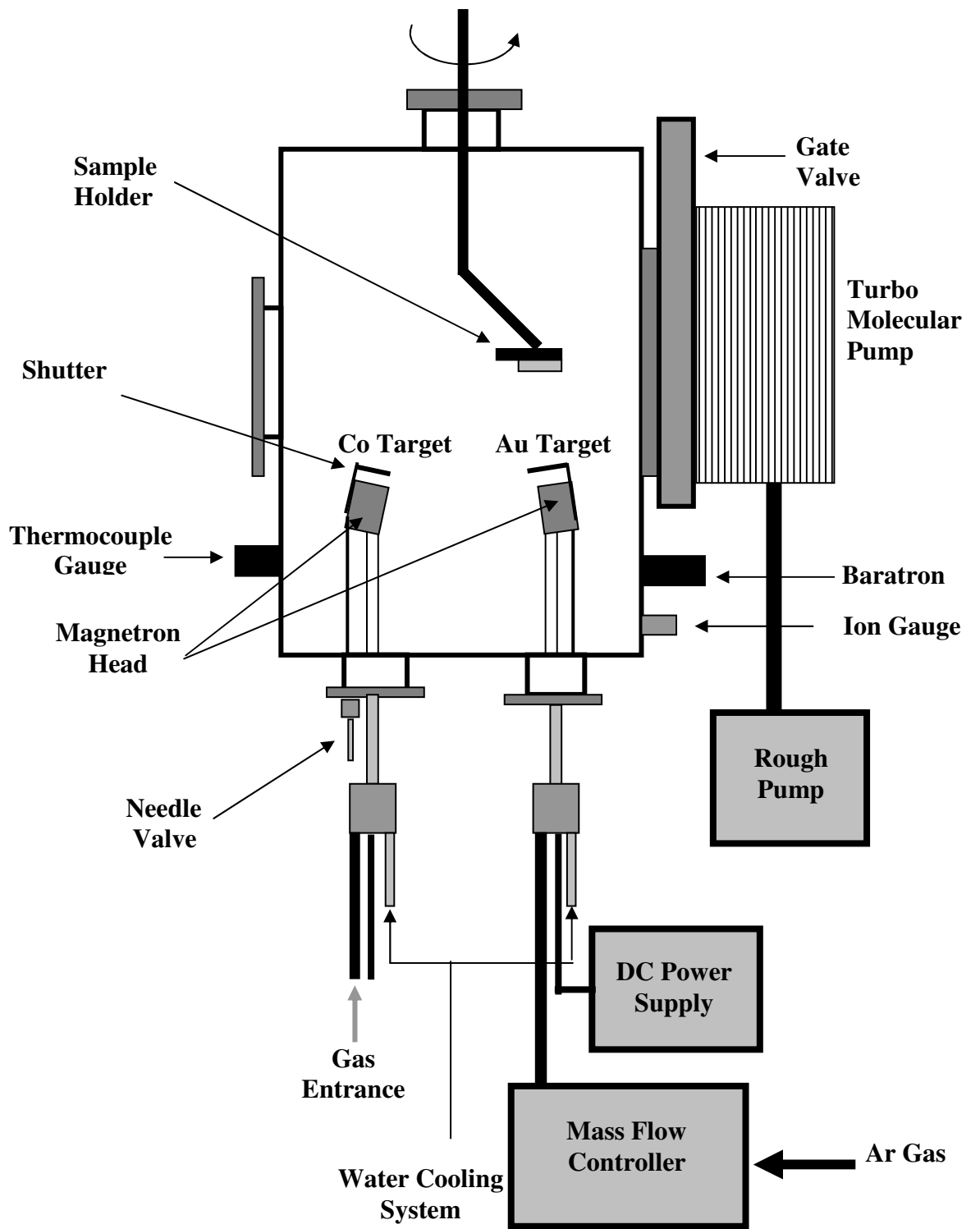
Figure 3.4. The schematic representation of Sputter system
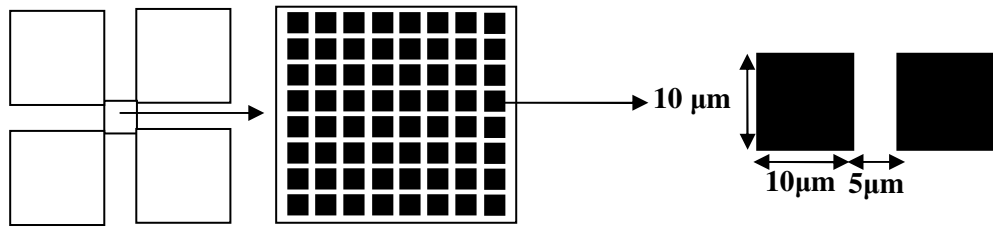
Figure 3.5.Schematic representation of holders and square area consisting of mesas
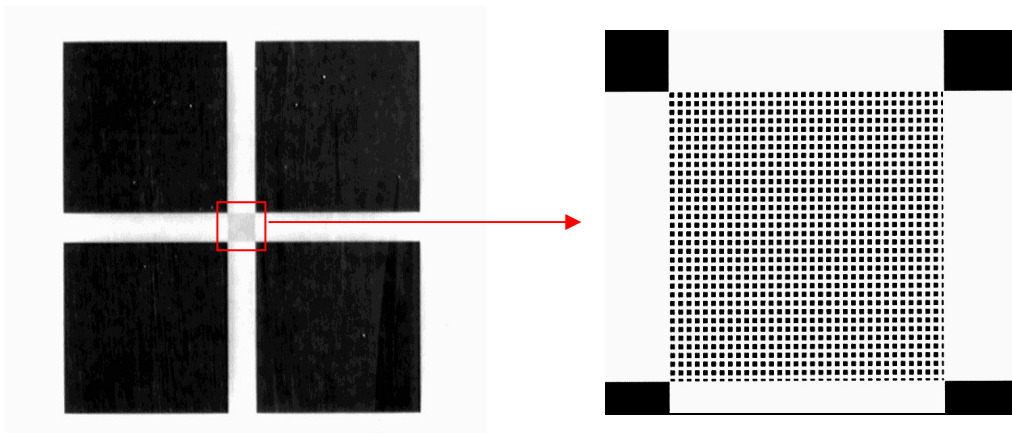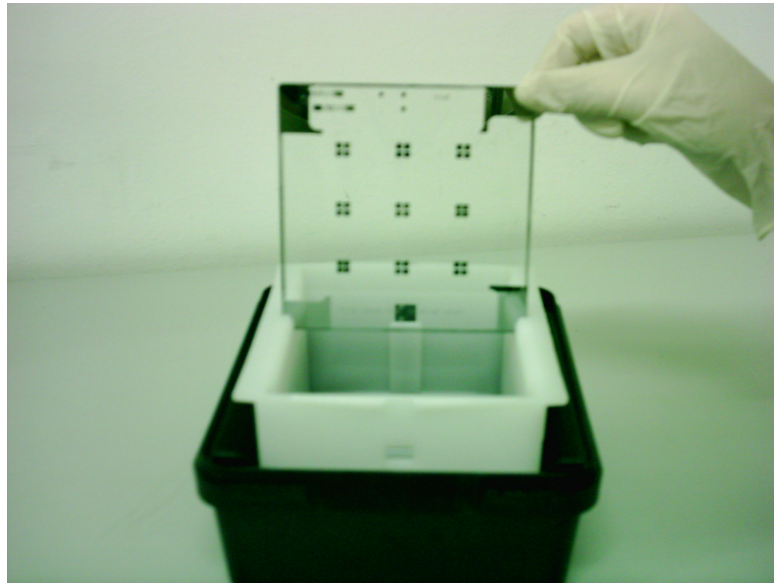
Figure 3.6. (a) The glass containing 9 different masks (b) and (c) is more detailed photography of mask

Positive photoresist

156 nm Au

80 nm Co

15 nm Au

Bi-2212
single crystal

Applying photoresist

UV light

Exposing UV

Argon ions

Argon ion beam etching

Mesa
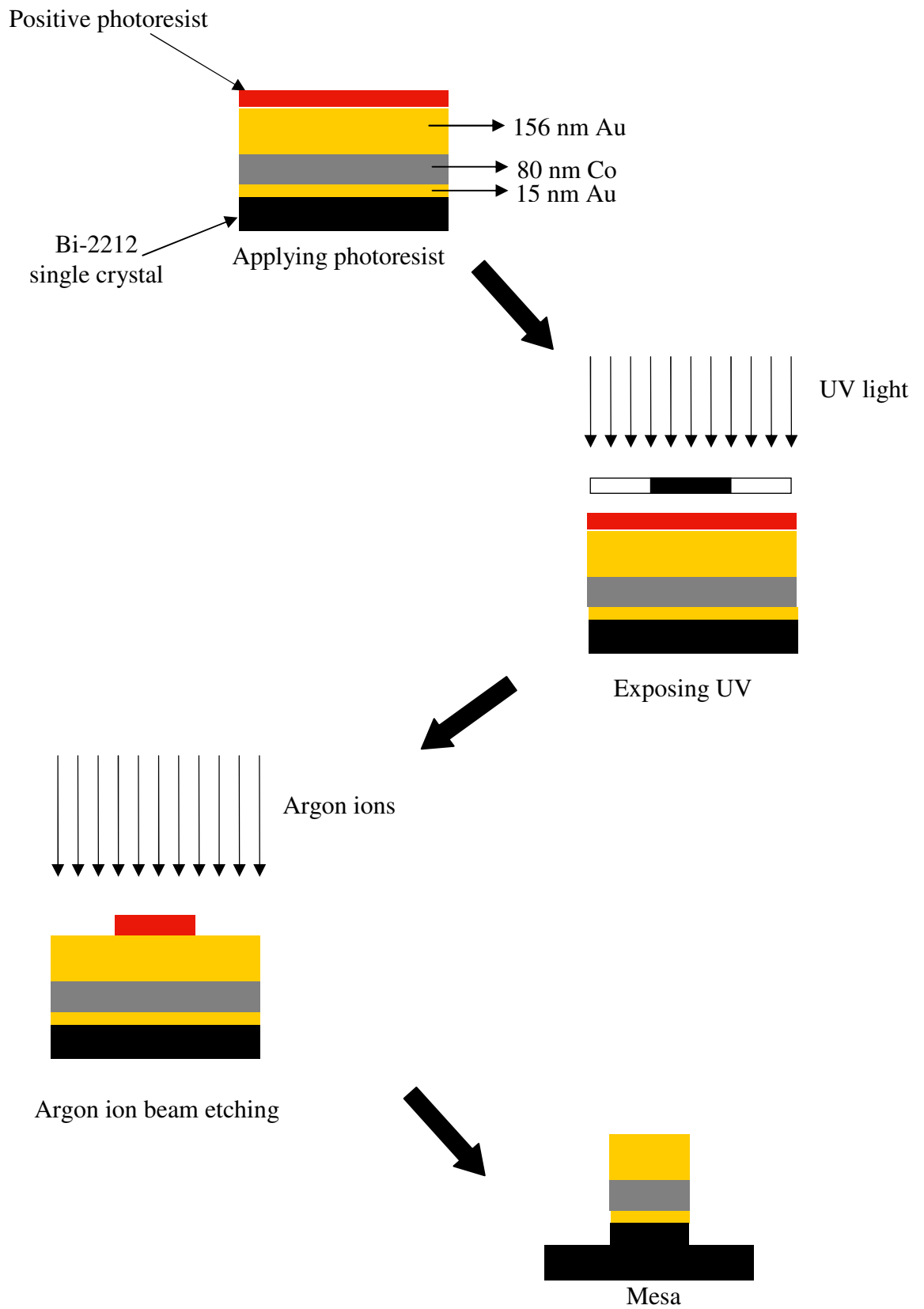
Figure 3.7. Schematic representations of photolithography steps
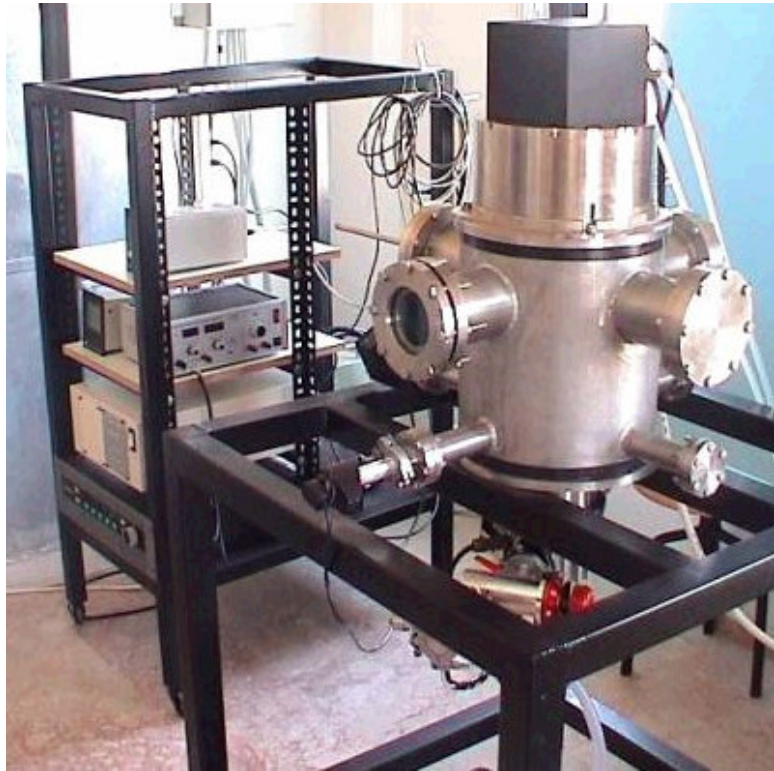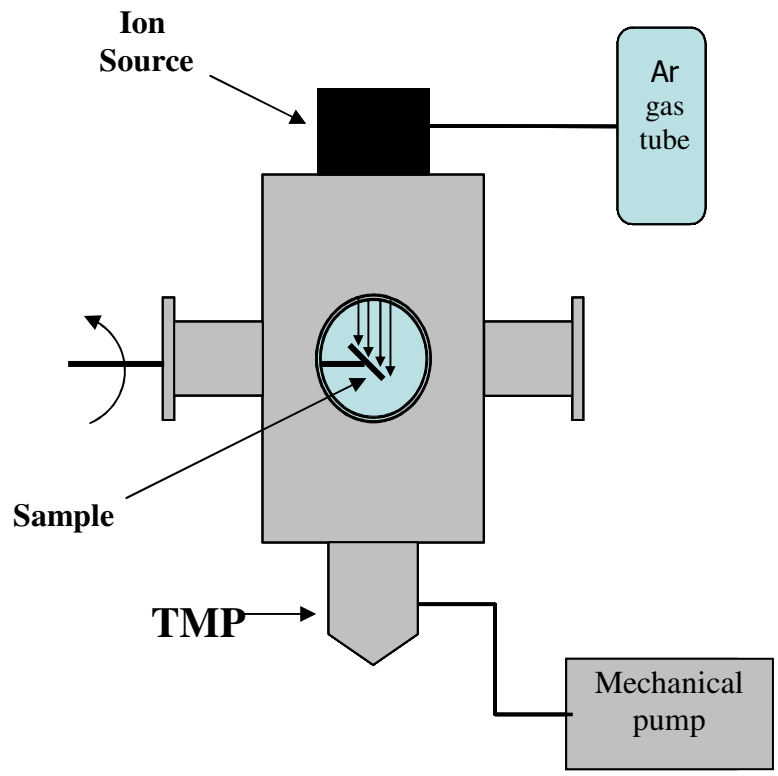
Figure 3.8. (a) Schematic representation of Ar-ion beam system (b) the photograph of
the same system.

Table.3.1 Deposition conditions of thin films

Target	Power (W)	Voltage(V)	Current(mA)	Gas Flow (SCCM)
Au	20	402	45	40
Co	20	346	48	20

3.3. Characterization Method

3.3. 1. Optical Microscopy

Firstly, to understand the quality of the photolithography, all mesas were examined with optically microscopy as a pre-characterization. This kind of characterization can give information about the degree of excellence transition of the mask pattern onto the single crystal surface. In other words, some problems originated from photolithography or etching such as poor contact between mask and crystal surface, undesired reflections because of glass mask, any contamination problem onto the mask surface such as remaining of photoresist skin after etching, excess or insufficient milling which can be easily understood from optical micrographs.

3.3. 2. Atomic Force Microscopy

After the pre-characterization, AFM was used to obtain more detailed image of mesas because of high resolution. And also AFM provide 3-dimensional topographic image of mesas.

Furthermore, the height of the mesa and multilayer thin film are very important and they were obtained using step height analysis of AFM. In order to determine height of multilayer film (Au, Co, Au) during the deposition onto the single crystal, a piece of lamella is mounted to the sample holder besides Bi-2212 single crystal. At the end of the sputtering, the multilayer film was expected to coat the glass surface with the same degree of quality and of course the same height on the crystal surface. For this reason a very narrow line is created on the thin film surface with an aid of extremely thin needle and AFM tip scanned the related slit, thickness of thin film could be easily found. Moreover, after height of the mesas determined, using the thickness of multilayer film,

height of single crystal into the mesa was determined. Dividing this value one SIS junction size in the unit cell, which is around 21 Å for intercalated Bi-2212 single crystal, the number of IJJ in mesa was calculated.

3.3. 3. Point Contact Tunneling

Among the other techniques Point Contact Tunneling is the most convenient and simplest method to investigate the quasi-particle density of states (DOS) near the Fermi level of superconductors, and has been often employed in the study of high-T_c superconductors. And also the best energy resolution ($\sim k_B T$) at low temperatures makes it favorable technique (Ozyuzer, 1999). Zimmerman and Silver first used point contacts in 1966 to obtain easily made superconducting weak links, which would exhibit the Josephson effect.

In all cases pressing a pointed rod onto a flat surface formed the point contact so that the contact area is sufficiently very small. However, there are some problems about the influence of the point contact pressure on the sample surface, which may bring extrinsic spectrum characteristics because of some surface damages. On the other hand, it is known that a cleaved surface Bi-2212 single crystal easily suffers from such damages, due to the weak bonding strength between the (Bi-O) double layers (Murakami, 2000). Such kind of problems is possible in many other surface sensitive probes but experiments performed with IJJ are not affected from such kind of problems because they naturally formed inside crystal with high degree homogeneity and they can reproduce. Understanding from the point mentioned, surface deformation does not affect the measurements in IJJ.

In this thesis, using point contact tunneling technique spin polarized and spin degenerate current was driven along the c-axis of Bi-2212. Tunneling measurements provided a direct measure of the temperature dependence changing from 4.2 K to 195 K and magnetic field dependence changing from 0 G to 1100 G as perpendicular to the sample surface.

CHAPTER 4

RESULT AND DISCUSSION

This chapter includes characterization results, which were obtained from Optical Microscope, Atomic Force Microscopy and Point Contact Tunneling Technique, and consensuses of results of $HgBr_2$ intercalated samples with the critical temperature of 74 K.

4.1. Optical Microscopy Results

Optical microscopy was used as a pre-characterization method at the beginning of investigation to obtain rough idea about the surfaces of mesa structures. This kind of characterization gives information about the quality of the photolithography such as the degree of excellence of images which are supposed to be replicated to the single crystal surface. During the photolithograph some problems can occur because of poor contact between mask and crystal surface, photoresist remaining from previous photolithography process or any contaminations onto the mask surface, excess or insufficient etching with $NaOH_2$. However some problems can occur during the Ar ion beam etching process for example photoresist skin remain onto the surface due to insufficient etching. After etching process if there is still photoresist skin onto the crystal surface Oxygen etching must be done.

Figure 4.1 shows an optical micrograph of a representative sample containing 12x12 μm^2 mesas on Bi-2212 single crystal; the separation between two squares is 5 μm in photomask. Figure 4.2 shows an optical micrograph of another sample containing same sized mesas.

When we look at the Figure 4.1 we can easily understand that square image of mask replicated to the surface perfectly. In this Figure, while square yellow areas are mesa structures, black areas are Bi-2212 single crystal. From this image and also we can understand that etching process is sufficient for this sample.

On the other hand Figure 4.2 show that image of photo mask could not be transfer onto crystal surface well because of contact problem between the mask and crystal surface. If there is a contact problem between mask and single crystal surface, the reflection of UV light occur edge of square pattern. However, the region of between

the mesas is not black. From this point we can understand that etching process is insufficient for this sample. Furthermore, there is photoresist remaining onto the single crystal.
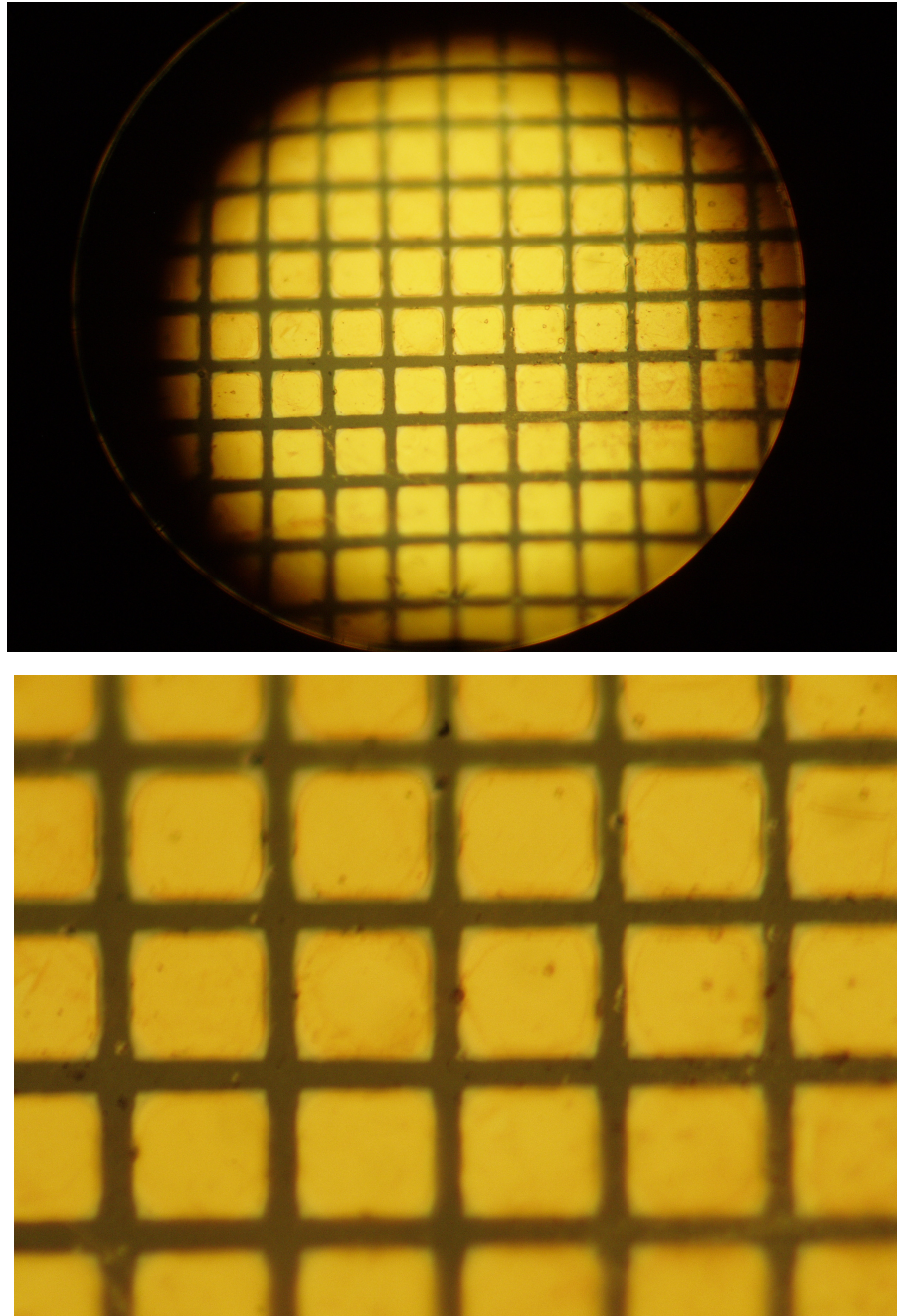

Figure 4.1 (a) Image of MMc with Arrays of squares with the area of 10x10 μm^2 on Bi-2212 single crystal (b) more detailed image
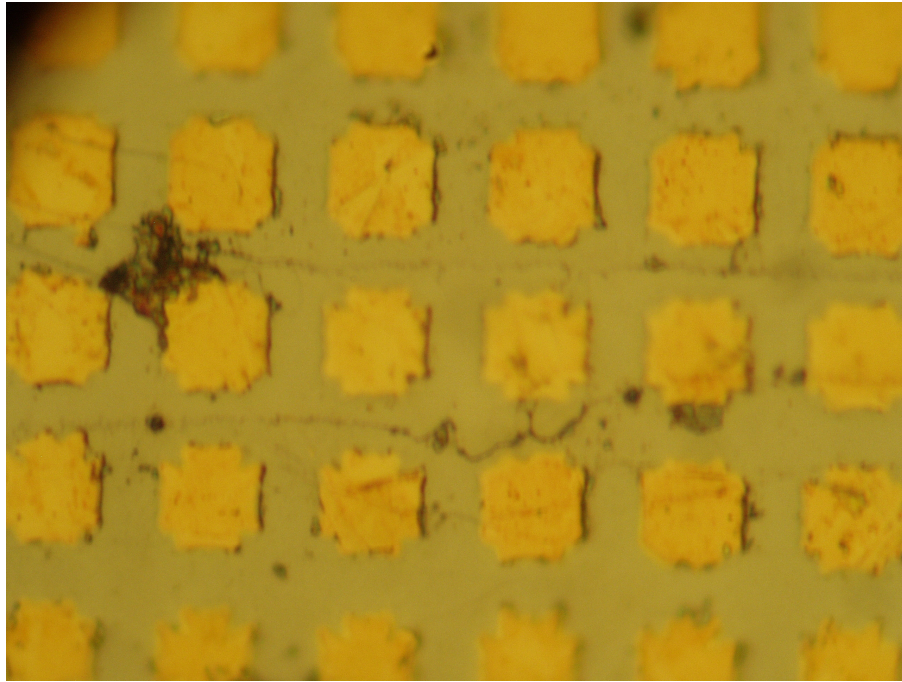
Figure 4.2. Image of MMb with Arrays of squares with the area of 10x10 μm^2 on Bi-2212 single crystal

4.2. Atomic Force Microscopy Results

Using Atomic Force microscopy, samples surface can be examined much more detailed. Figure 4.3(a) and (b) show the topographic image and three dimensional images of MMe samples, which have the same size with the other samples mesas. When the images are examined, it is easily seen that there is thin photoresist skin onto the mesas.

The measurements done with tapping mode of the AFM can reveal the exact thickness of the multilayer thin film sputtered onto the crystal surface and thickness of the mesas Figure 4.4(a) and 4.4(b) respectively. So, the number of IJJ in the concerned mesa can be calculated easily. The height of the single crystal into the mesa can be found with simple calculation. The height of the single crystal into the mesa structure corresponds to the total height of IJJ into the mesa. Using these results, number of the IJJs into the mesa can be calculated dividing total height (730 Å) by one SIS junction size in the unit cell which is around 21.3 Å for intercalated Bi-2212. From this simple calculation the number of IJJs was found nearly 35.
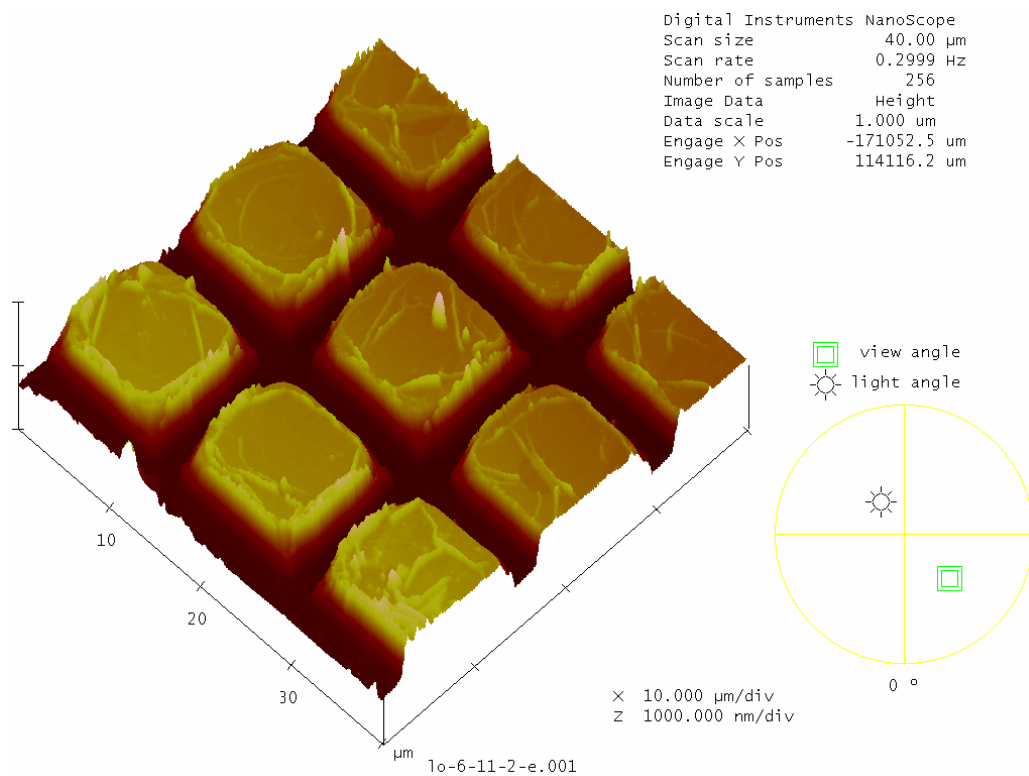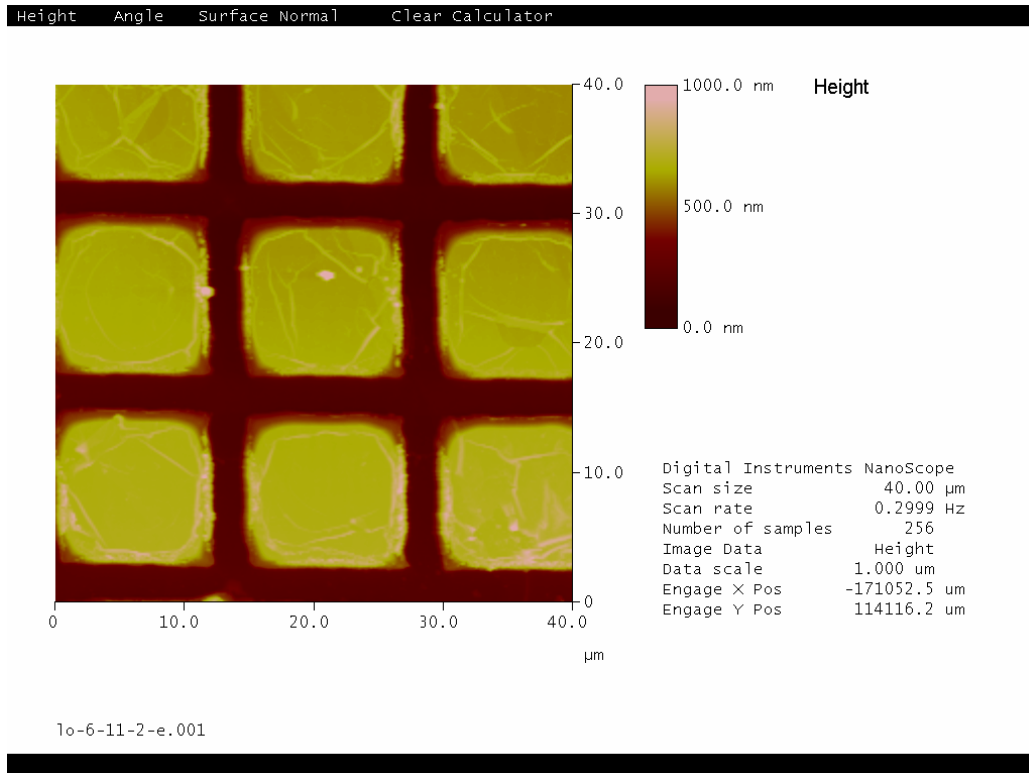
Figure 4.3. (a) The topographic image of the mesa arrays of squares with the area of $12 \times 12 \ \mu m^2$ on Bi–2212 single crystal (b) Three dimensional image of mesas
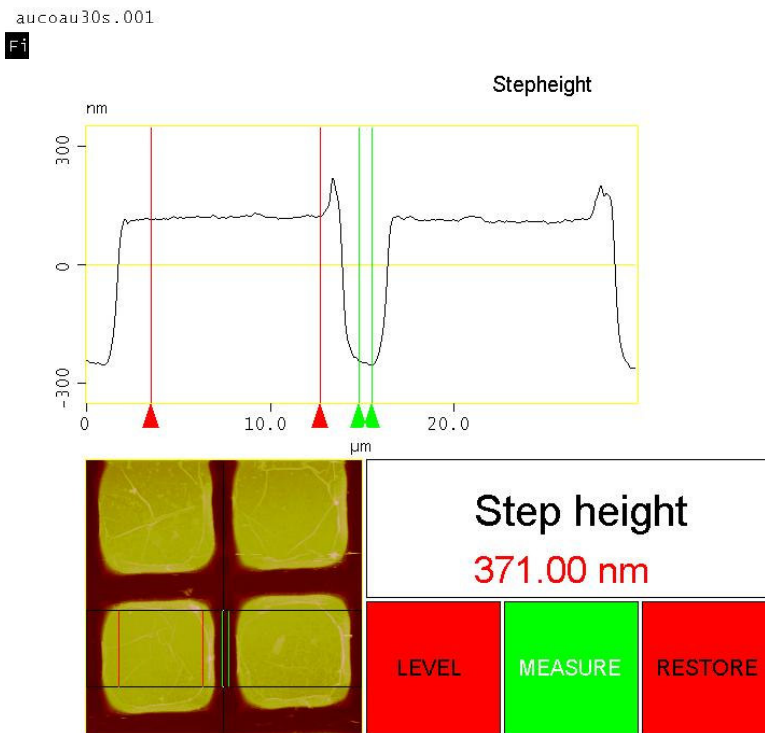
Figure 4.4. (a) The step height analyses of multilayer thin film (b) That of 12x12 μm^2 mesas obtained by AFM

The color differences in the AFM images indicate the height difference. While the bright areas correspond to the high height, dark areas correspond to the low height. This can be seen easily from the three dimensional topographic image Figure 4.3. When we look at the topographic images, while the yellow areas correspond to the mesas, dark areas correspond to the Bi-2212 single crystal. And also color difference easily can be seen on the mesa areas. This means that the surfaces of the mesas are not flat and roughness is pretty high. This problem also can be deduced from section analyses, the height of the mesa surface changes from point to point because of the uneven feature of the mesa areas because of unequal exposure of Ar ions during the etching process. Furthermore, reason of uneven surface can be photoresist remaining after the Ar ion beam etching. And also the height of the photoresist skin can be obtained from the section analyses. Figure 4.5 shows the section analyses of MMc sample surface. On the other hand this photoresist skin is not a problem for PCT measurements because during the measurements due to heating skin disappeared.
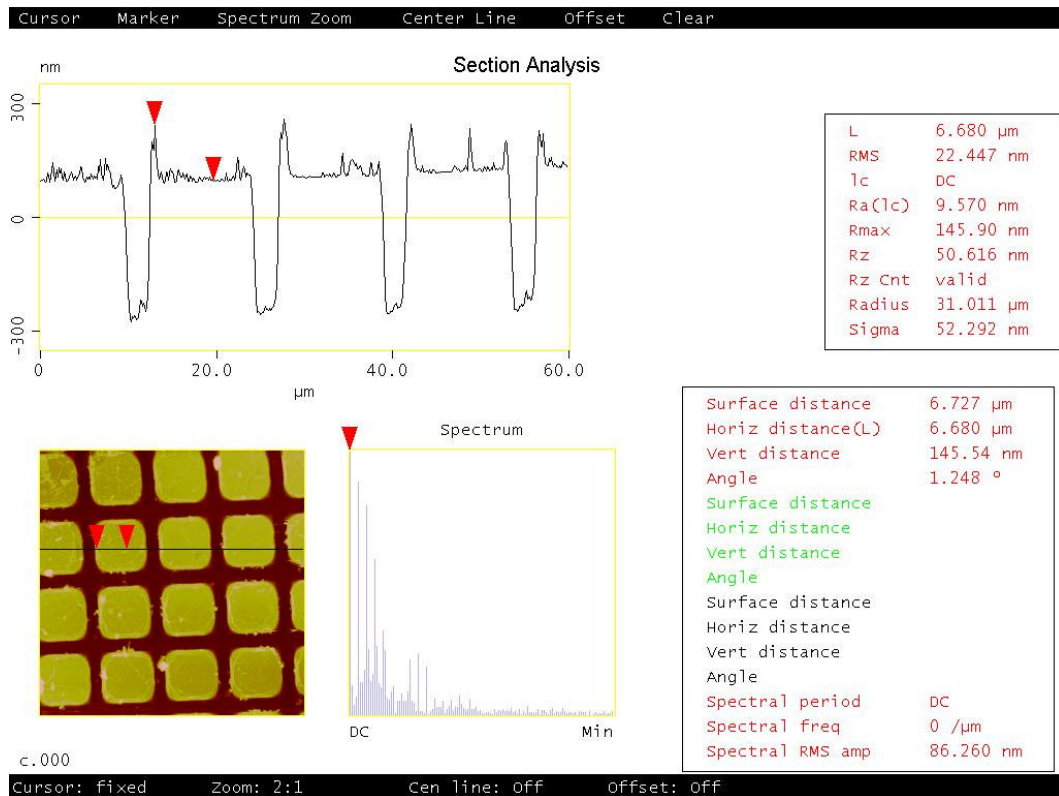

Figure 4.5 The section analyses of 10x10 μm^2 mesa areas.

4.3. Point Contact Tunneling Measurements

4.3.1. Tunneling Characteristics of Mesa with Au Top Layer

Point contact tunneling measurements were used to obtain the tunneling spectroscopy of intercalated Bi-2212 single crystal with T_c= 74 K. Tunneling experiments were performed on micron sized mesa arrays of $HgBr_2$ intercalated superconducting Bi-2212 single crystals. Two different configurations are used for covering top of the mesas; one is ferromagnetic multilayer (Au/Co/Au) and the other one is just single Au layer. The spin degenerate current is driven along the c-axis of 2 different junctions (BH19a#1 and BH19a#2) on sample BH19a. The spin-polarized current is driven along the c-axis of 3 different junctions (MMc#1, MMc#2 and MMc#3) on sample MMc by the aid of ferromagnetic Co layer. Dimensions of these square mesas are 12x12 μm^2 and separation between them is 5 μm^2.
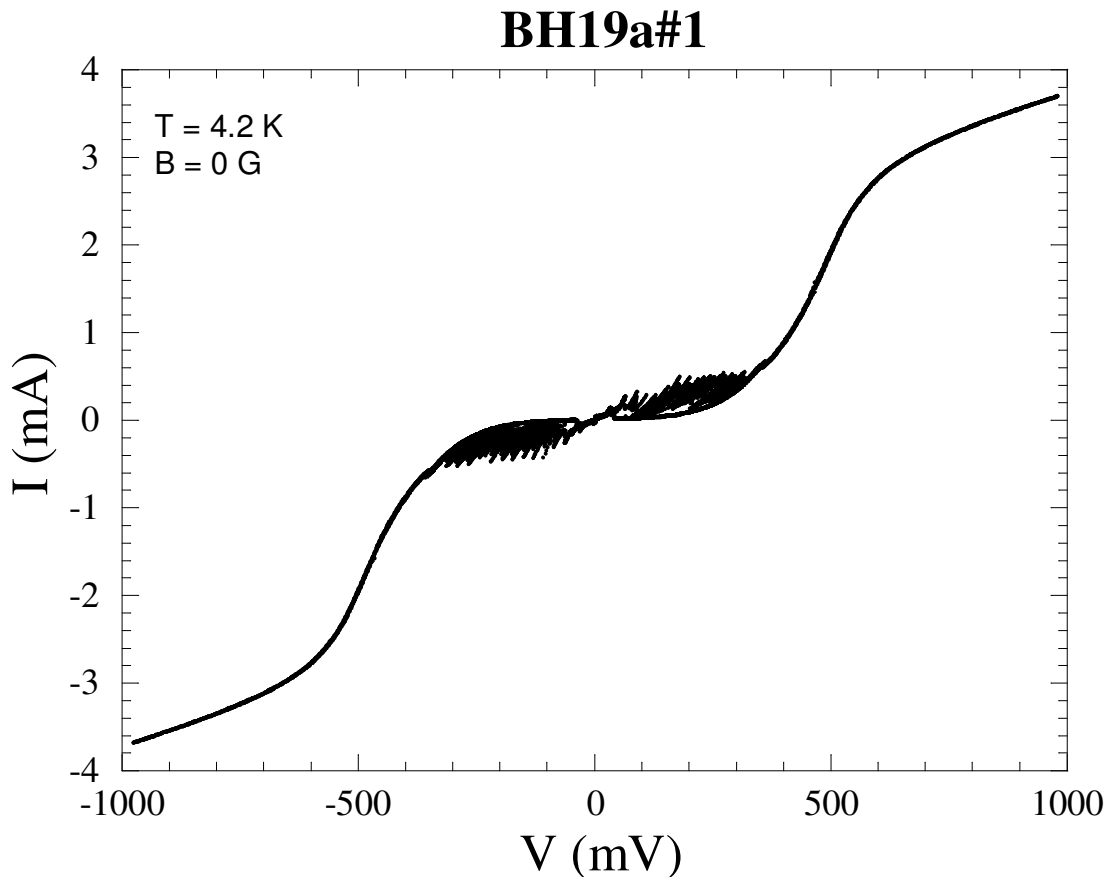

Figure 4.6. The I-V characteristic of BH19a#1 at 4.2 K
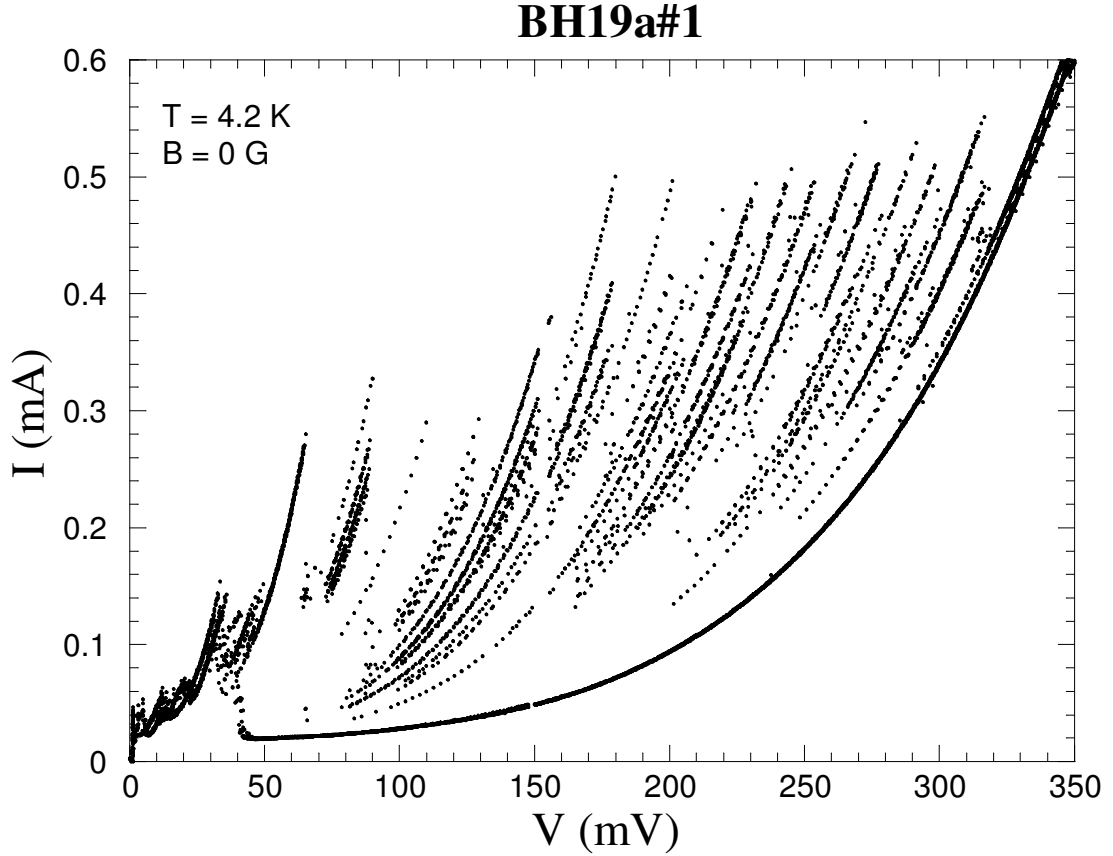
Figure 4.7. The I-V characteristic of BH19a#1 at 4.2 K in detail

Figure 4.6 shows the I-V tunneling characteristic of the IJJ of the BH19a#1 and more detailed part of this graph is shown in Figure 4.7. From the tunneling characteristics the hysteretic quasiparticle braches have been obtained. These branches can be easily counted. Each quasiparticle branches corresponds to the different IJJ within the constructed mesa. For these reason, counting these branches, the number of the IJJ can be obtained. Since the number of branches observed is equal to the number of IJJs in the mesa, such I-V curves have been interpreted as a direct evidence of the interlayer Josephson tunneling.

From the more detailed part of the I-V characteristics of the BH19a#1, 20 quasiparticle branches are identified. All of these branches can not be seen from the Figure because of continues switching of the bias. However, the separation between the all branches must be same normally. If Figure 4.7 is examined these space between the quasiparticle branches become smaller as being approached to higher bias values even unclear at the values between -1000 meV and 1000 meV. The decrease of space between the branches can be a Joule heating in the mesa. Furthermore, between the 0

meV and 50 meV the quasiparticle branches can not be seen because of degradation of single crystal surface by thin film layer.

And also the number of IJJs is determined from AFM results. The height of the single crystal into the mesa, which is 32 nm, divided by height of unit cell of intercalated Bi-2212, which is 21.3 Å, and it has been found as approximately 16 branches. This value is close to the value of IJJ number obtained from I-V curve.
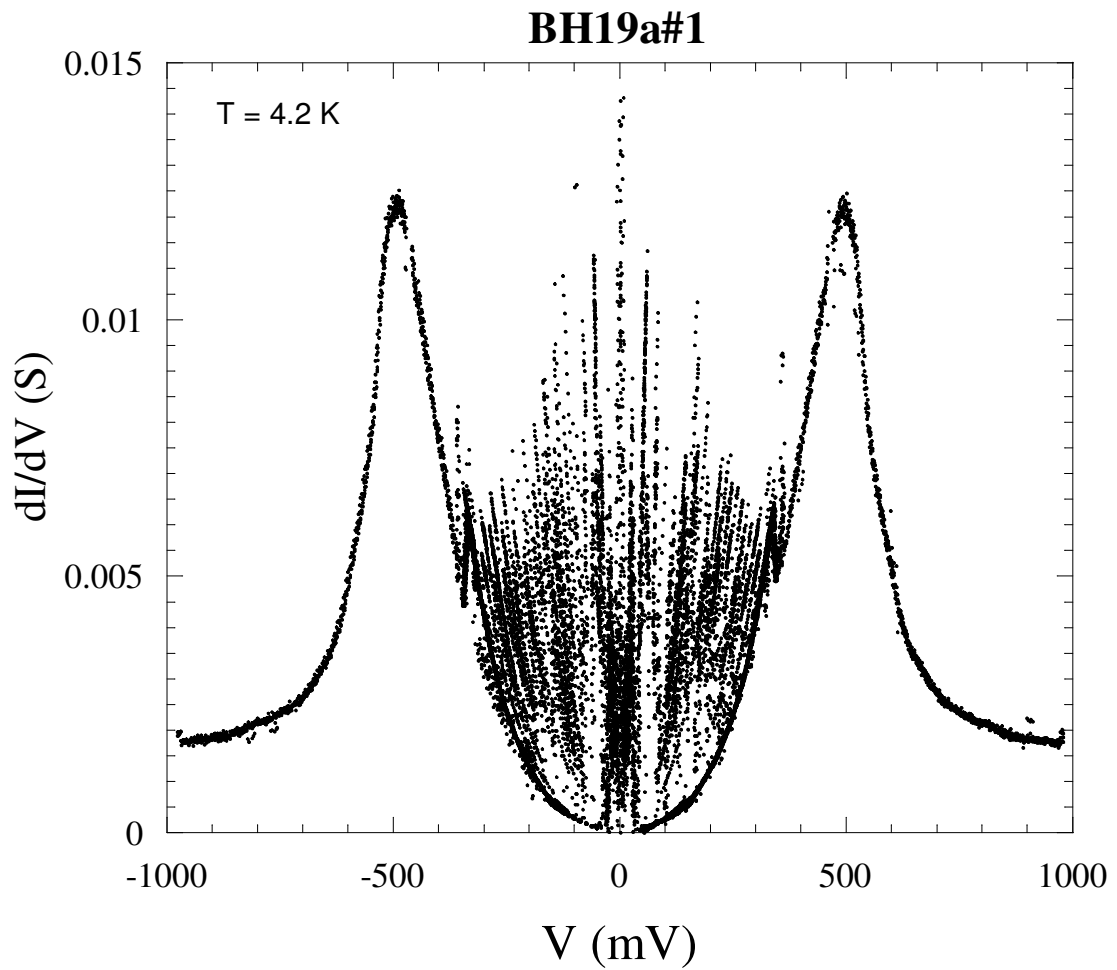
BH19a#1

Figure 4.8. The dI-dV characteristic of BH19a#1 at 4.2 K

Figure 4.8 shows the dI/dV – V characteristics of the BH19 #1. From the tunneling conductance, sharp and narrow quasiparticle peaks have been obtained at the ± 495 meV, which is equal to the total energy gap of the IJJs. So to obtain the accurate the dynamical conductance gap voltages with the accurate values, the value of the total voltage should be divided with the number of the IJJs in the mesas. After the simple calculation energy gap has been found as 12,5 meV. However, tunneling spectroscopy experiments usually give value of about 25 meV for the energy gap Δ (Wu, 2004). In our study 12.5 meV seems too small to be the energy gap. This illustrates a great suppression of the energy gap. In literature the suppression of the energy gap attributed to a quasiparticle injection nonequilibrium effect and a Joule heating. These effects originate from a high quasiparticle current density, it is difficult to distinguish the two effects and hard to say which effect is more important than the other for suppression of the energy gap.

And also Figure 4.9 shows the I-V characteristic of Bi-2212 IJJs for different mesa (BH19a#2) at 4.2 K. The characteristic properties of the branches of the mesa show the similarity with the BH19a#1. Quasiparticle branches are seen more apparently in Figure 4.10 and the separation between the all quasiparticle branches are same and equal to $2\Delta = 25$ meV which show the parallelism with the calculated value for the BH19a#1. Moreover, value of switching current is nearly same. This value is change only between 0.2 and 0.3 mA.

Magnetic field dependence of tunneling characteristic of BH19a#1, 2 has been also investigated with applied magnetic field along the c-axis. Changing the applied magnetic field from 100 G to 2000 G, the effect of magnetic field on switching current was investigated. From Figure 4.11, one can understand that the value of sumgap voltage does not change with applied magnetic field. However, when the quasiparticle branches are examined the gradual increase of switching current through the sumgap can be seen from Figure 4.12. On the other hand, without any applied magnetic field value of switching current is remain same through the sumgap. Because the fact that when we applied magnetic field along the c-axis of the crystal, magnetic field penetrates from the edge of several layers of top of the mesa so critical current decrease in these layers. At the bottom of the mesa magnetic field can not penetrate from the layers whilst value of the critical current must be larger.
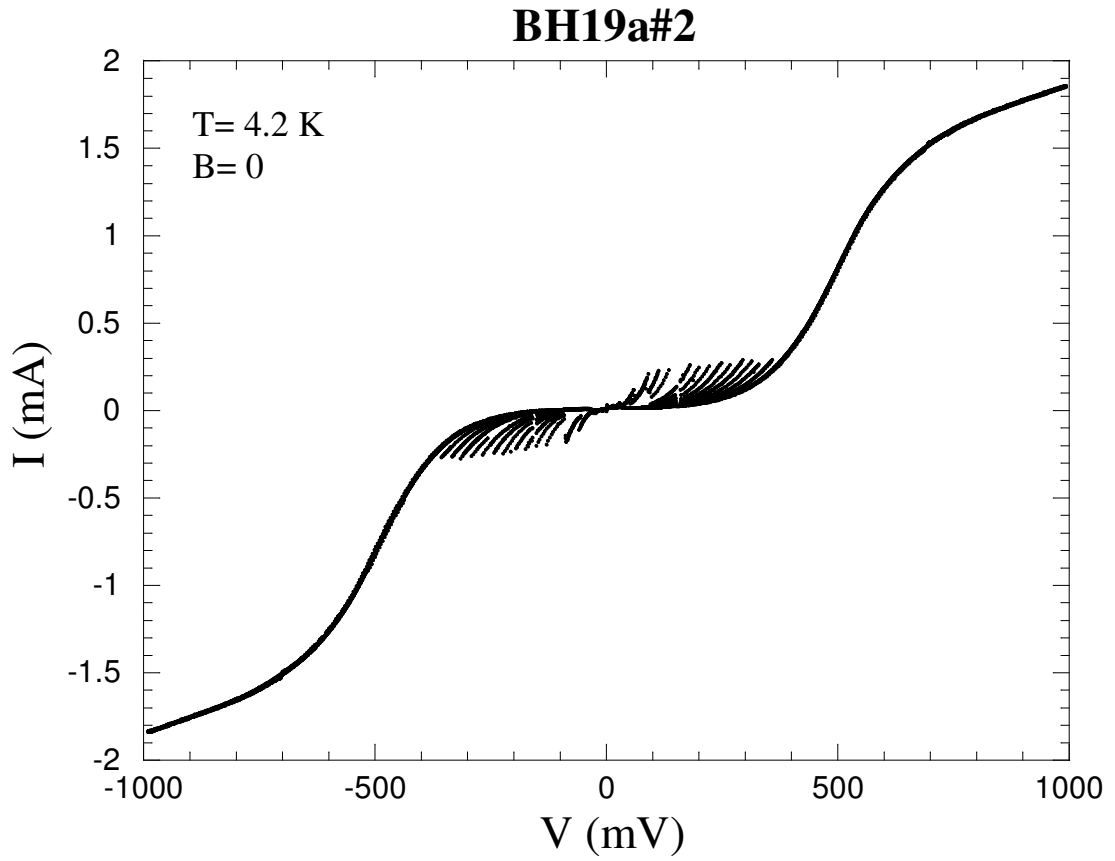
BH19a#2

Figure 4.9. The I-V characteristic of BH19a#2 at 4.2 K and B= 0 G
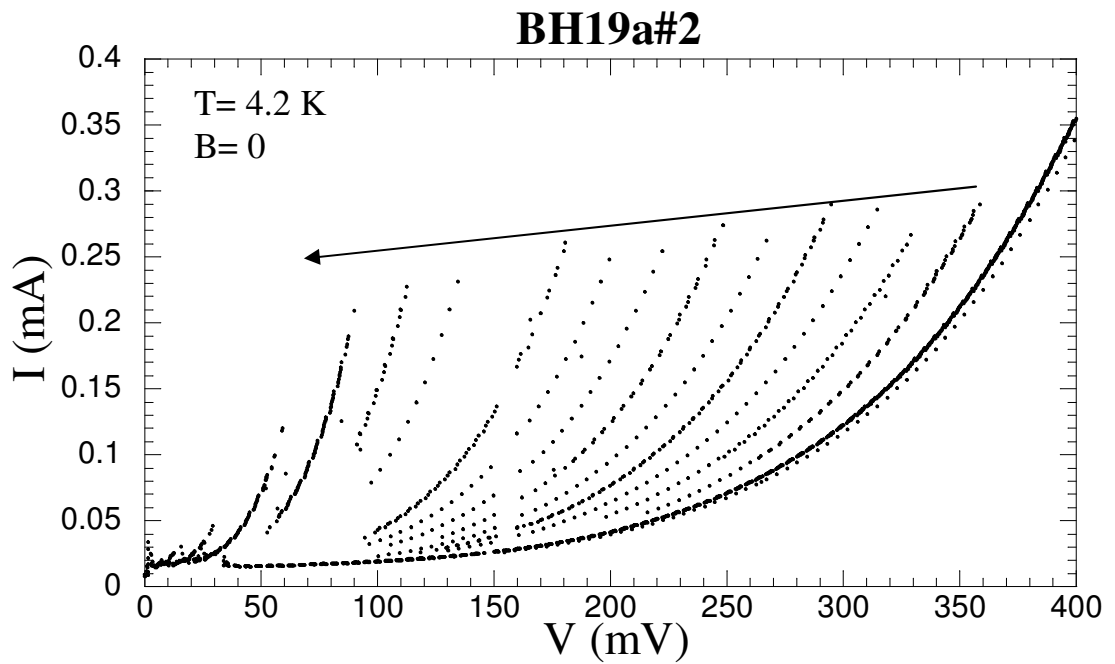
BH19a#2

Figure 4.10. The I-V characteristic of BH19a#2 at 4.2 K and B= 0 in detail
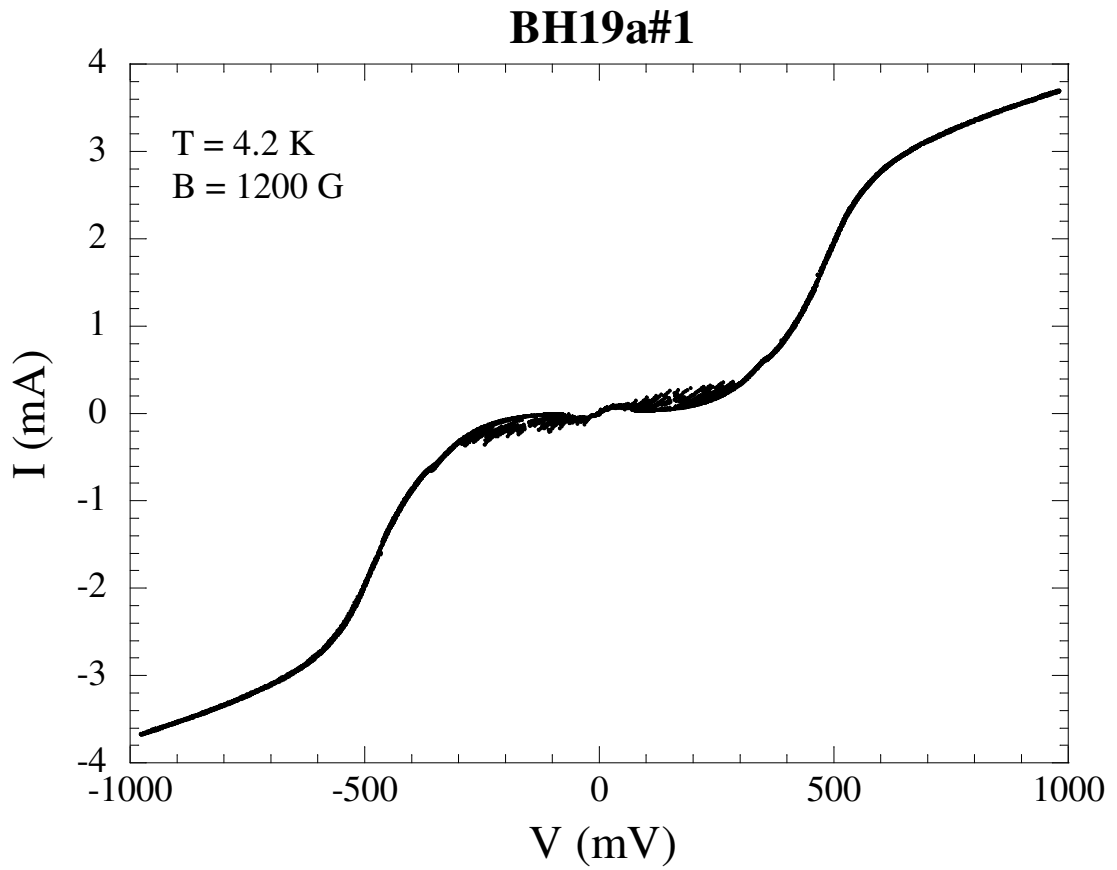
Figure 4.11. The I-V characteristic of BH19a#1 at 4.2 K and B= 1200 G
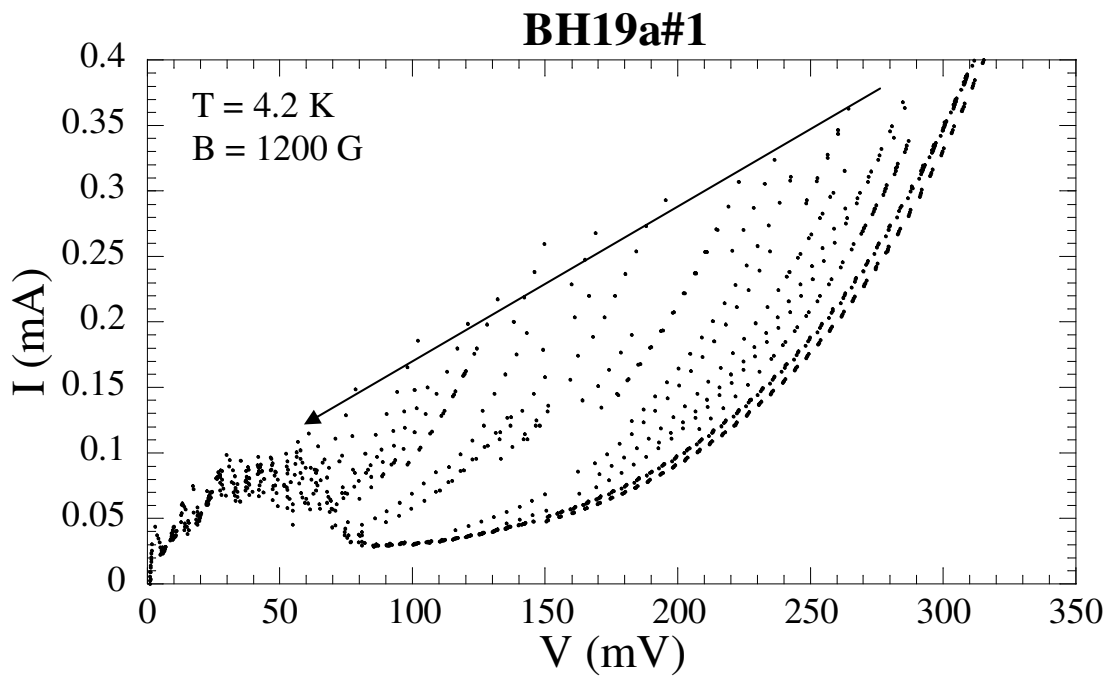
Figure 4.12. The I-V characteristic of BH19a#2 at 4.2 K and B=1200 G in detail
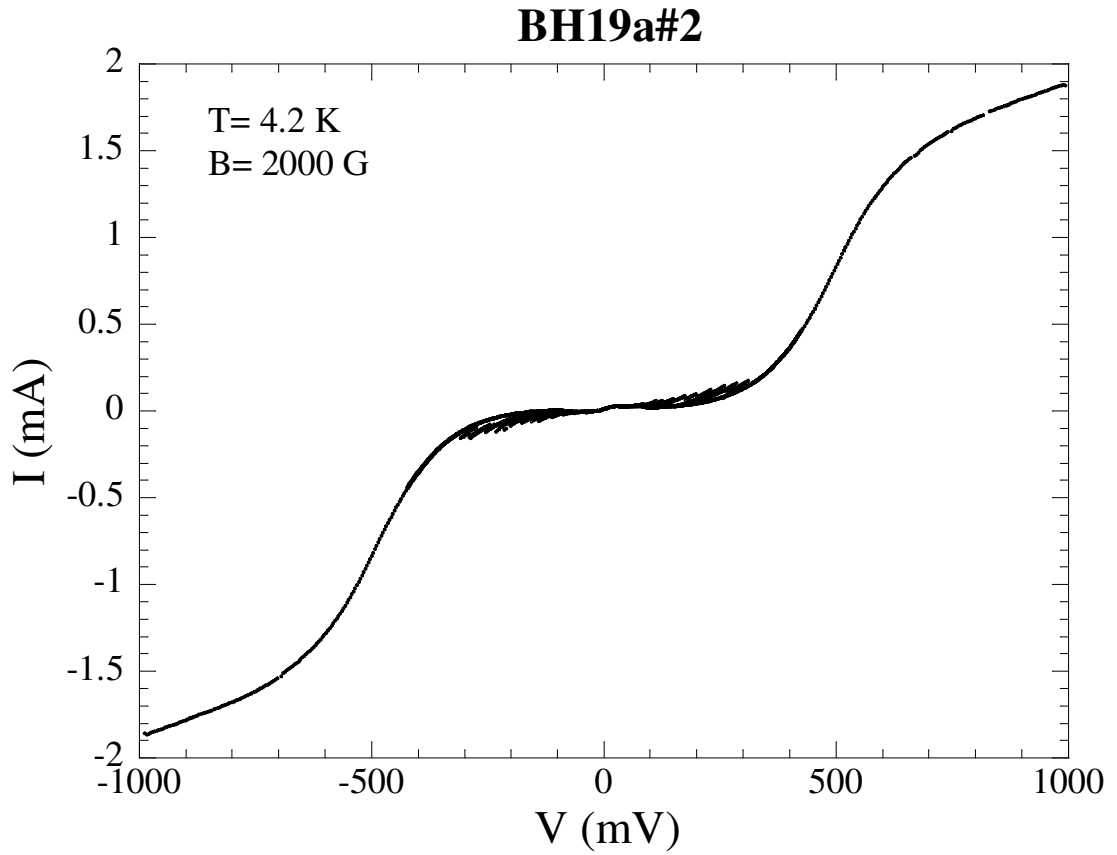
BH19a#2

T= 4.2 K
B= 2000 G

Figure 4.13. The I-V characteristic of BH19a#1 at 4.2 K and B= 2000 G
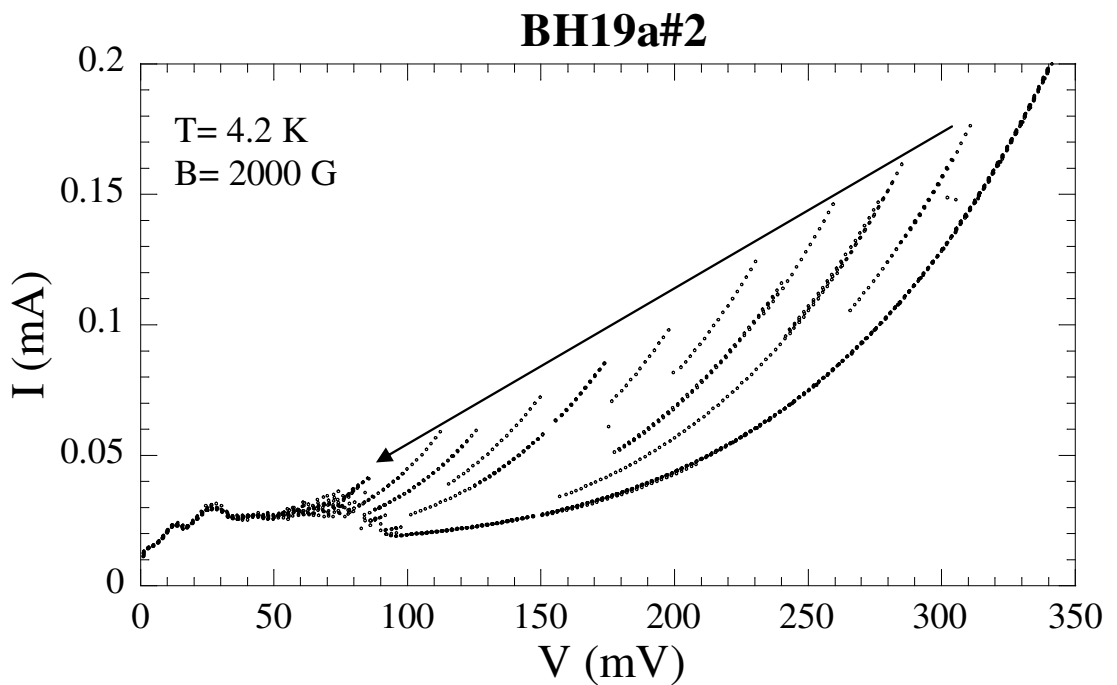
BH19a#2

T= 4.2 K
B= 2000 G

Figure 4.14. The I-V characteristic of BH19a#2 at 4.2 K and B= 2000 G in detail

BH19a#1

T= 4.2 K

I (mA) 100G
I (mA) 200G
I (mA) 300G
I (mA) 400G
I (mA) 600G
I (mA) 800G
I (mA) 1000G
I (mA) 1200G
I (mA) 1600G
I (mA) 2000G
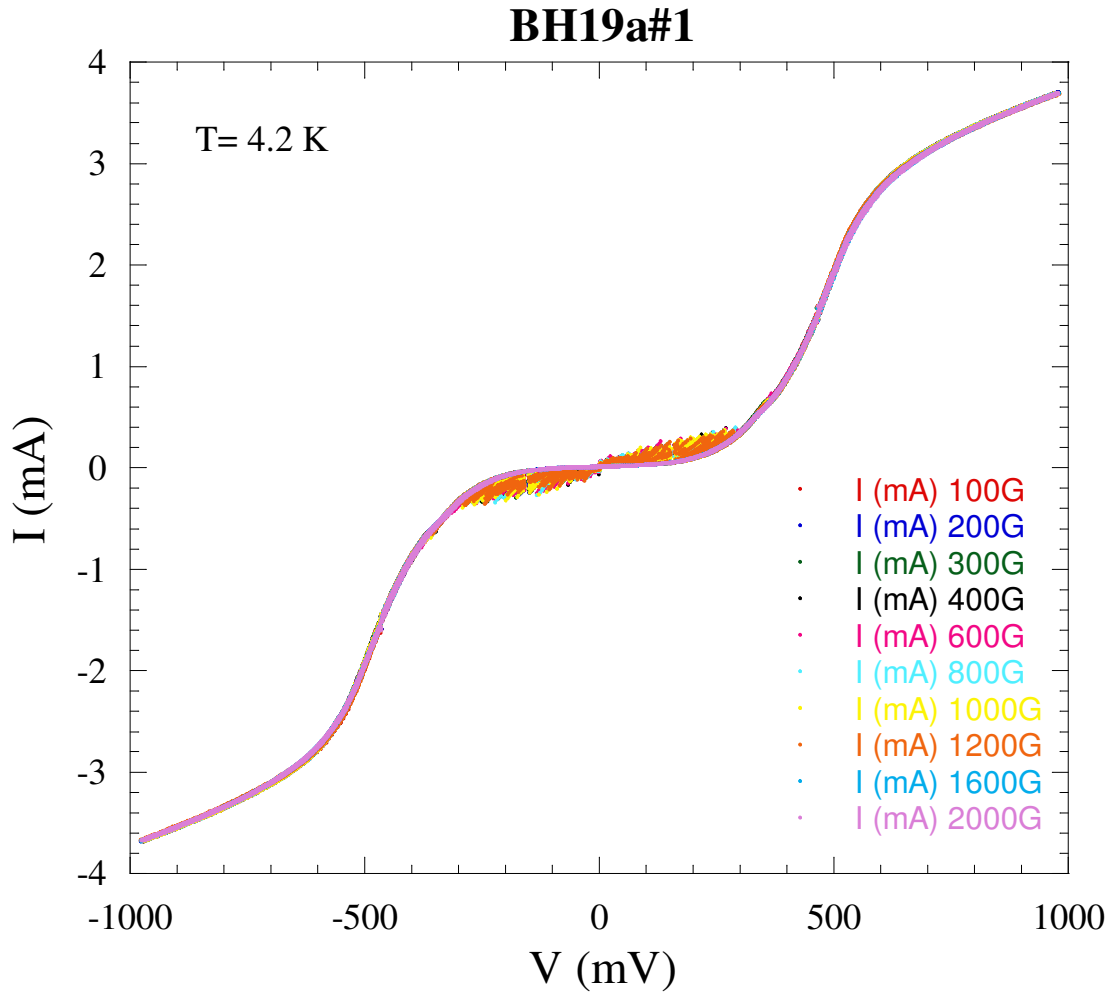
Figure 4.15. Magnetic field dependence of I-V characteristic of BH19a#1

Figure from 4.15 to 4.18 illustrate the tunneling characteristics in various magnetic fields at 4.2 K. Figure 4.15 shows the magnetic field dependencies of the I-V curves of the BH19a#1 for the field increasing stepwise up to 2000 G ,which much lower than the upper critical field of the material. The switching current of the quasiparticle branches exhibits a gradual distribution. Value of the switching current decrease with increasing magnetic field because when the magnitude of the magnetic field increased, more magnetic field penetrate to the crystal so critical current is more reduced in relevant layers. Indeed, we can not see any quasiparticle branch above the 1200 G and only return branches are observed.
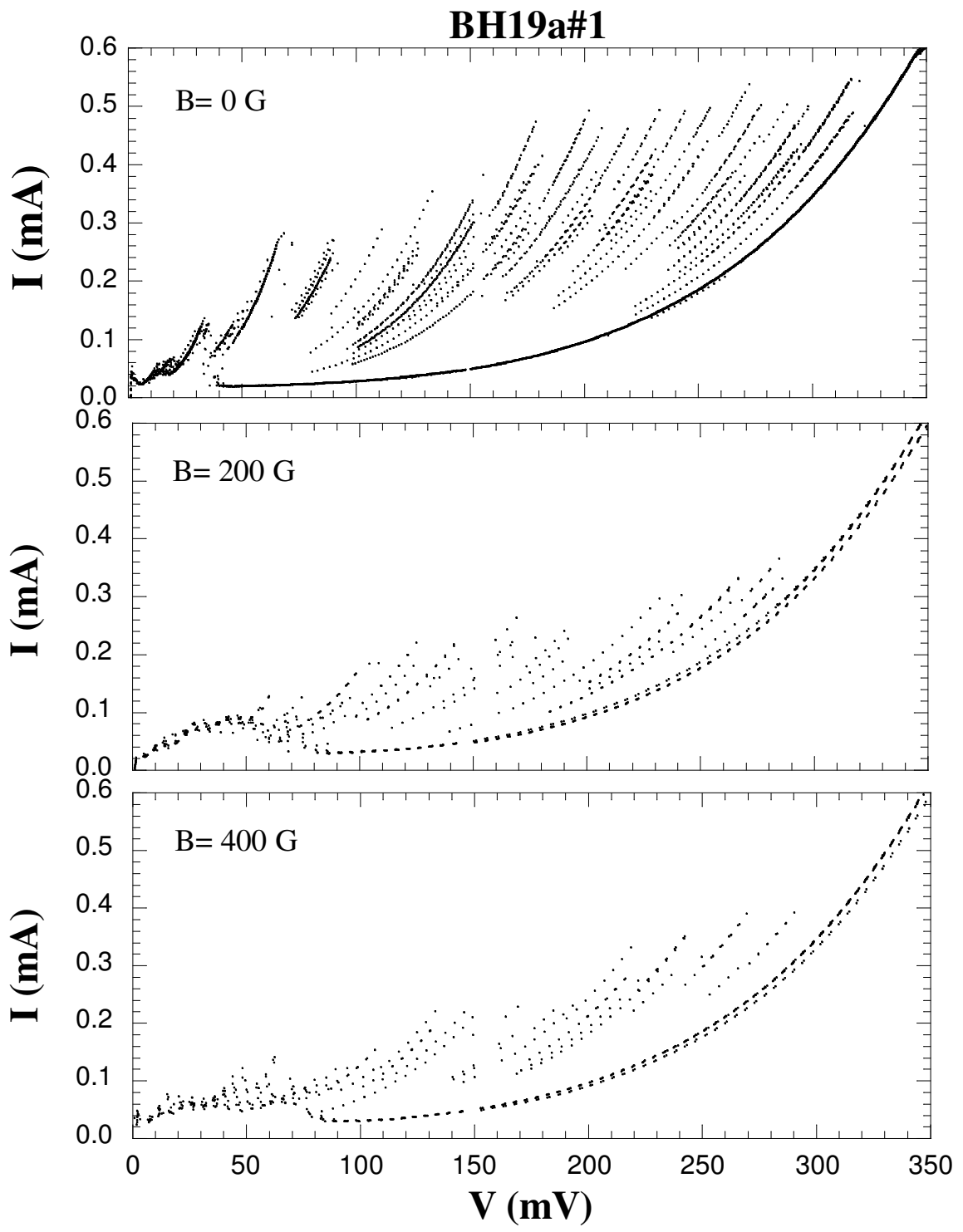
BH19a#1

Figure 4.16 Magnetic field dependence of I-V characteristic of BH19a#1 in detail at
0 G, 200 G and 400 G respectively
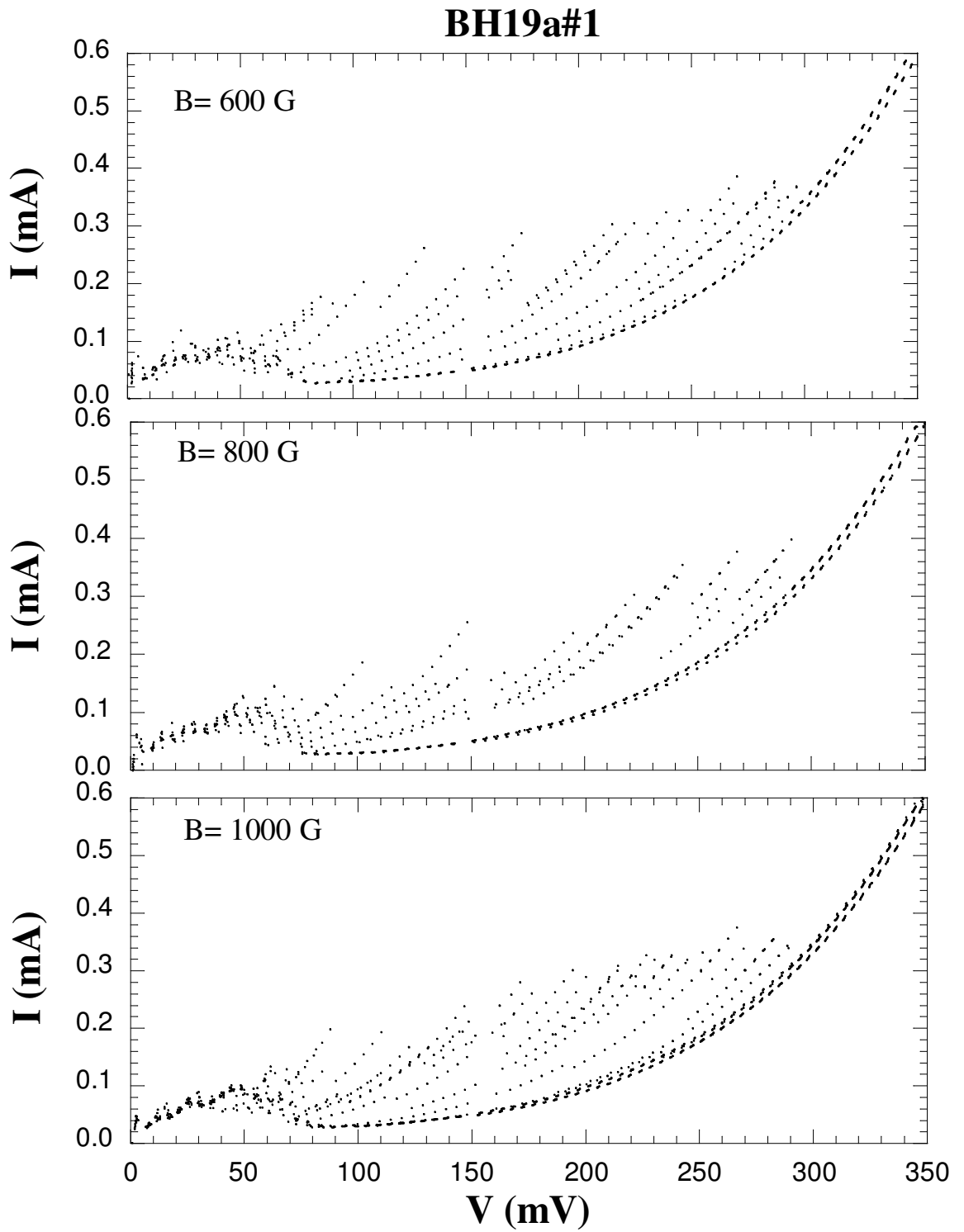
BH19a#1

Figure 4.17 Magnetic field dependence of I-V characteristic of BH19a#1 in detail at
600 G, 800 G and 1000 G respectively
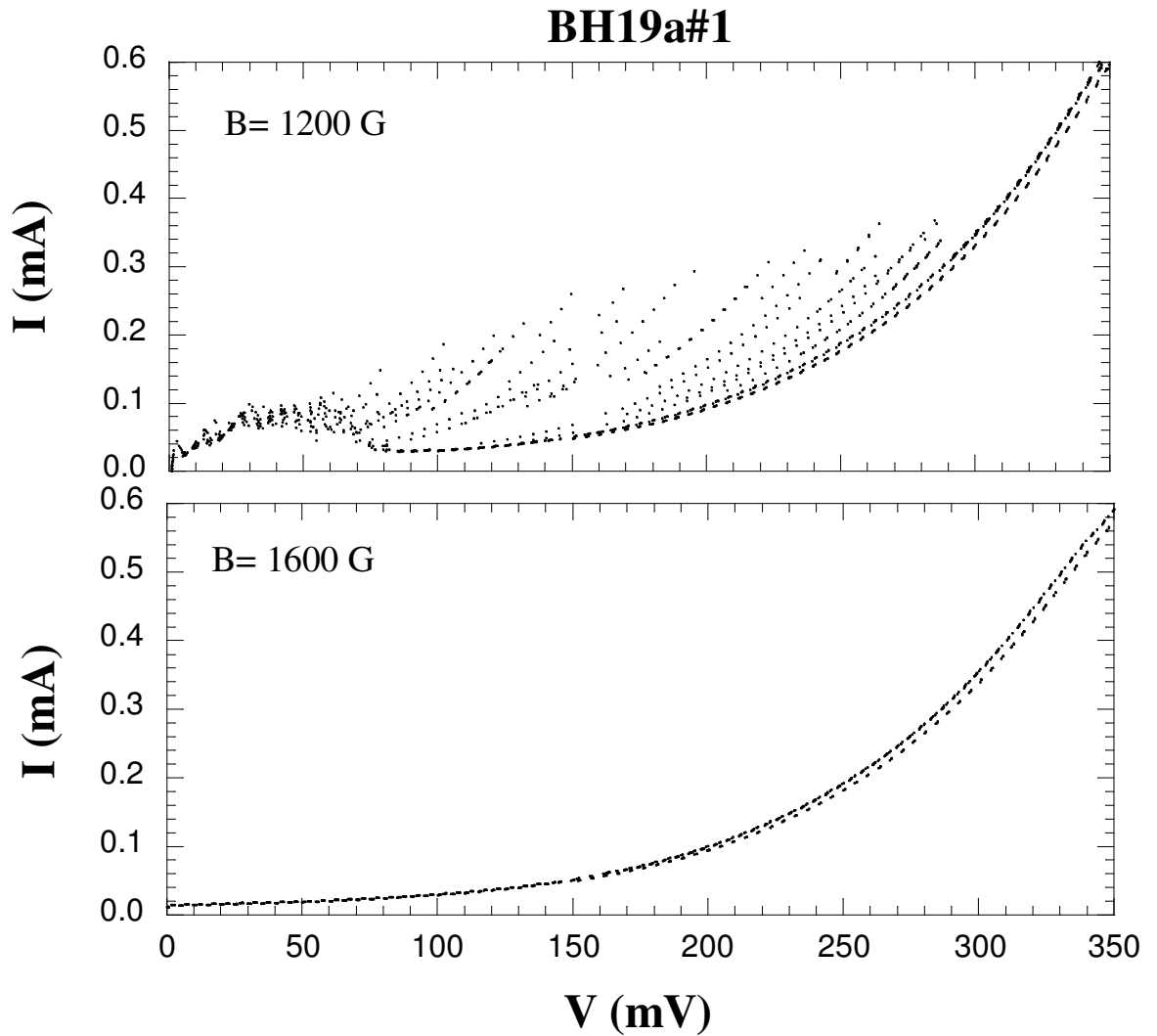
BH19a#1

Figure 4.18 Magnetic field dependence of I-V characteristic of BH19a#1 in detail at
1200 G and 1600 G respectively

And also, from Figure 4.16 to 4.18 magnetic field dependence of switching current can be seen in more detail. Moreover, in these figures the first several branches can not be seen up to 50 meV, presumably first layers just underneath Au film are not cleaved properly or inhomogeneous intercalation of the crystal may cause such kind of effect.
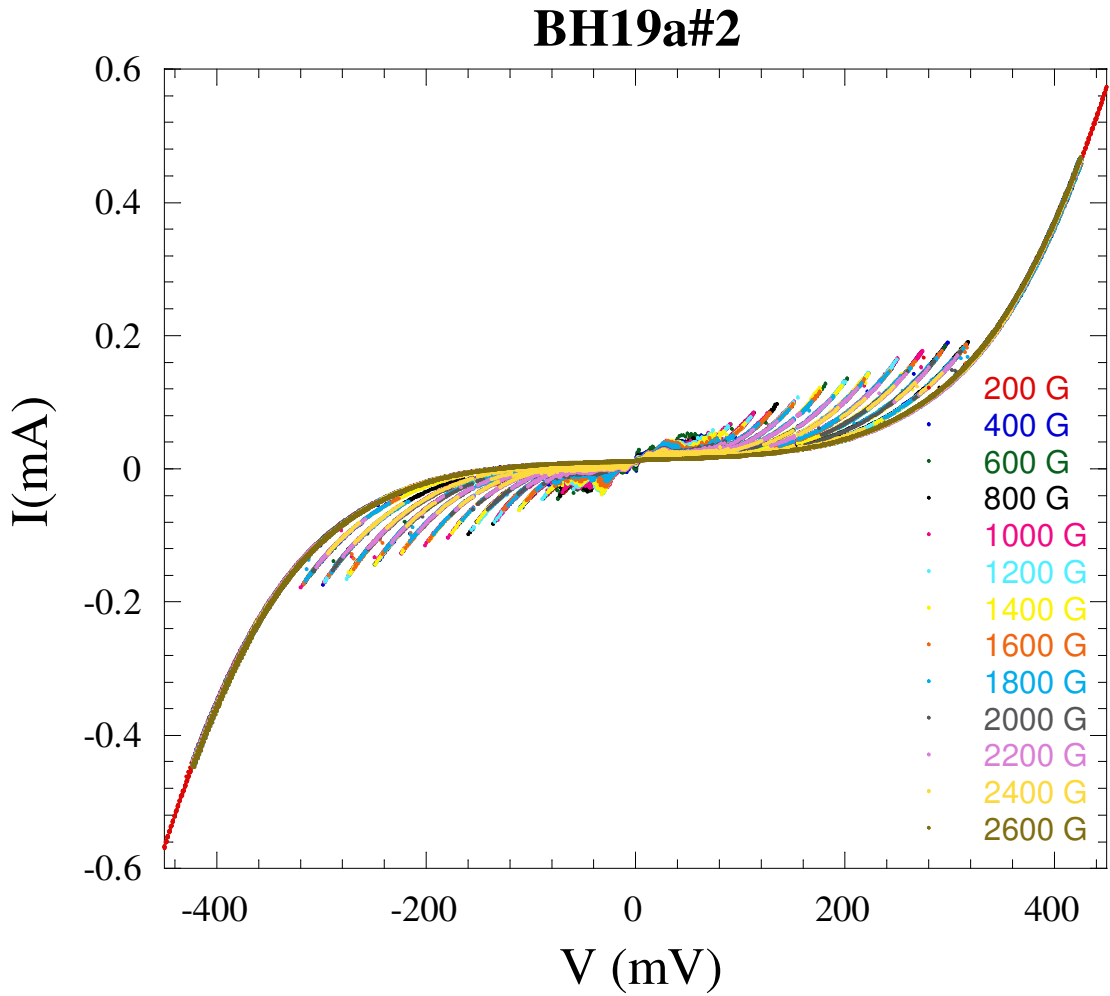
BH19a#2

Figure 4.19. Magnetic field dependence of I-V characteristic of BH19a#2

Figure 4.19 shows the magnetic field dependence of the other mesa BH19#2 at 4.2 K. This mesa also has the same properties with the BH19#1. On the other hand, the quasiparticle branches of BH19#2 totally diminish at 2400 G while that of BH19#1 diminish at 1600 G. The deference is because of various mesa. Data were taken from different mesa. During the photolithography because of inhomogeneous etching process, thickness of the mesas can be different so the number of IJJs is different. However, inhomogeneous intercalation might cause such kind of effect.
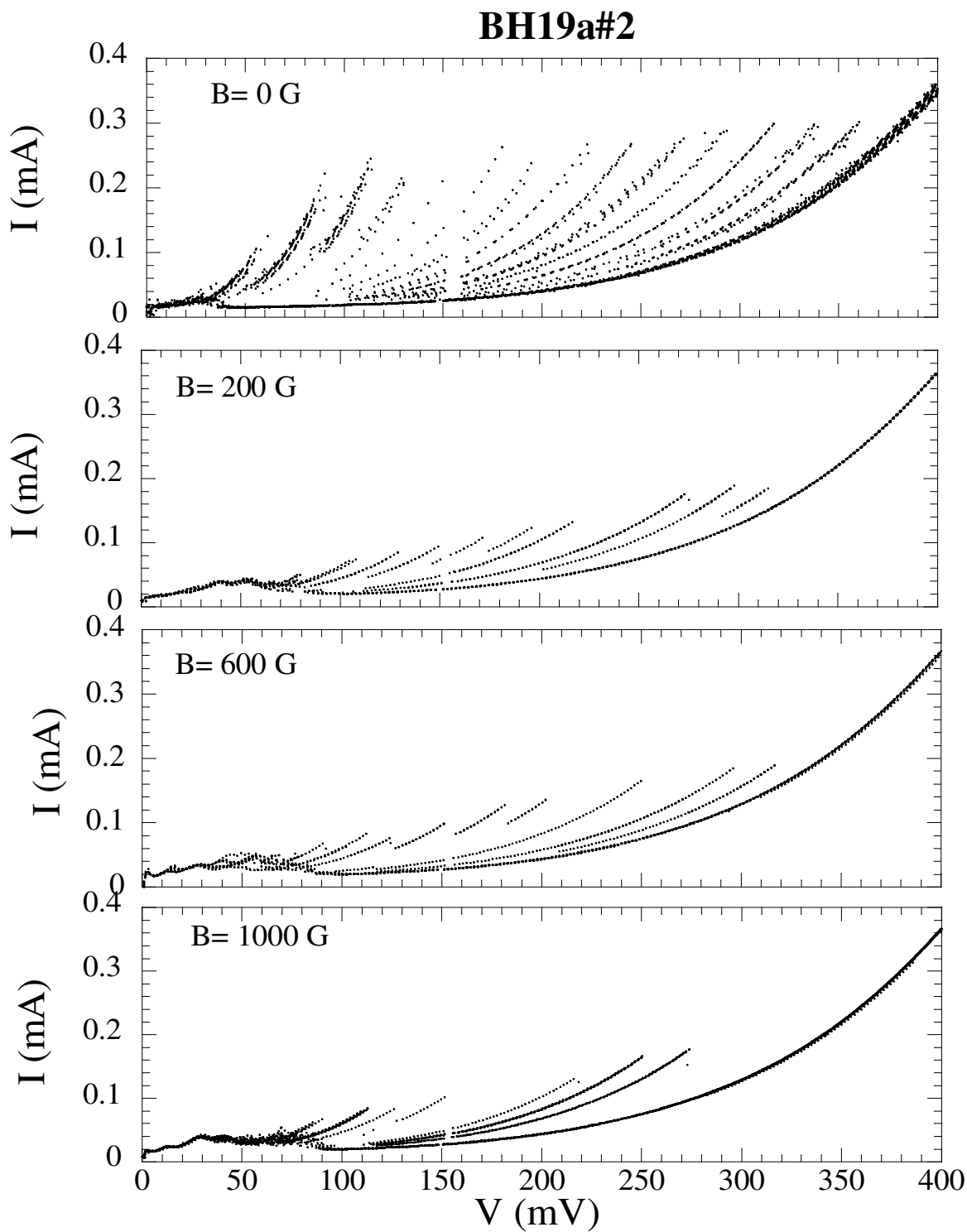
BH19a#2

Figure 4.20 Magnetic field dependence of I-V characteristic of BH19a#1 in detail at
0 G, 200 G, 600 G and 1000 G respectively
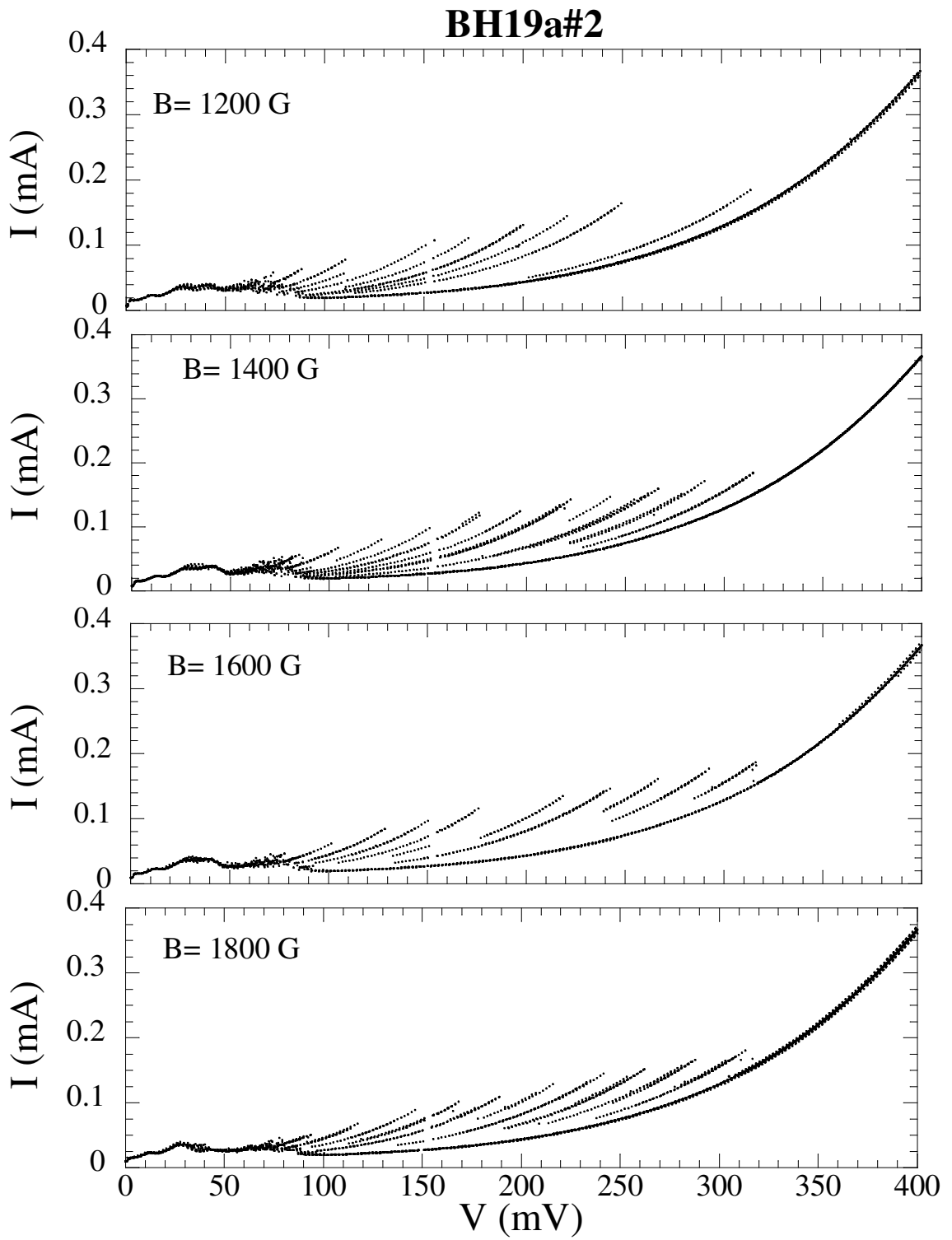
BH19a#2

Figure 4.21 Magnetic field dependence of I-V characteristic of BH19a#1 in detail at
1200 G, 1400 G, 1600 G and 1800 G respectively
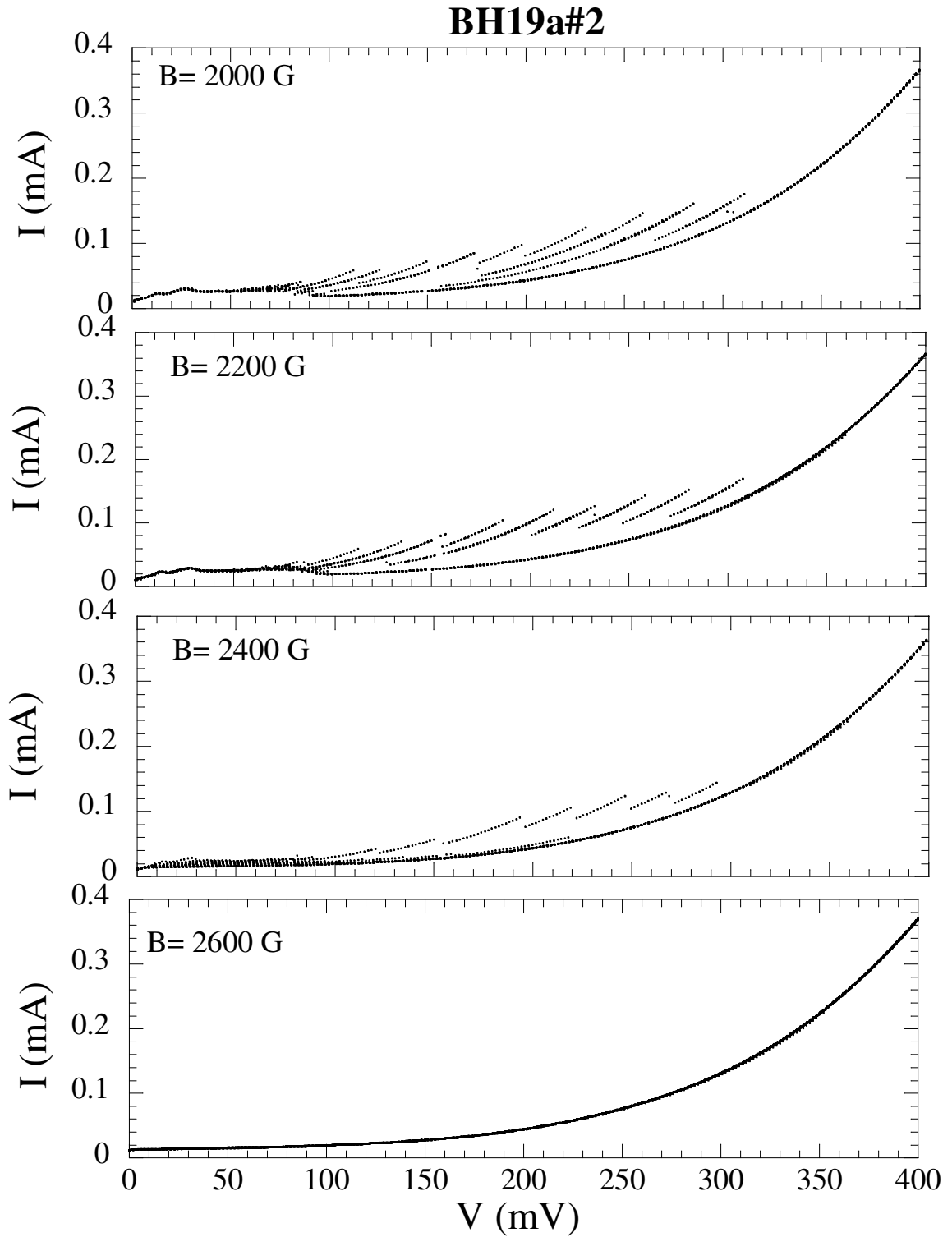
BH19a#2


Figure 4.22 Magnetic field dependence of I-V characteristic of BH19a#1 in detail at 2000 G, 2200 G, 2400 G and 2600 G respectively
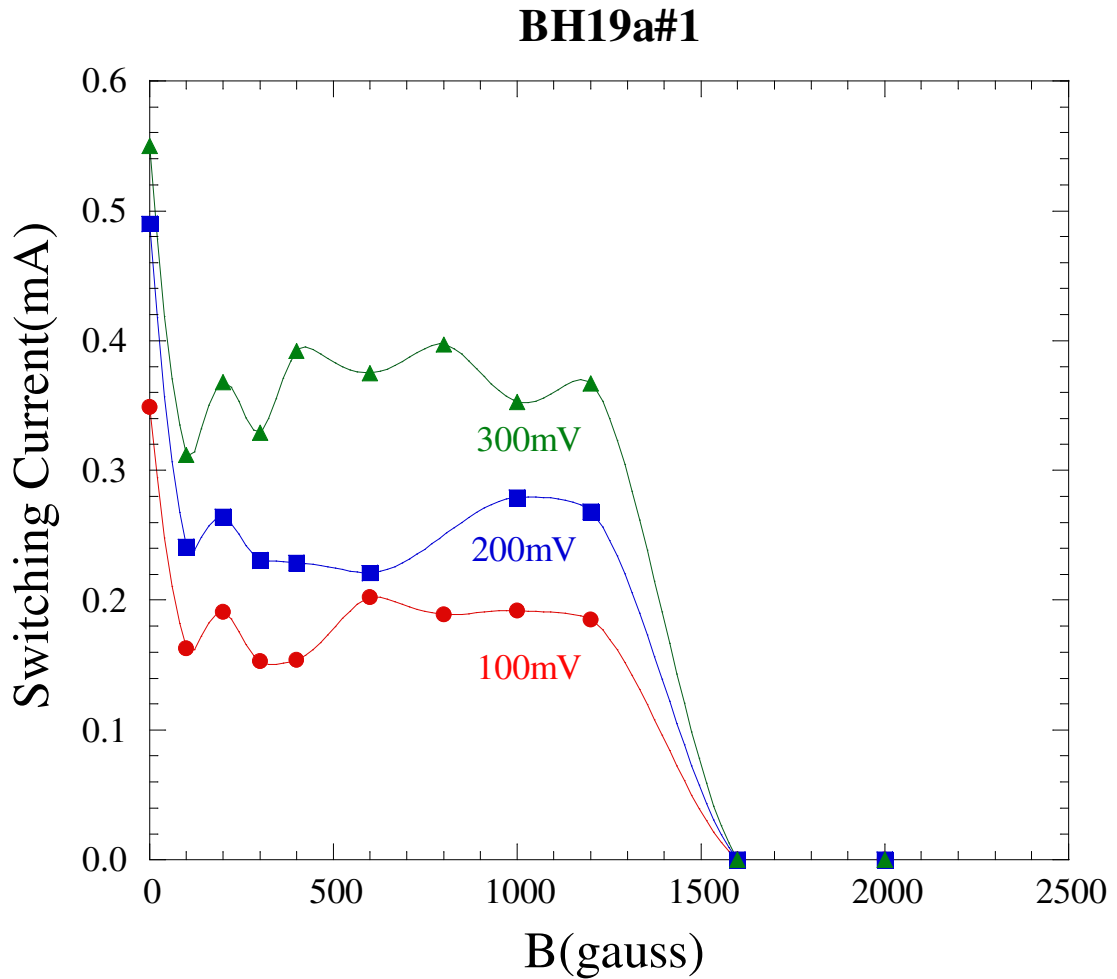
BH19a#1

Figure 4.23. Magnetic field dependence of critical Josephson current for spin degenerate current to BH19a#1

Figure 4.23. exhibits magnetic field dependence of critical Josephson current for spin-degenerate current to BH19a#1. The switching current increase with applied votage. On the other hand, the switching current is nearly constant while the applied magnetic field increase up to 1600 G. When the magnetic field reach to the 1600 G, switching current suddenly decrease. Becase after this value magnetic field totally penetrates into the superconductor.
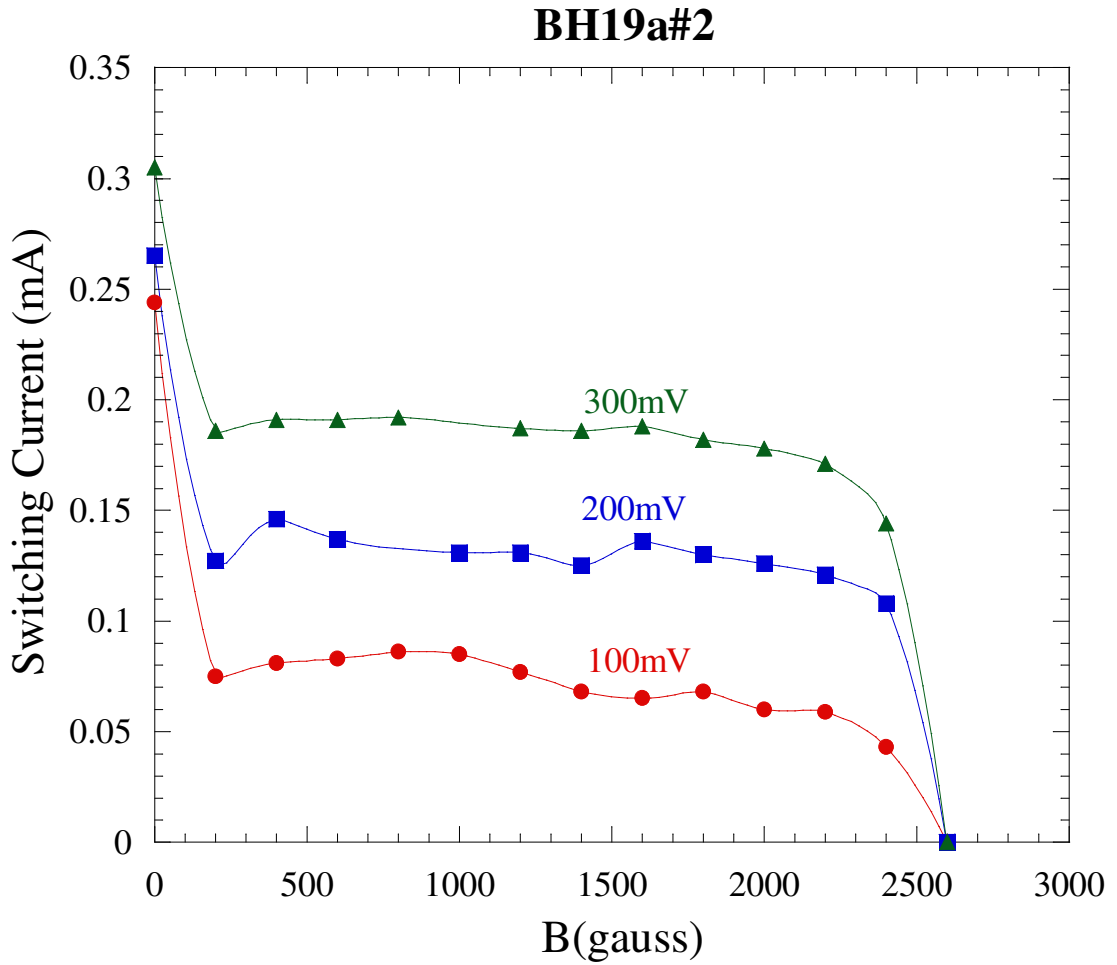
Figure 4.24. Magnetic field dependence of critical Josephson current for spin degenerate current to BH19a#2

Figure 4.24 shows magnetic field dependence of critical Josephson current for spin-degenerate current to other mesa BH19a#2. The properties of this mesa also shows the parallelism with the other mesas.

4.3.2. Tunneling Characteristics of Mesa with Cobalt Top Layer

Tunneling experiments were performed on $HgBr_2$ intercalated sample with Co top layer. Data were obtained from 3 different mesas using PCT technique.

Figure 4.25 exhibits I-V characteristic of MMc#1 mesa. And also Figure 4.26 show the more detailed part of Figure 4.25. As it can be seen, the quasiparticle branches are fairly clear, which provides to count them and to determine the number of branches with a great accuracy. The quasiparticle branches were traced out by sweeping the bias up and down repeatedly (not all the branches were traced out). The I-V curves exhibit approximately 24 resistive quasiparticle branches, the number of which coincides with the estimated mesa thickness of 73 nm divided by the spacing between neighboring CuO_2 layers 21.3 Å. After the simple calculation branches number found as 34 branches. This indicates that whilst doing PCT measurements, all the problems related to heating were virtually minimized, which can be the most important indication of intercalation. If we examine the I-V characteristics more detail, the sharp current jumps can be seen at ± 1100 meV, which determine the location of the quasiparticle peaks in the tunneling conductance graph. And also this value is corresponds to total energy gap of the IJJs in the mesa. To find the individual energy gap of each junction obtained total energy gap value, 1100 meV as shown in Figure 4.27, divided by 24 and found as $2\Delta = 45$ and the value of energy gap is around the 23 meV. This value is coincides with the literature.

From the Figure 4.26 it can be seen that there is a gradual increase of quasiparticle branches through the sumgap. These differences can be associated with spin polarized tunneling into a superconductor or magnetic field generated by the ferromagnetic material Co. On the other hand, the amount of the spin polarization into a high temperature superconductor is not known because spin injection technique utilizes the excellent lattice match for epitaxial film growth of the FIS junction. However, Cobalt is not epitaxialy grown on Au. It is reasonable to think that decrease of switching current can be self magnetic field of Co film.
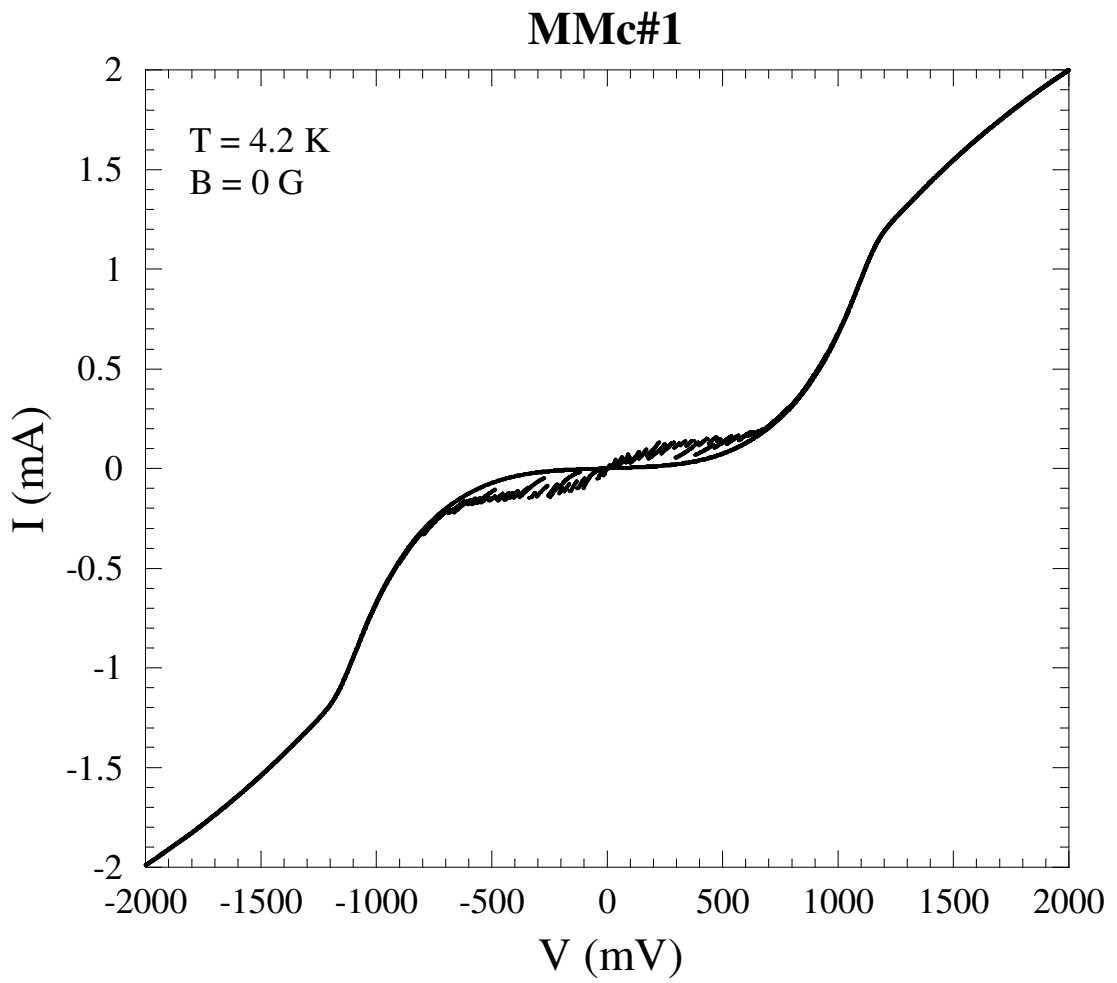
MMc#1

Figure 4.25. I-V characteristics of MMc#1 mesa at 4.2 K without any applied magnetic field

MMc#1

T = 4.2 K
B = 0 G

I (mA)

V (mV)
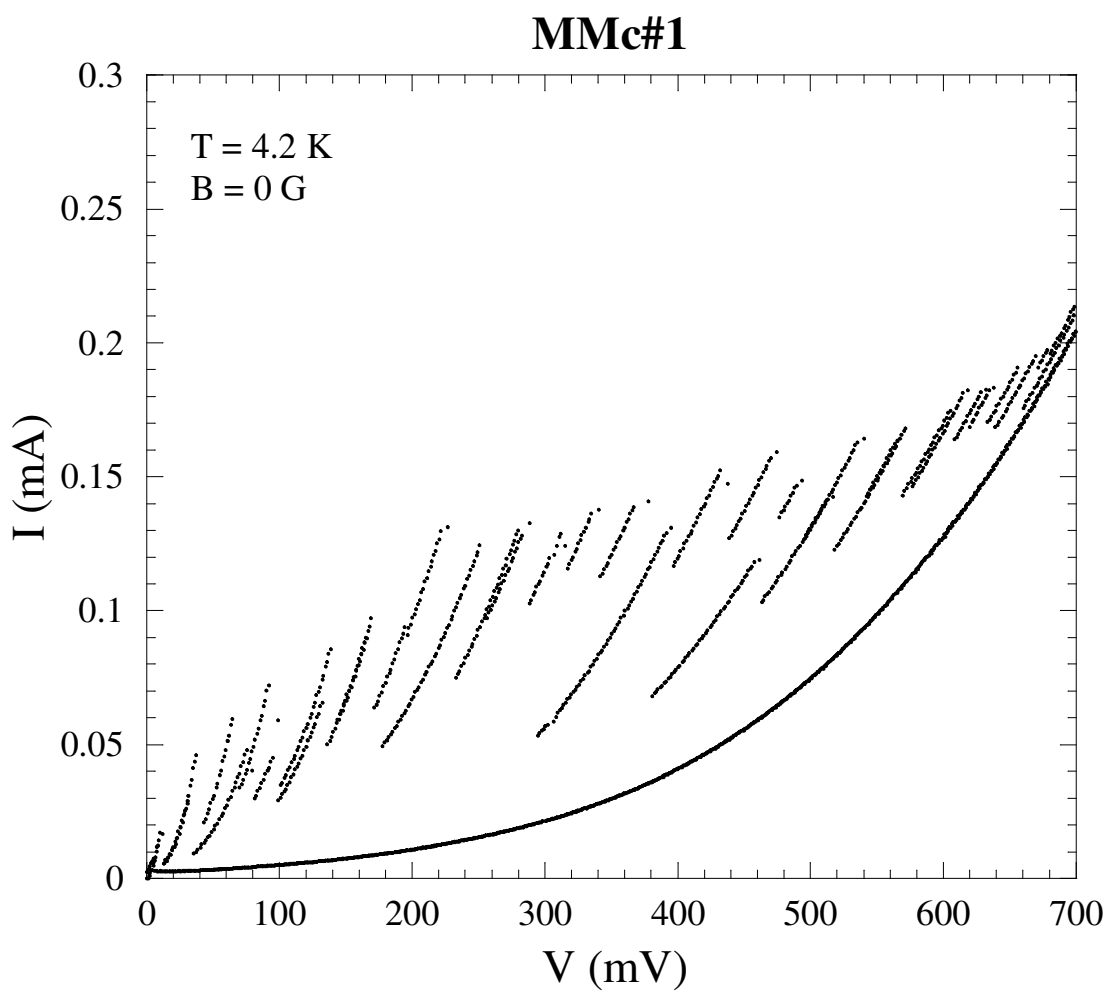
Figure 4.26. I-V characteristics of MMc#1 mesa at 4.2 K without any applied magnetic
field in detail

MMc#1
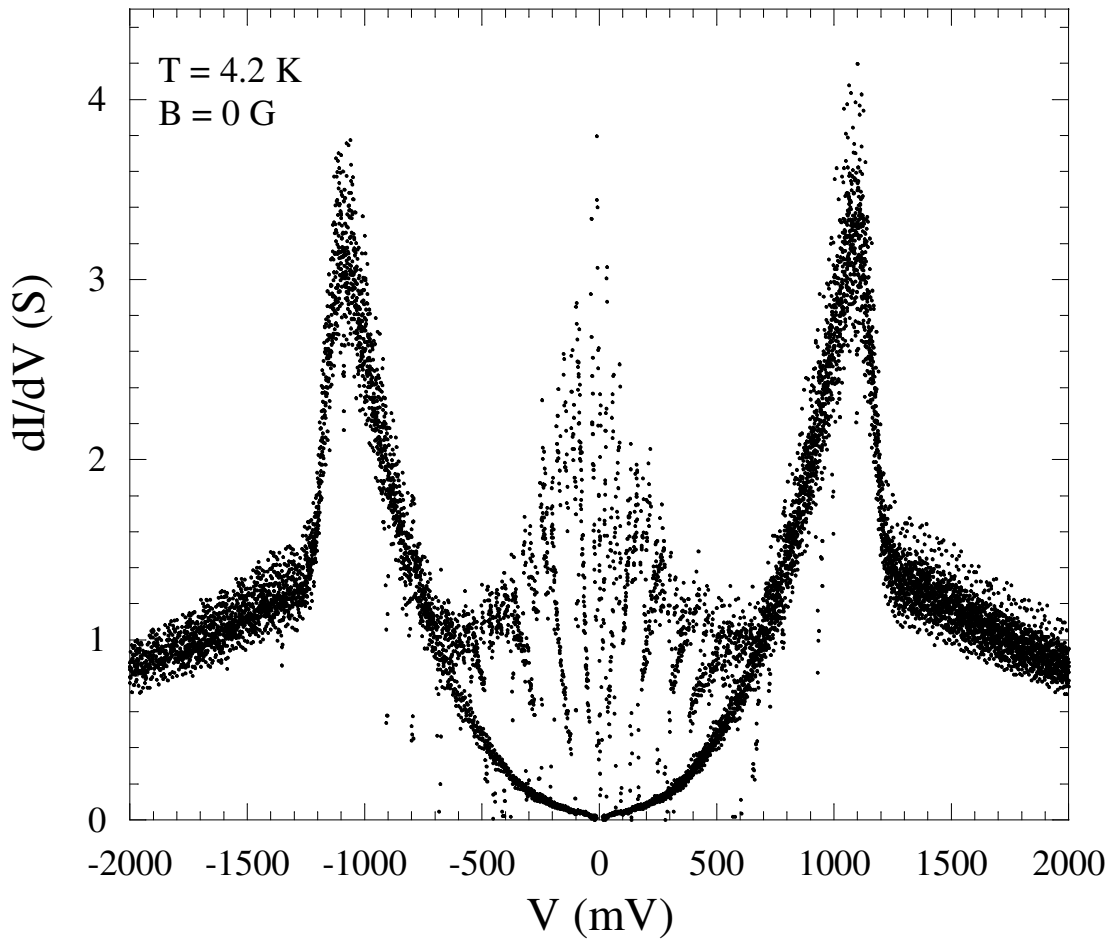
Figure 4.27. dI/dV-V characteristics of MMc#1 mesa at 4.2 K without any applied magnetic field
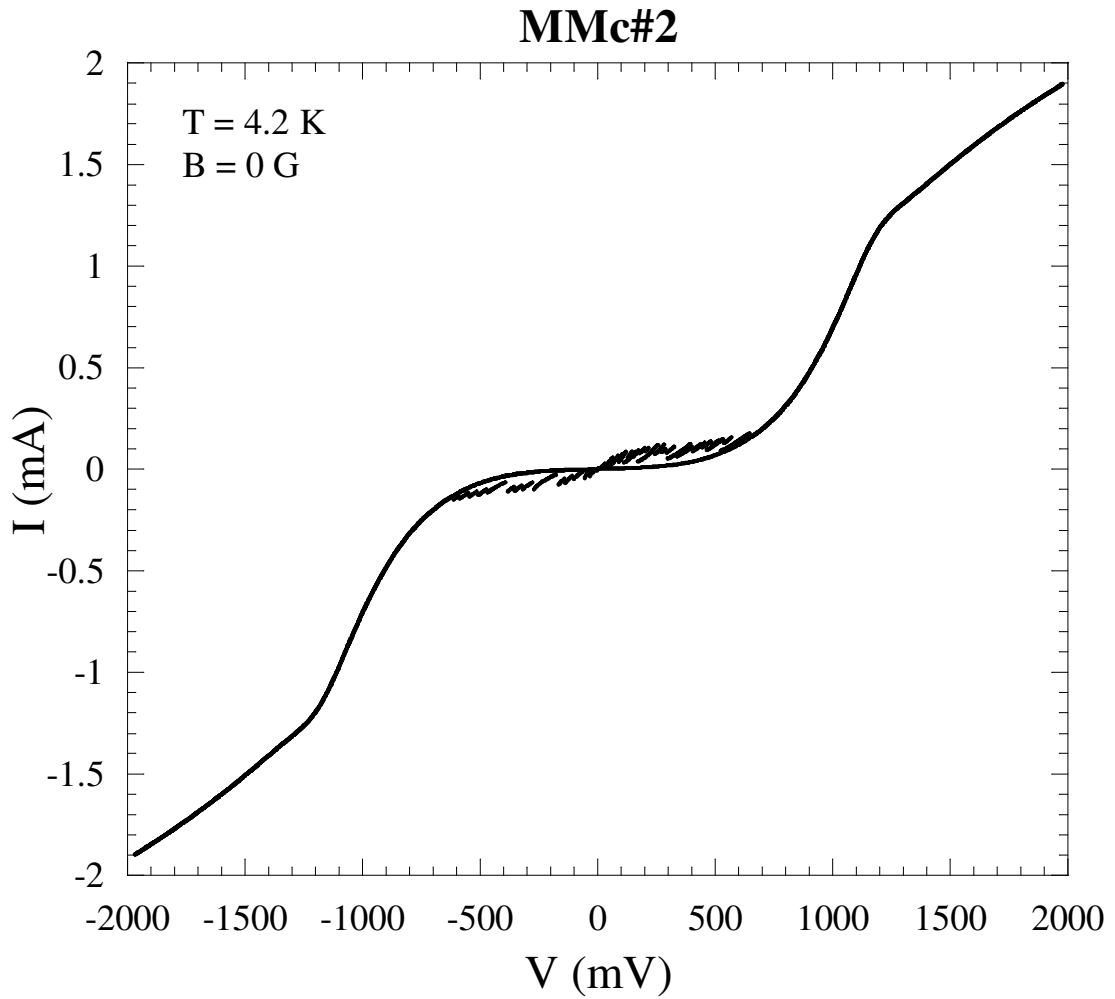
Figure 4.28. I-V characteristics of MMc#2 mesa at 4.2 K without any applied magnetic field

Figure 4.28 shows the I-V characteristic of the different mesa called as MMc#2. 22 quasiparticle branches were obtained from the I-V curve and this value is very close to number of IJJ obtained from the MMc#1. This result indicate that the homogeneous etching process was carried out during the experiment. And the other tunneling properties show the similar behavior as observed from the MMc#2 and also MMc#3 in Figure 4.30 and 4.31.
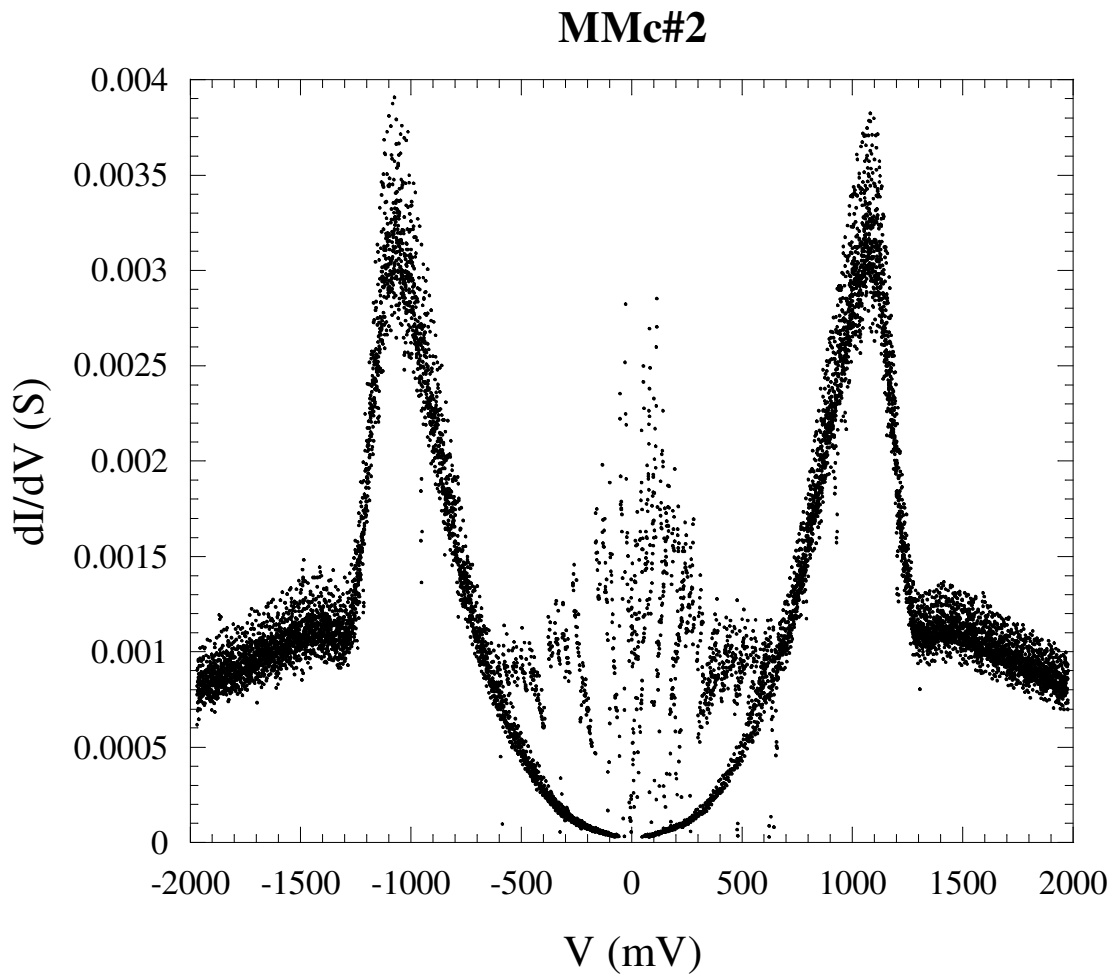
MMc#2

Figure 4.29. dI/dV-V characteristics of MMc#2 mesa at 4.2 K without any applied magnetic field

From Figure 4.29 we can obtained the dip and hump features at ± 1300 meV and at ± 1450 meV respectively. These are the indication of less heating because in the experiment intercalate Bi-2212 single crystal was used.
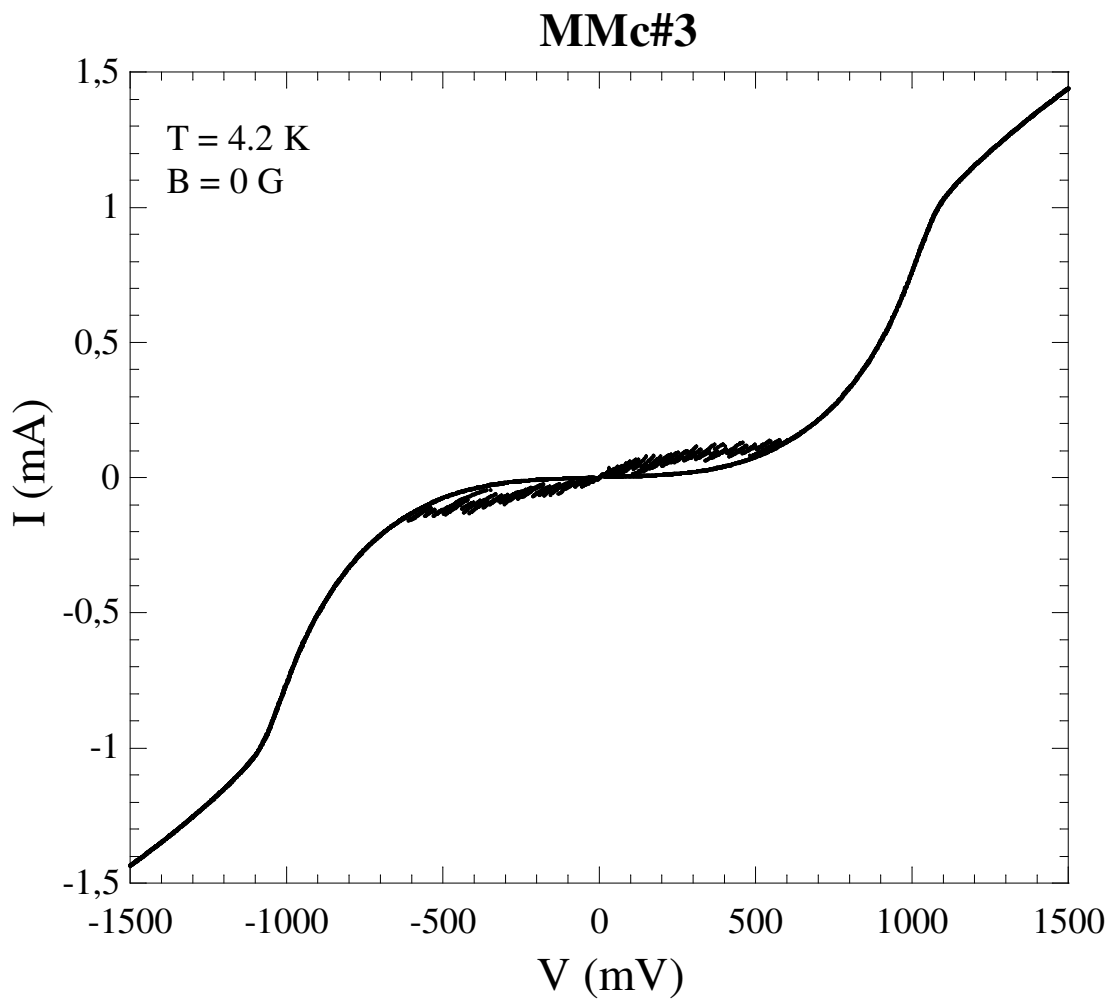
MMc#3

T = 4.2 K
B = 0 G

Figure 4.30. I-V characteristics of MMc#3 mesa at 4.2 K without any applied magnetic field

MMc#3
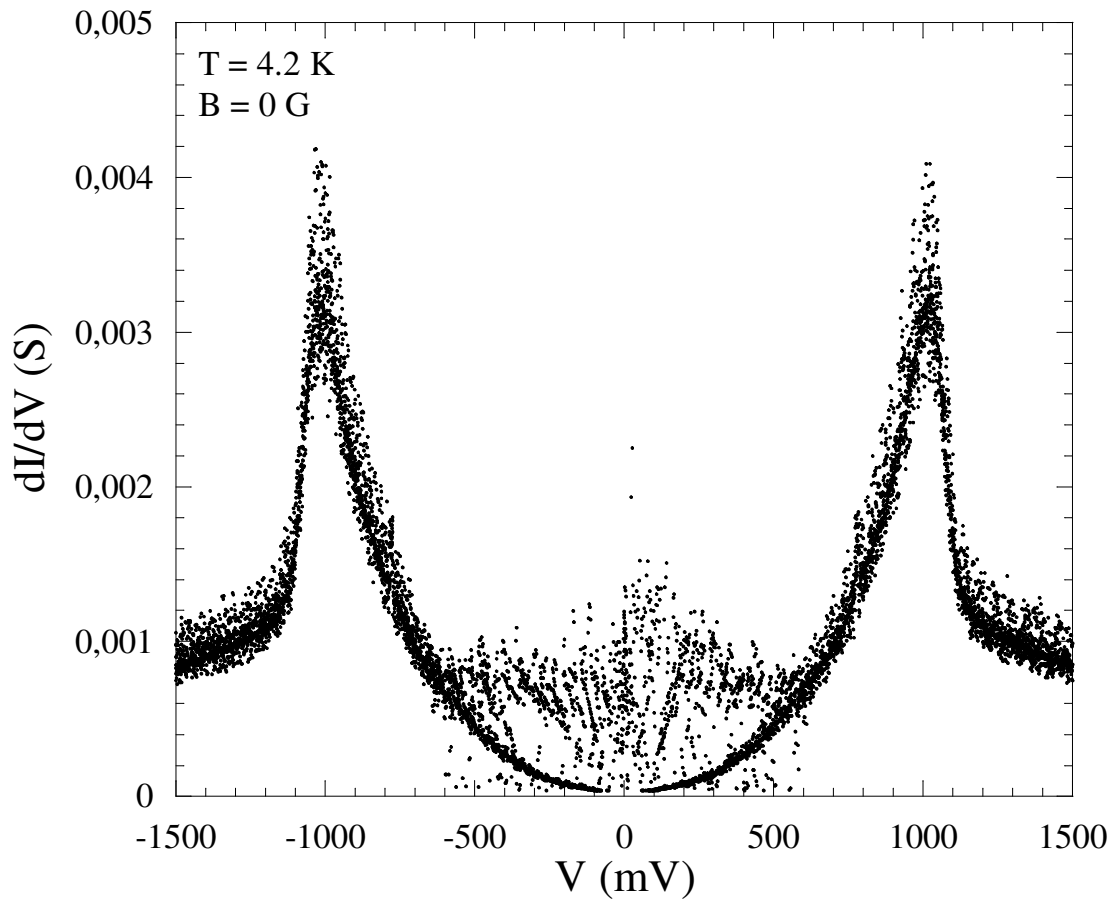

Figure 4.31. dI/dV-V characteristics of MMc#3 mesa at 4.2 K without any applied magnetic field
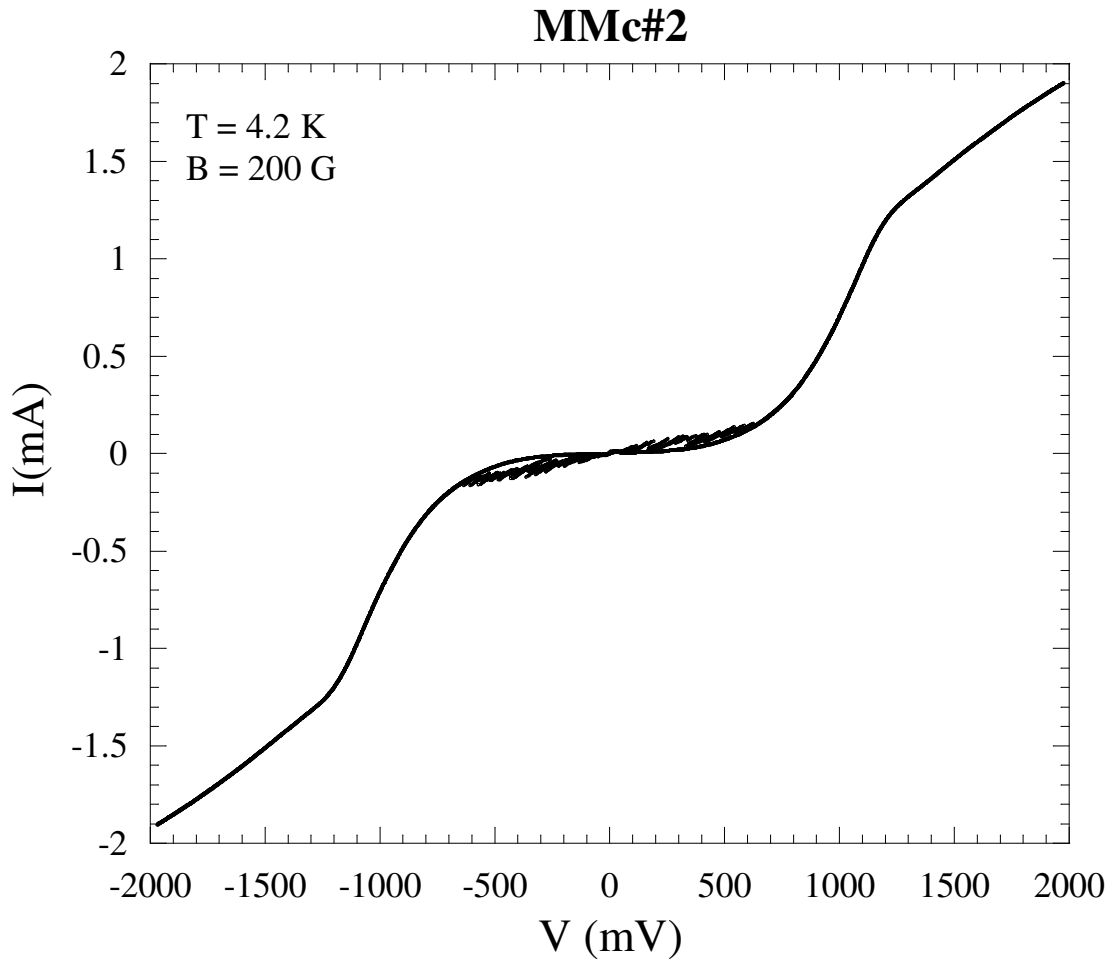
Figure 4.32. I-V characteristics of MMc#2 mesa

After the I-V characteristics were investigated without any applied magnetic, I-V characteristics were obtained with increasing magnetic field up to 1100 G. Figure 4.32 shows the magnetic field dependence I-V characteristic of the MMc#2. Firstly, one can understand sumgap voltage does not change with the applied magnetic field. Moreover, the gradual increase of the switching current through the sumgap can be seen in Figure 4.33 in detail. The gradual distribution of critical currents is either due to spin polarized current or self field of ferromagnetic Co layer. The spins might penetrate through the mesa and scattering might decrease the degree of polarization. Injected spin polarized quasiparticles through the multilayer top layer to the IJJ stack begin to loose their direction memory, when they reach to some CuO_2 planes far away from

ferromagnetic layer. These effects are also obtained from the other mesa MMc#3 as seen in Figure 4.34 and 4.35.

MMc#2

T = 4.2 K
B = 200 G
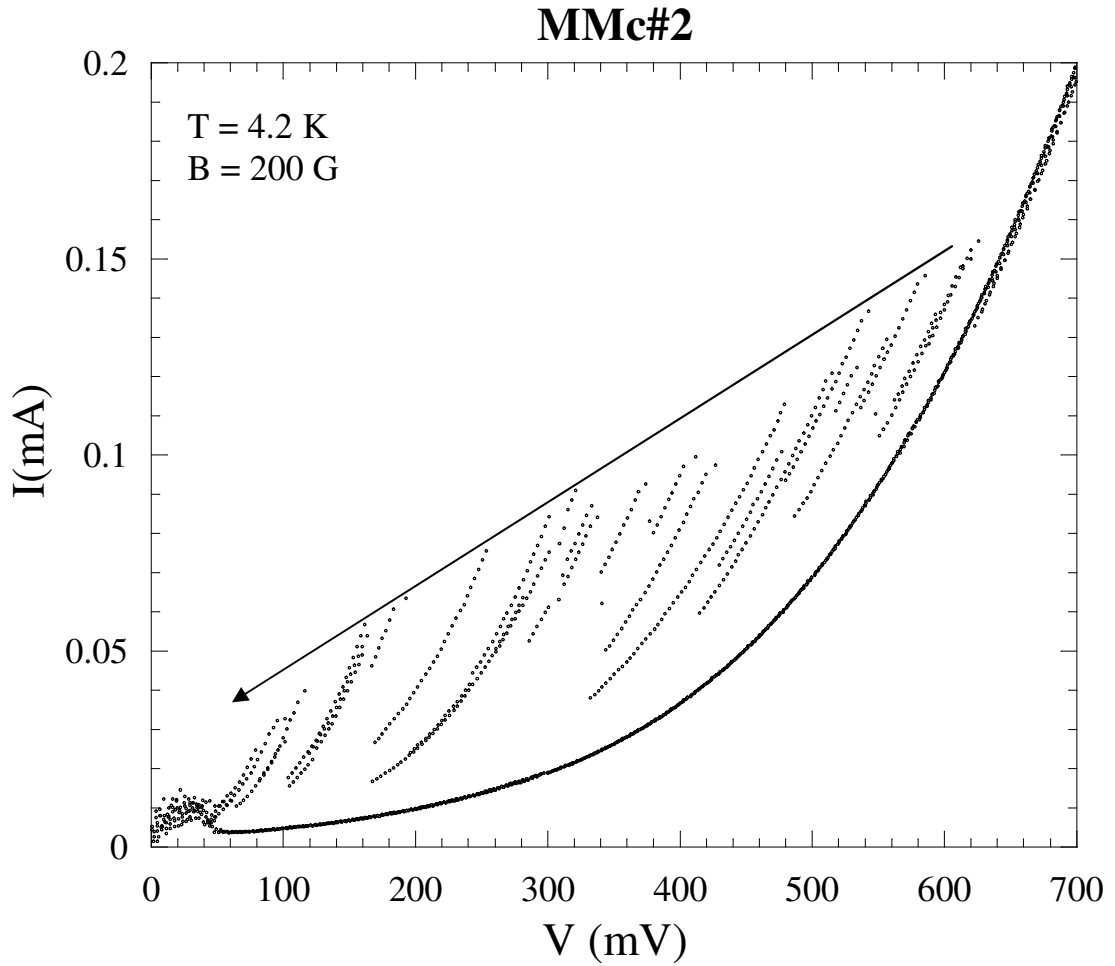
Figure 4.33. I-V characteristics of MMc#2 mesa in detail
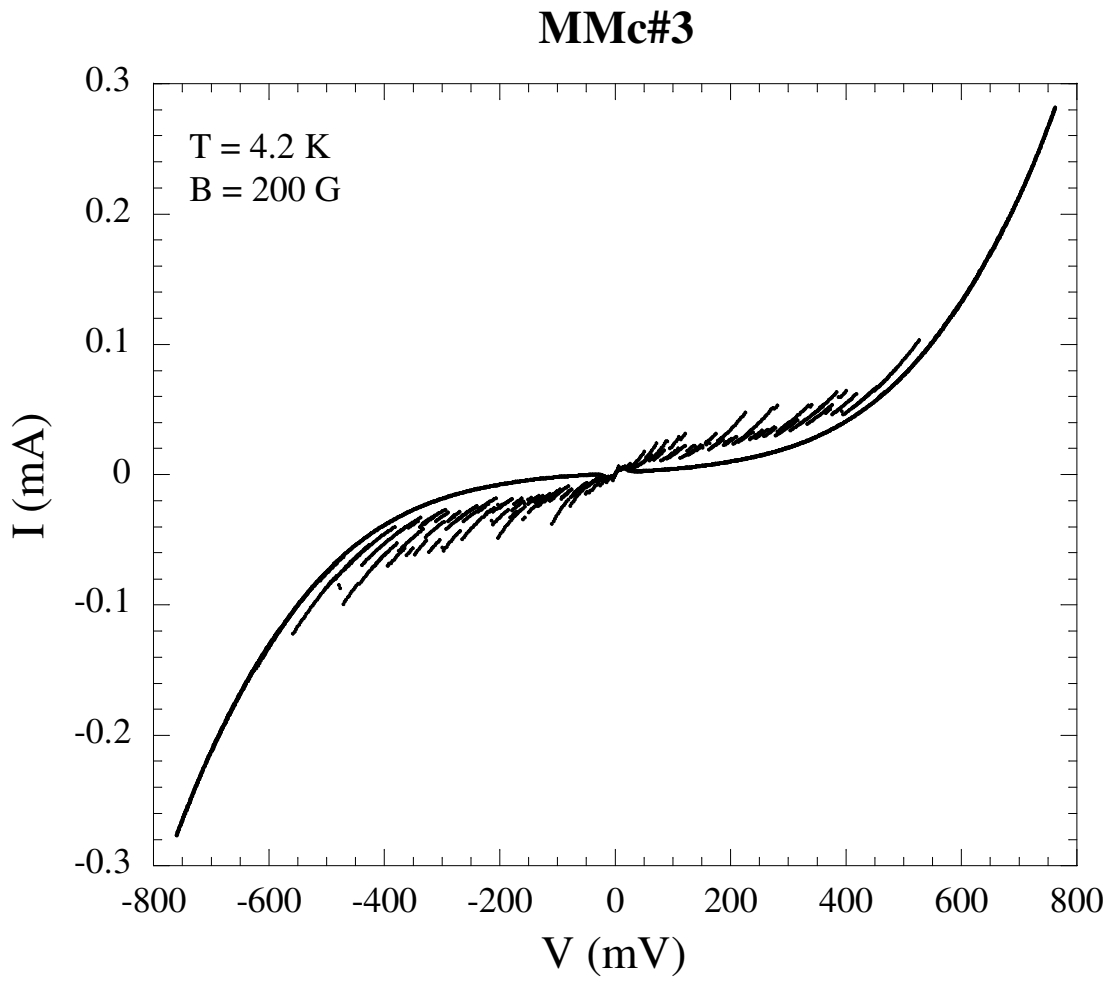
MMc#3

Figure 4.34. I-V characteristics of MMc#3 mesa
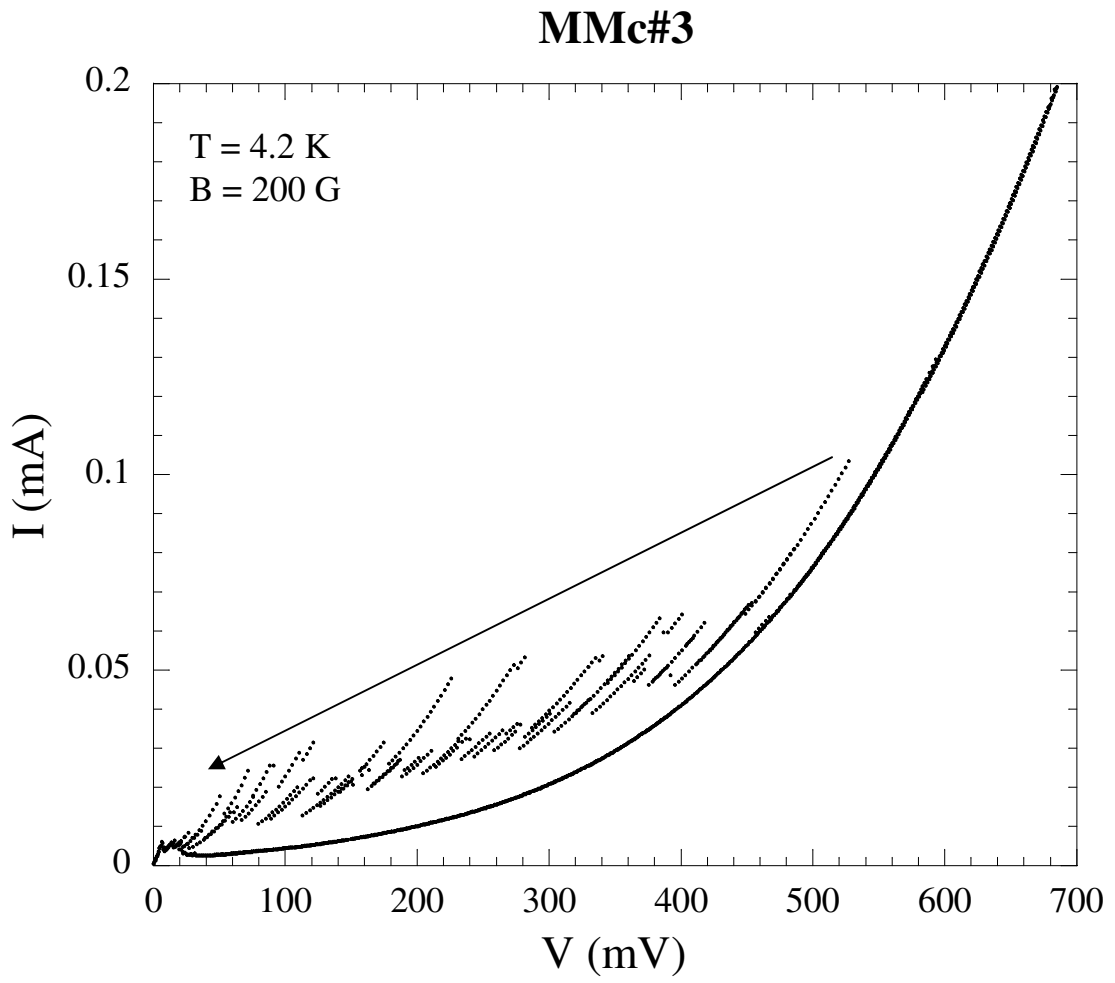
MMc#3

Figure 4.35. I-V characteristics of MMc#3 mesa in detail
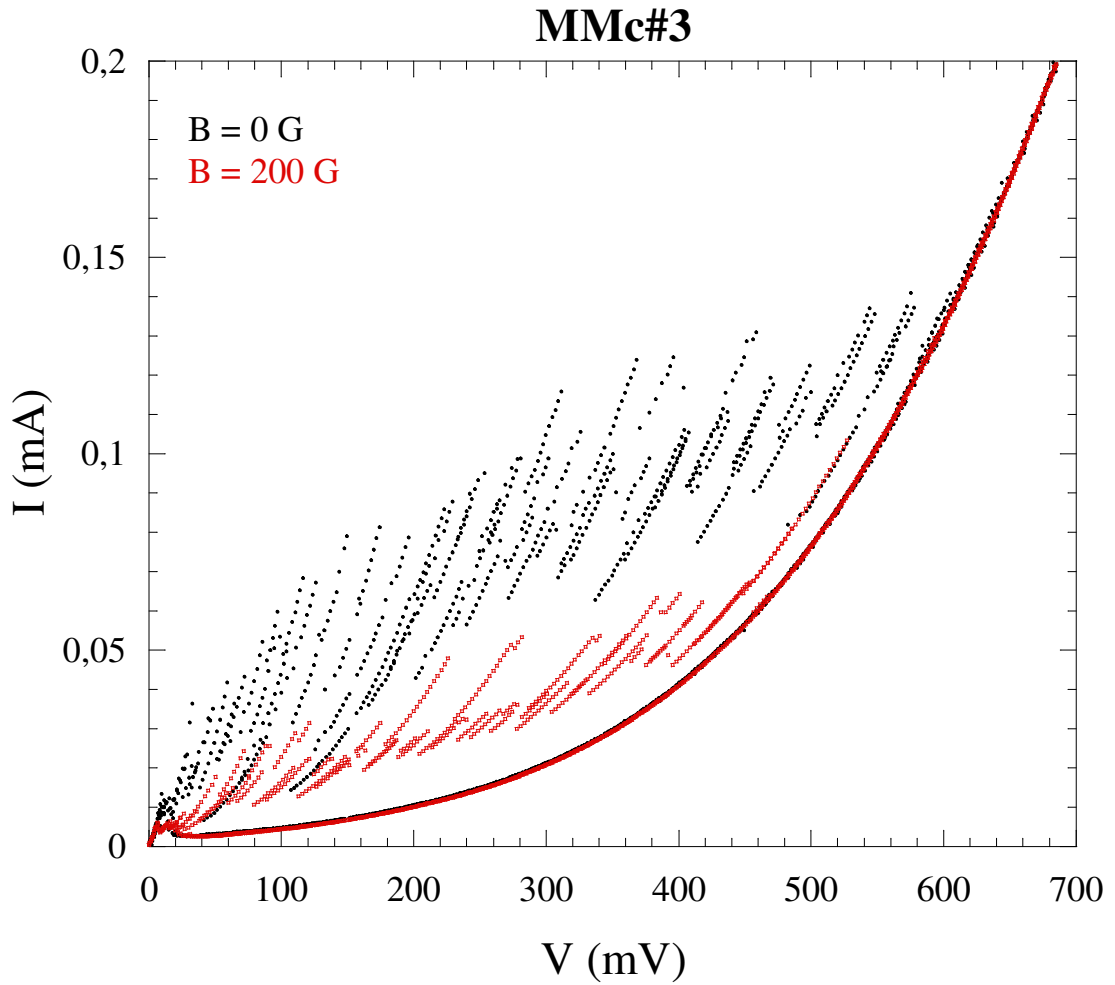
Figure 4.36. I-V characteristics of MMc#3 mesa with and without magnetic field in detail

Figure 4.36 shows the I-V characteristics of MMc#3 mesa with and without magnetic field in detail. It can be easily seen that spin polarized current strongly suppress the superconductivity as mentioned before.

To investigate the magnetic dependence of the tunneling spectroscopy, during the measurements magnetic field was applied to the single crystal along the c-axis. The I-V curves were measured by ramping a bias current up and down repeatedly to trace out all of the quasiparticle branches for the field increasing stepwise up to 1100 G.

Figure 4.37 shows the I-V characteristics of the Bi-2212 mesa covered with ferromagnetic Co top layer for changing magnetic field from 100 G to 1100 G. In experiments it can be think that the effective magnetic field H can be result from a combination of the externally applied magnetic field and the self-field of the ferromagnet. At the superconductor, the direction of the externally applied magnetic field may be opposite that of the self-field of the ferromagnet, resulting in a decrease in H as the external field is increased (Jiang, 2003)

Especially from Figure 4.38 we can see the magnetic field effect on the critical current of quasiparticle branches. These branches exhibit a gradual distribution with applied magnetic field. When the magnetic field is increased, height of the switching current is decrease. Although the applied magnetic field is much lower than upper critical magnetic field of the Bi-2212 (B_{c2}=60 T), this field increase the spin polarization of the current. As we mentioned at previous chapter, superconductivity is strongly suppressed with the spin polarized current because of pair-breaking. The dynamic pair breaking effects of spin polarized quasiparticle is result of excess magnetic moments and quasiparticle redistribution .On the other hand these results attributed to excellent lattice match for epitaxial film growth but Cobalt is not grown epitaxially on Au. The amount of the spin polarization of quasiparticle injected into a Bi-2212 is not known.

The other consensus in literature about reduction of the Josephson current with increasing field is because of ''pancake vortices''. Pancake vortices in general misaligned along the c-axis direction because of the thermal disorder and induce flux trap between the neighboring CuO_2 layers, so critical current is reduced (Bang, 2005). Beyond the 700 G, the all quasiparticle branches diminish and only return branches are observed.

However, when the Figure 4.38and 4.39 is examined, the gradual increase of the switching current is seen easily through the sumgap. Because when the magnetic field is applied to the single crystal along the c-axis, the applied field penetrates through the several top layers of mesa and switching current decreases in these layers

because of penetrated field. As soon as go away form the top of the mesa, switching current is increase and bottom of the mesa reach to the maximum value.
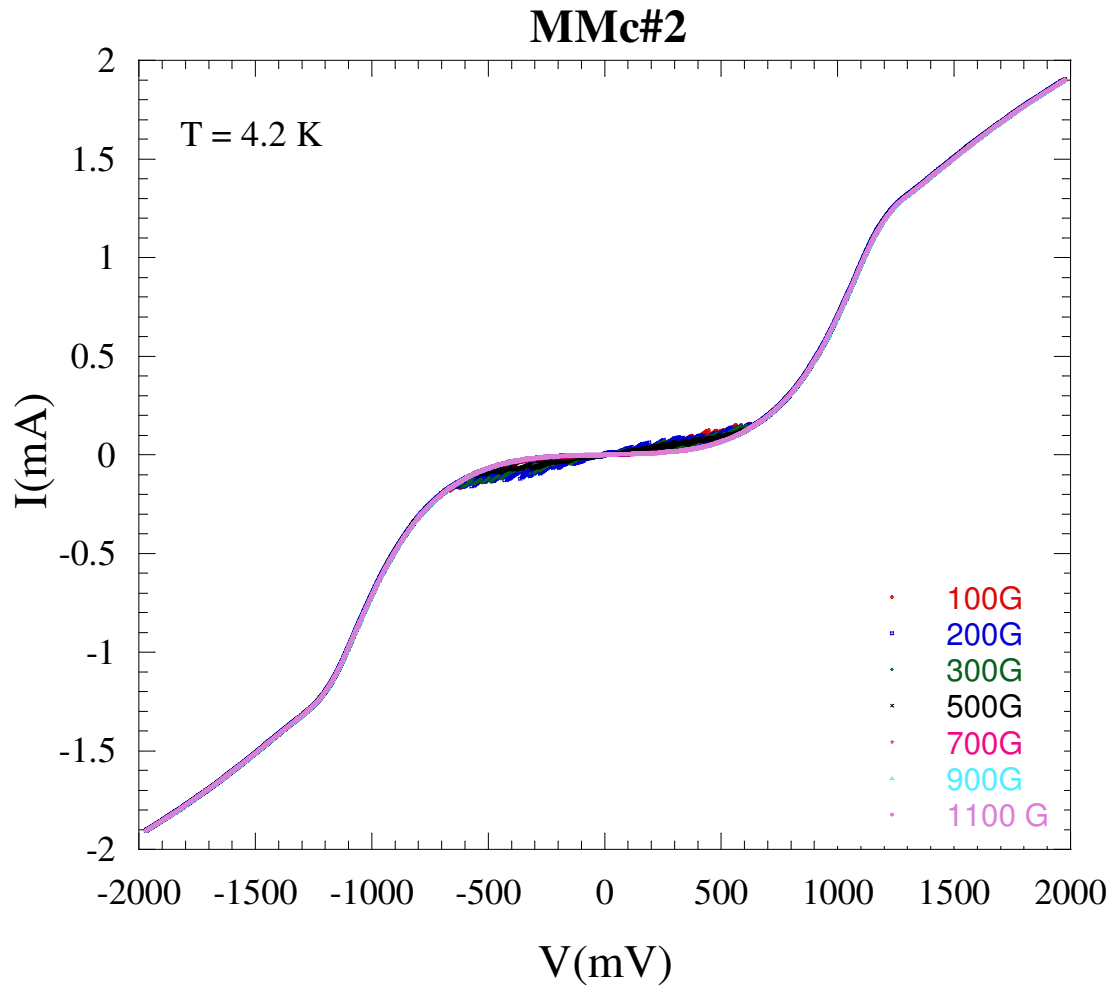
MMc#2

Figure 4.37. Magnetic field dependence of I-V characteristic of MMc#2 mesa at 4.2 K
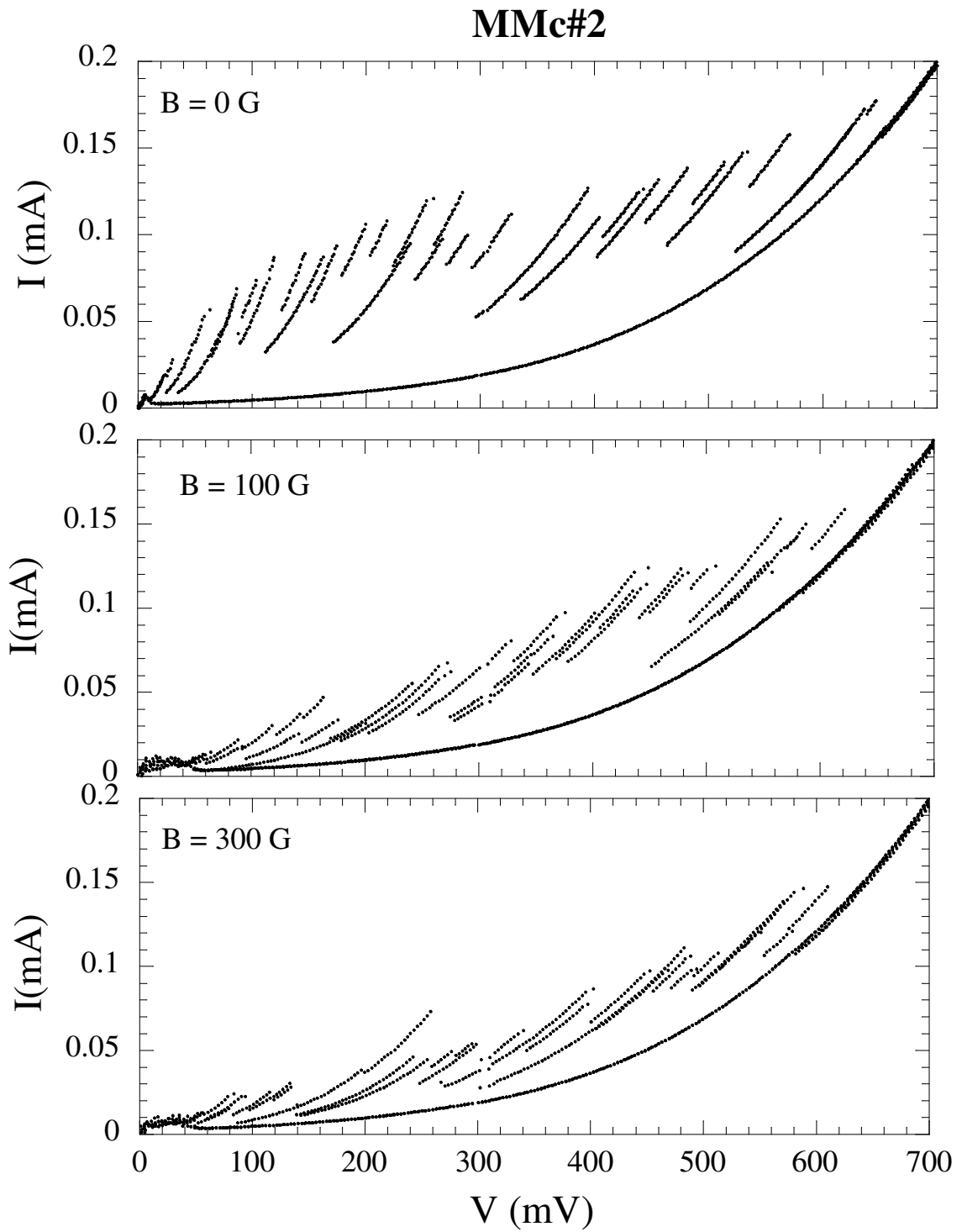
MMc#2

Figure 4.38. More detail part of magnetic field dependence of I-V characteristic of
MMc#2 mesa at 0 G, 100 G and 300 G
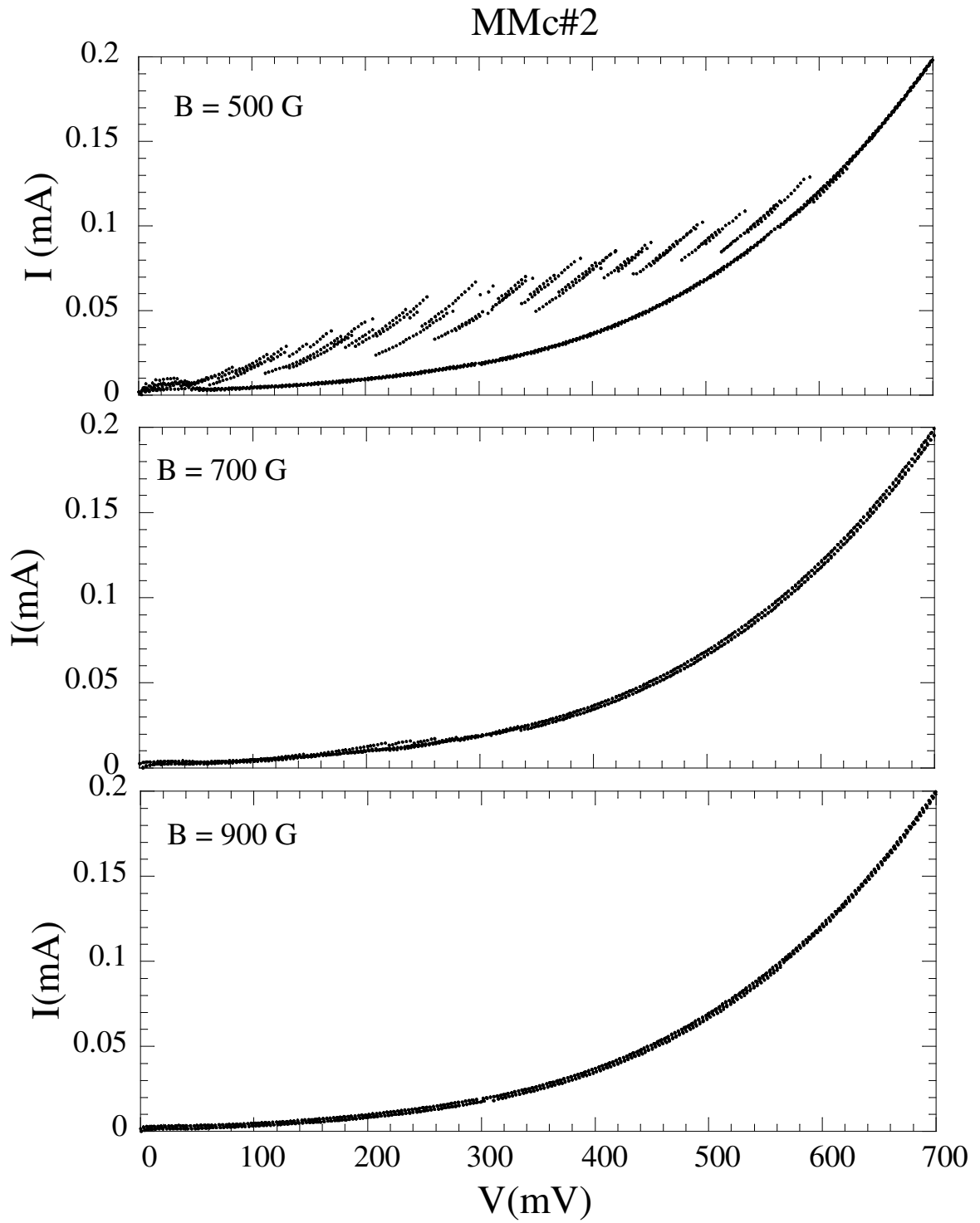
MMc#2

Figure 4.39. More detail part of magnetic field dependence of I-V characteristic of MMc#2 mesa at 0 G, 100 G and 300 G
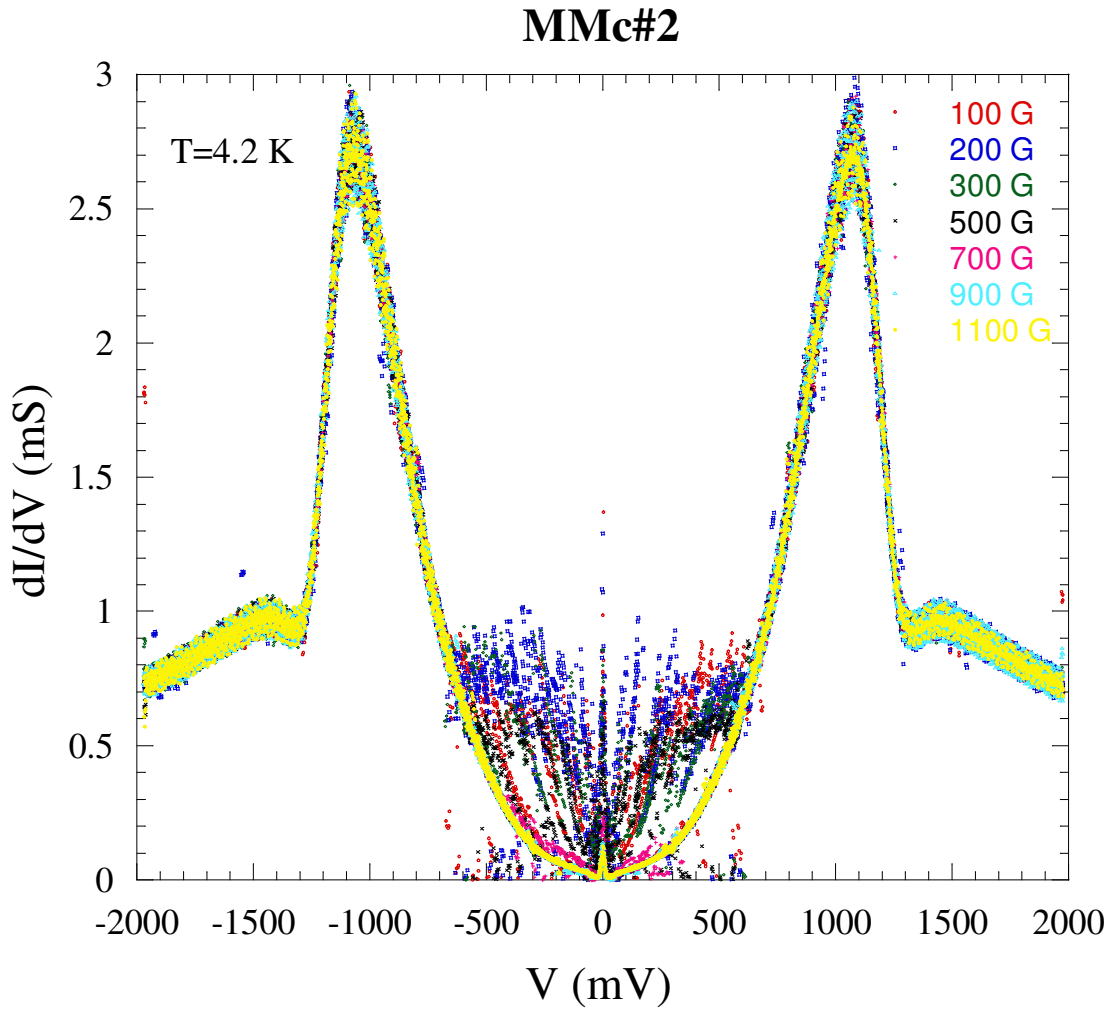
Figure 4.40. Magnetic field dependence of I-V characteristic of MMc#2 mesa at 4.2 K

From Figure 4.40 it is easily understand that the energy gap of the high-Tc superconductor does not change with applied magnetic field along the c-axis. The plot shows also dip features at ± 1300 meV and hump features at ± 1450 meV. These are the indication of less heating because in the experiment intercalated Bi-2212 single crystal was used.
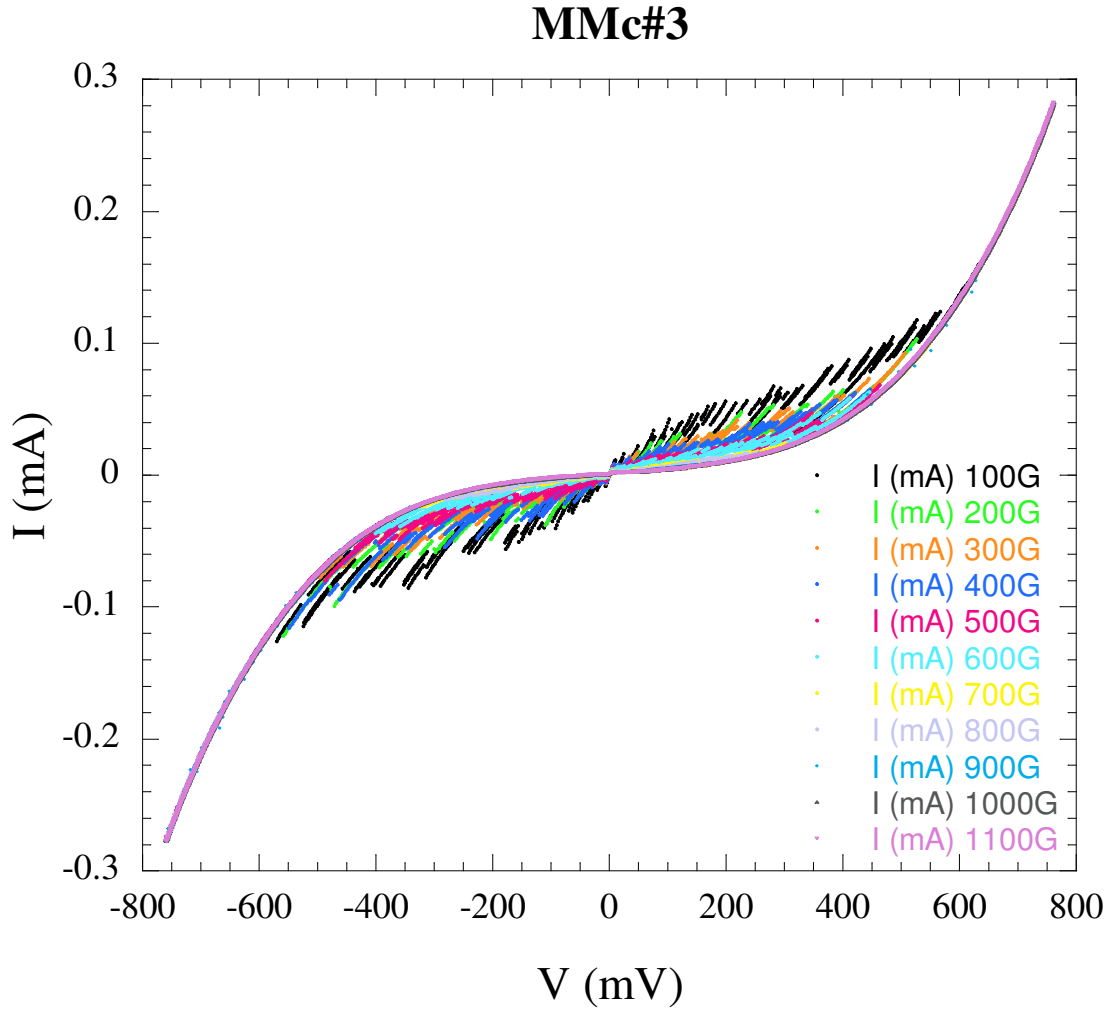
MMc#3

Figure 4.41. Magnetic field dependence of I-V characteristic of MMc#3 mesa

Figure 4.41 and Figure 4.42 and 4.43 shows the magnetic field dependence of the other mesa. The tunneling properties show similar behavior as mentioned mesa belong to Figure 4.38. In Figure 4.38 and 4.42, 4.43 up to 50 meV we can not see any quasiparticle branch because of inhomogeneous intercalation or degradation of the first layers with Au layer.
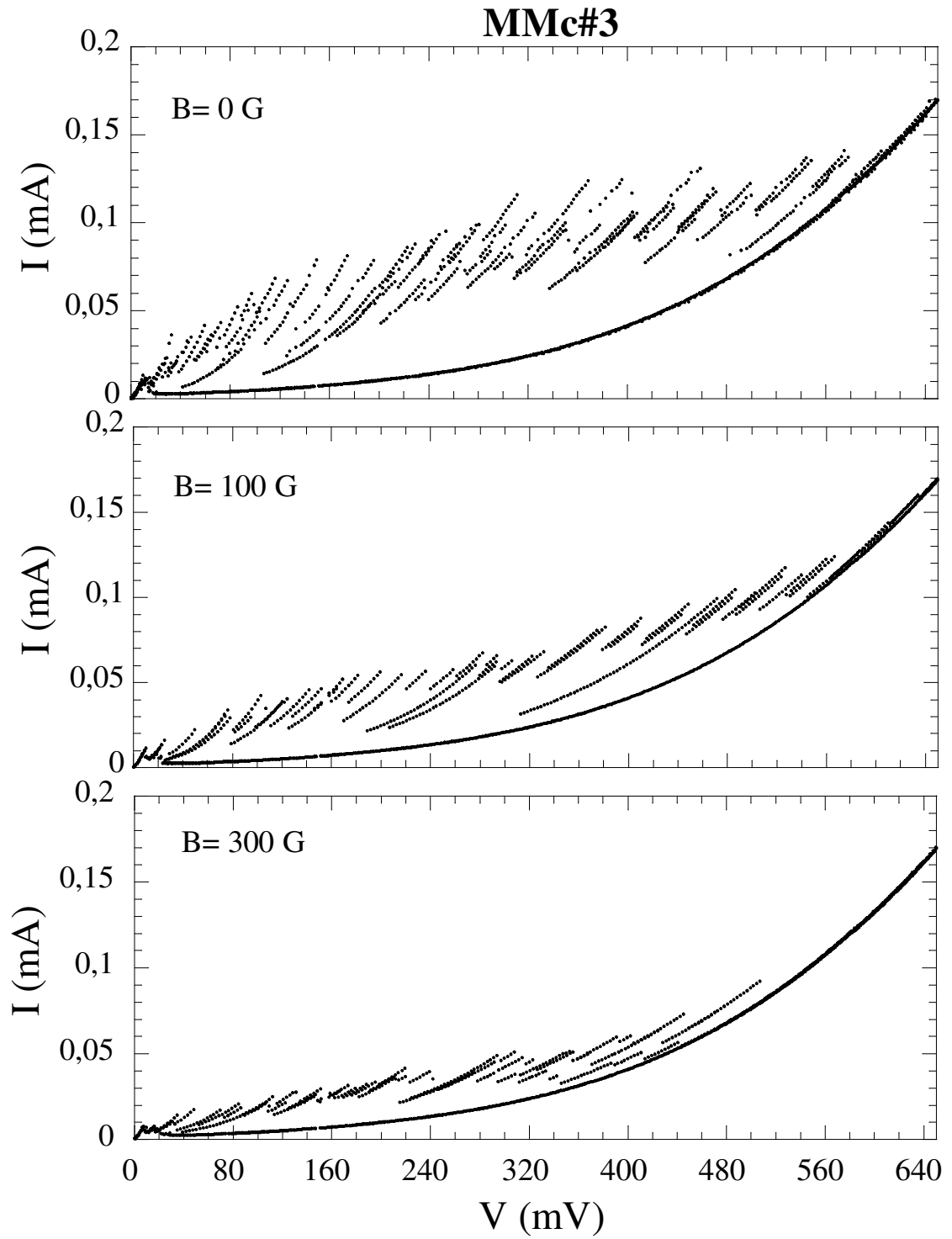
Figure 4.42. Magnetic field dependence of I-V characteristic of MMc#3 mesa
in detail at 0 G, 100 G, and 300 G
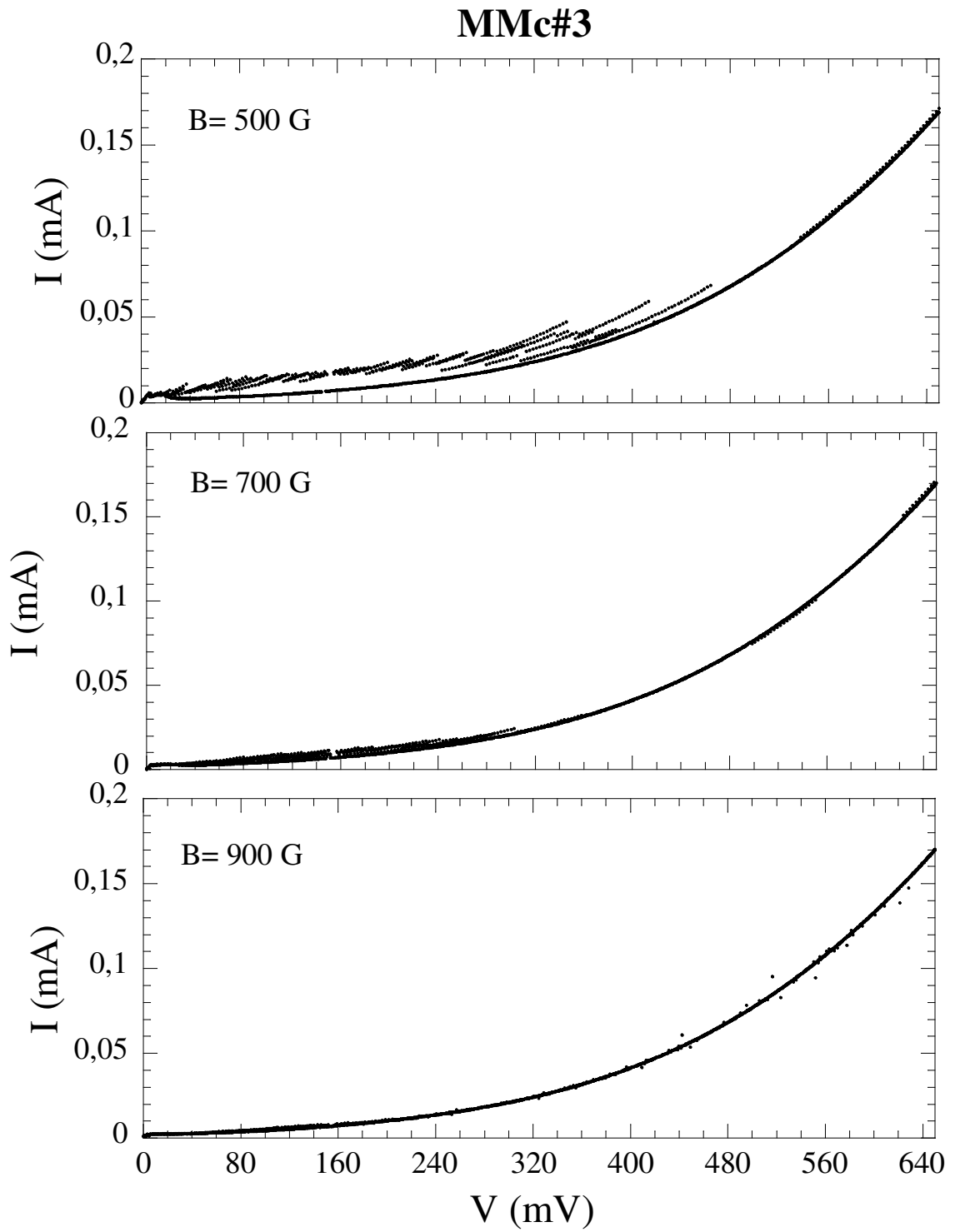
MMc#3



Figure 4.43. Magnetic field dependence of I-V characteristic of MMc#3 mesa
in detail at 0 G, 100 G, and 300 G
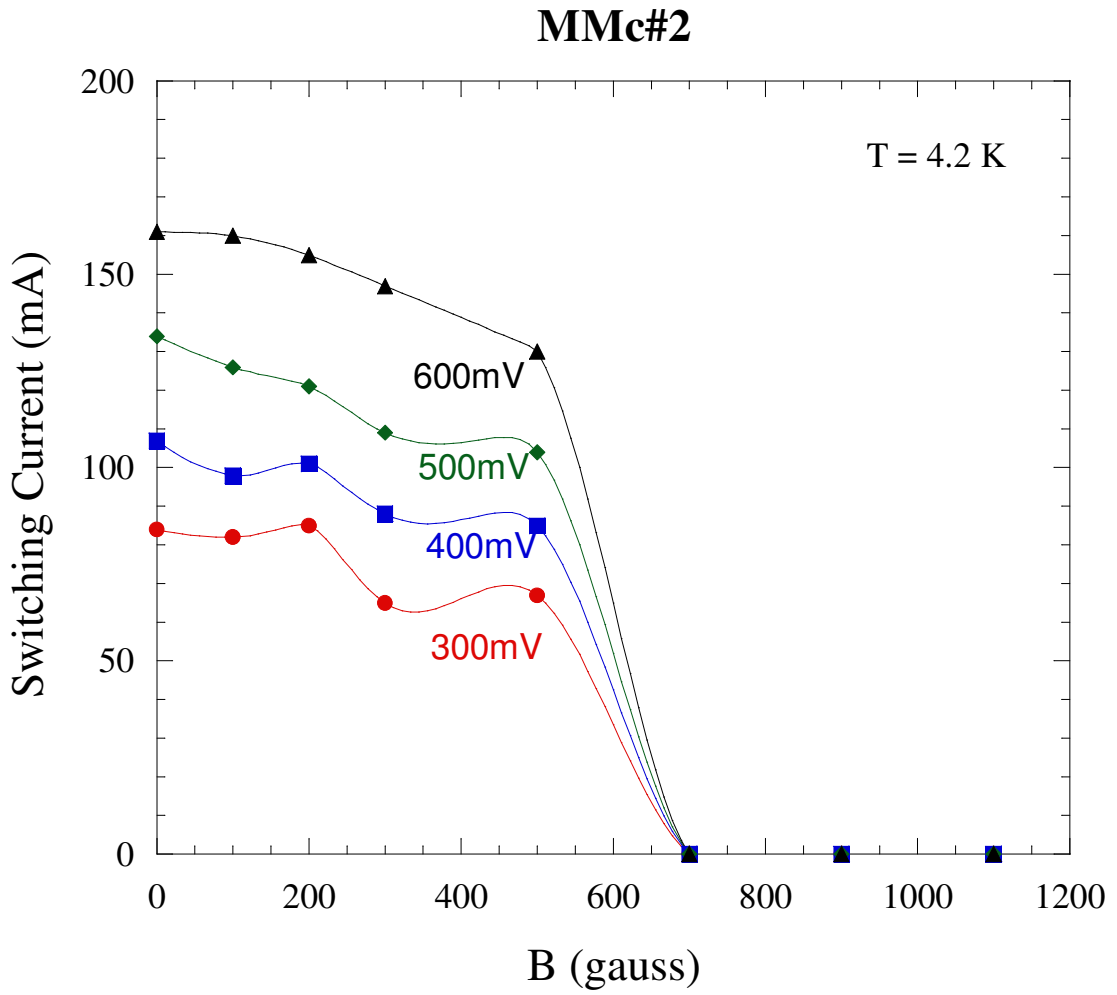
Figure 4.44. Magnetic field dependence of critical Josephson current for spin polarized current to MMc#2

Figure 4.44 shows the magnetic field dependence of switching current for spin polarized current to MMc#2.The magnitude of the switching current increase with applied voltage. However, figure exhibits that while switching current firstly gradually decreasing after that it suddenly decrease above 600 G. This features already mentioned in Figure 4.38 and 4.39. The reason of this effect does not known yet.
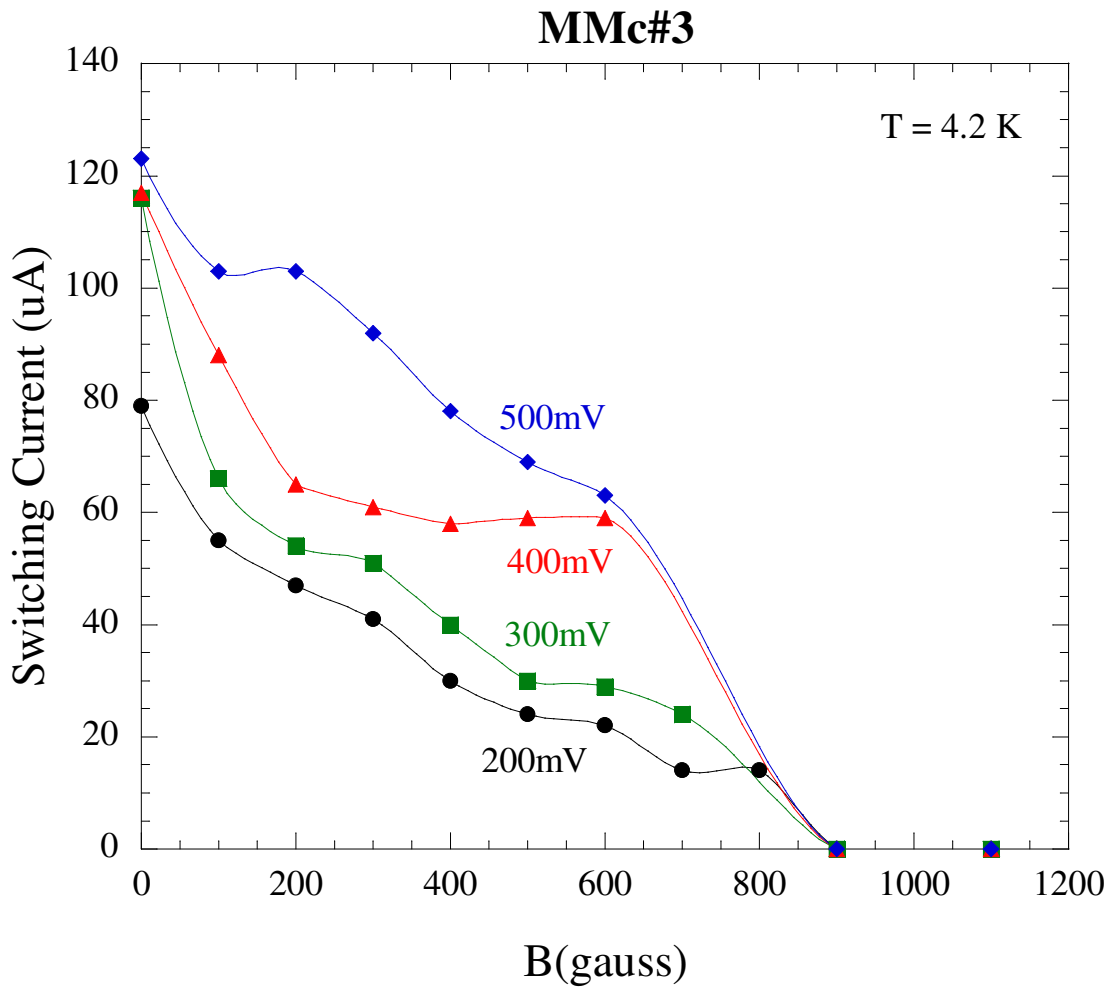
Figure 4.45. Magnetic field dependence of critical Josephson current for spin polarized
current to MMc#3

    Figure 4.45 shows the magnetic field dependence of switching current for spin polarized current to MMc#3. The magnitude of the switching current increase with applied voltage. Moreover, From the Figure it can be easily understand that switching current decreases gradually with increasing magnetic field. This feature is also seen from the Figures 4.41 and 4.42. When the magnetic reach to the 900 G all of the switching current diminishes. The reason of this effect is mentioned previous that it can be spin polarized current or ″pancake vortices″.

From Figure 4.46 and Figure 4.47, it can be easily understand that, there is a strong relation between the temperature and energy gap of superconductors. Figure 4.46 is examined; it can be obtained that I-V characteristic become almost linear beyond the 78 K. According to the BSC theory, when the temperature reaches to the critical temperature of superconductor, energy gap must be totally destroyed and I-V characteristics must show linearity. However, from Figure 4.47, one can understand, the conductance peak voltages gradually decrease with increasing temperature. And also when Figure 4.47 is looked at it is easily seen that the presence of the gap and the conductance peaks are estimated to have finished between 137 K and 161 K.
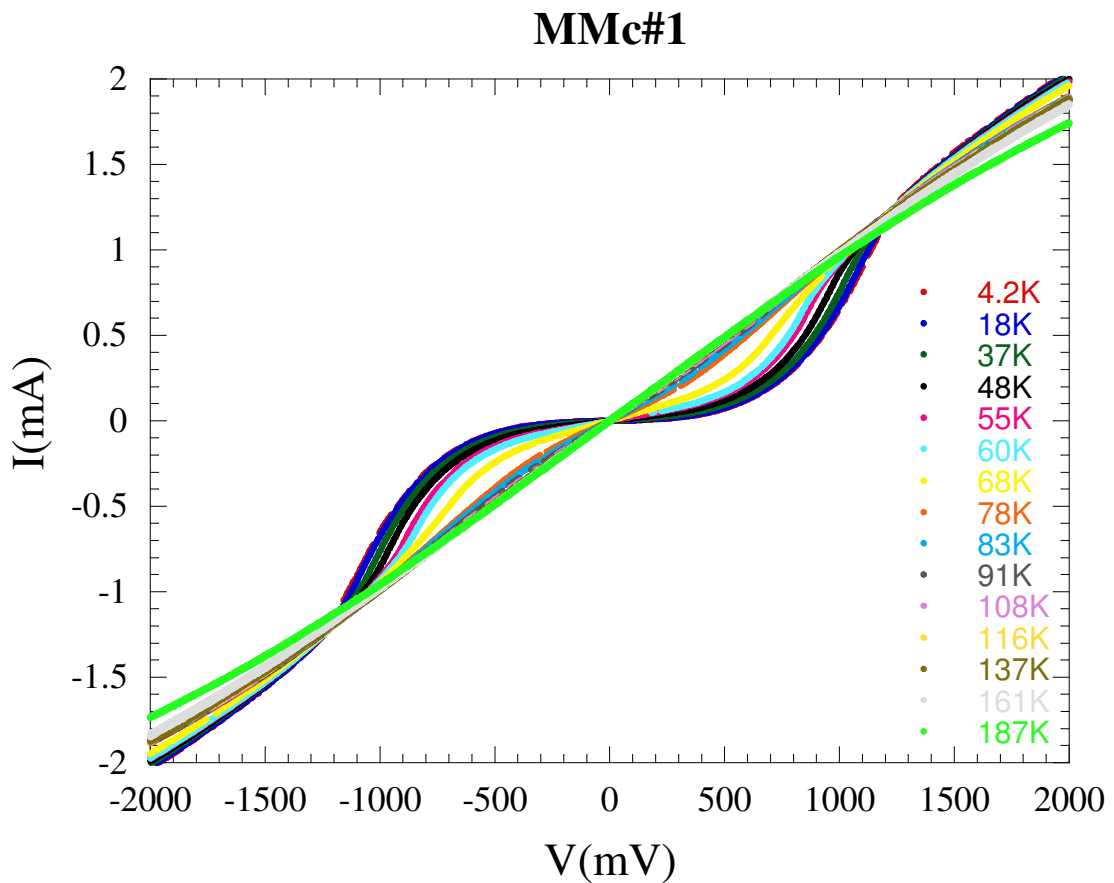
Figure 4.46. Temperature dependence of I-V characteristic of MMc#1 mesa
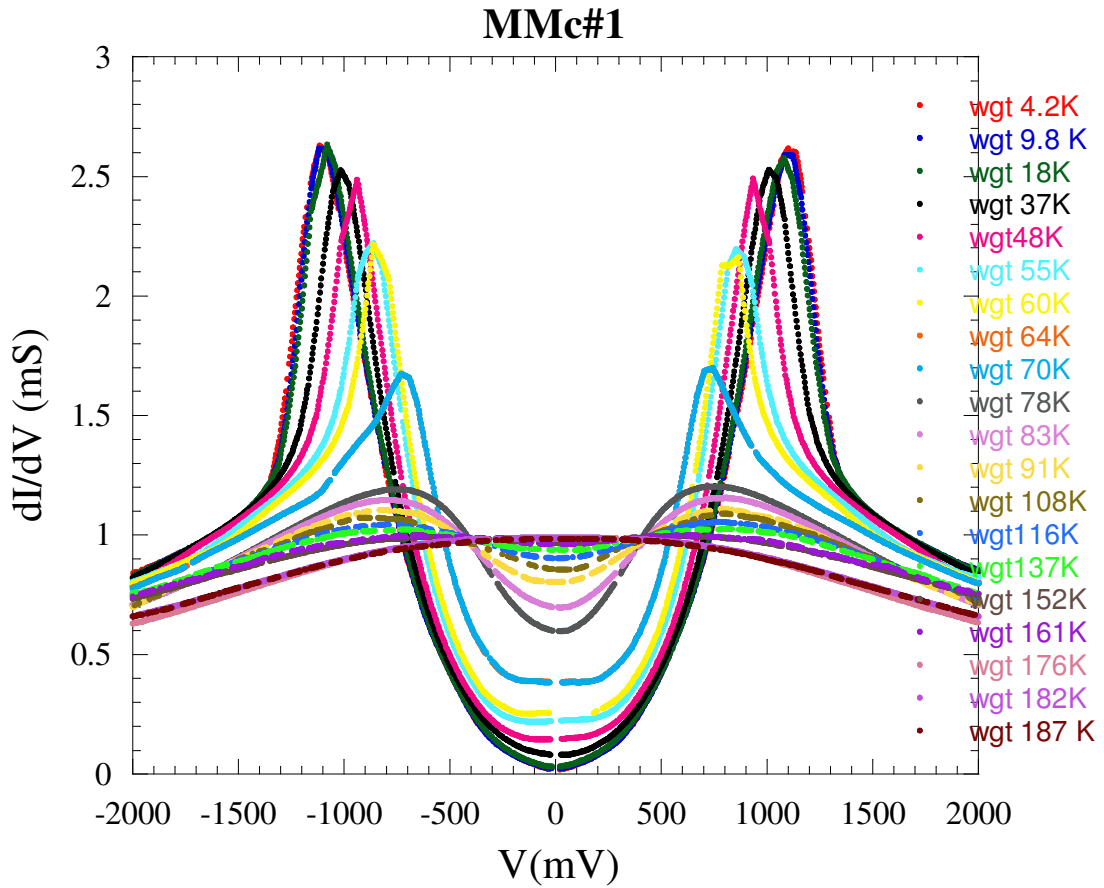
Figure 4.47.Temperature dependence of dI-dV-V characteristic of MMc#1 mesa

Indeed, it can be observed that there is a rapid decrease of quasiparticle height while temperature increases from the 70 K to 78 K. This value is very close to the critical temperature of single crystal (T_c= 74 K) but above the 74 K we can see the energy gap this indicates presence of the energy gap above the T_c. The availability of the energy gap above T_c might be a proof of pseudogap. Besides, while temperature increases, the quasiparticle peaks is closer to the curve which is supposed to be because energy gap began to destroy with increasing temperature. Up to 152 K, normal state conductances have a rising tendency but above 152 K curves begin to down.
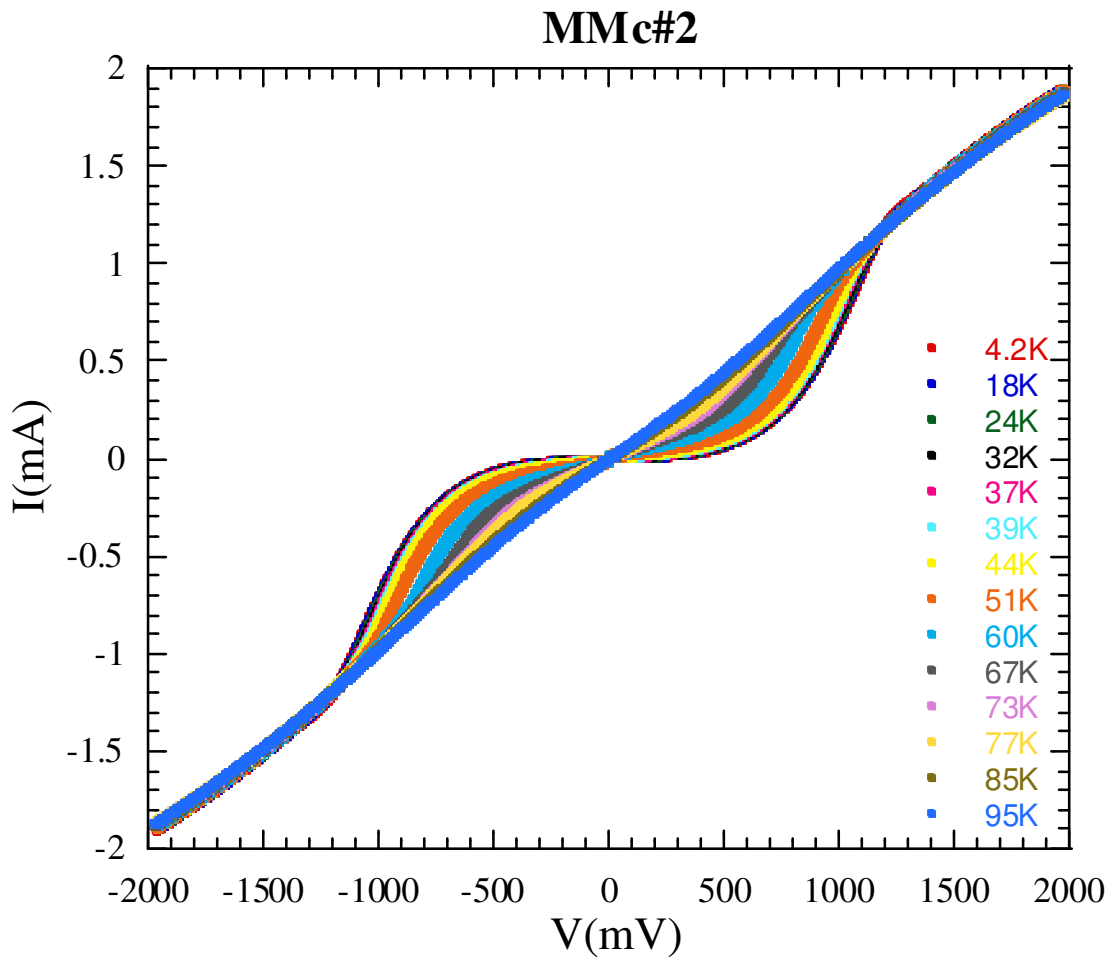
Figure 4.48.Temperature dependence of I-V characteristic of MMc#2 mesa

Figure 4.48 and 4.49 show the temperature dependence of I-V and dI/dV-V characteristic of different mesa called as MMc#2. These characteristics are shows similar peculiarities with the previous one. Symmetric conductance peaks show the gradual decrease with increasing temperature. While going higher temperatures, I-V characteristic show a linear tendency but there is no exact linearity in the experimental data even at higher temperatures.
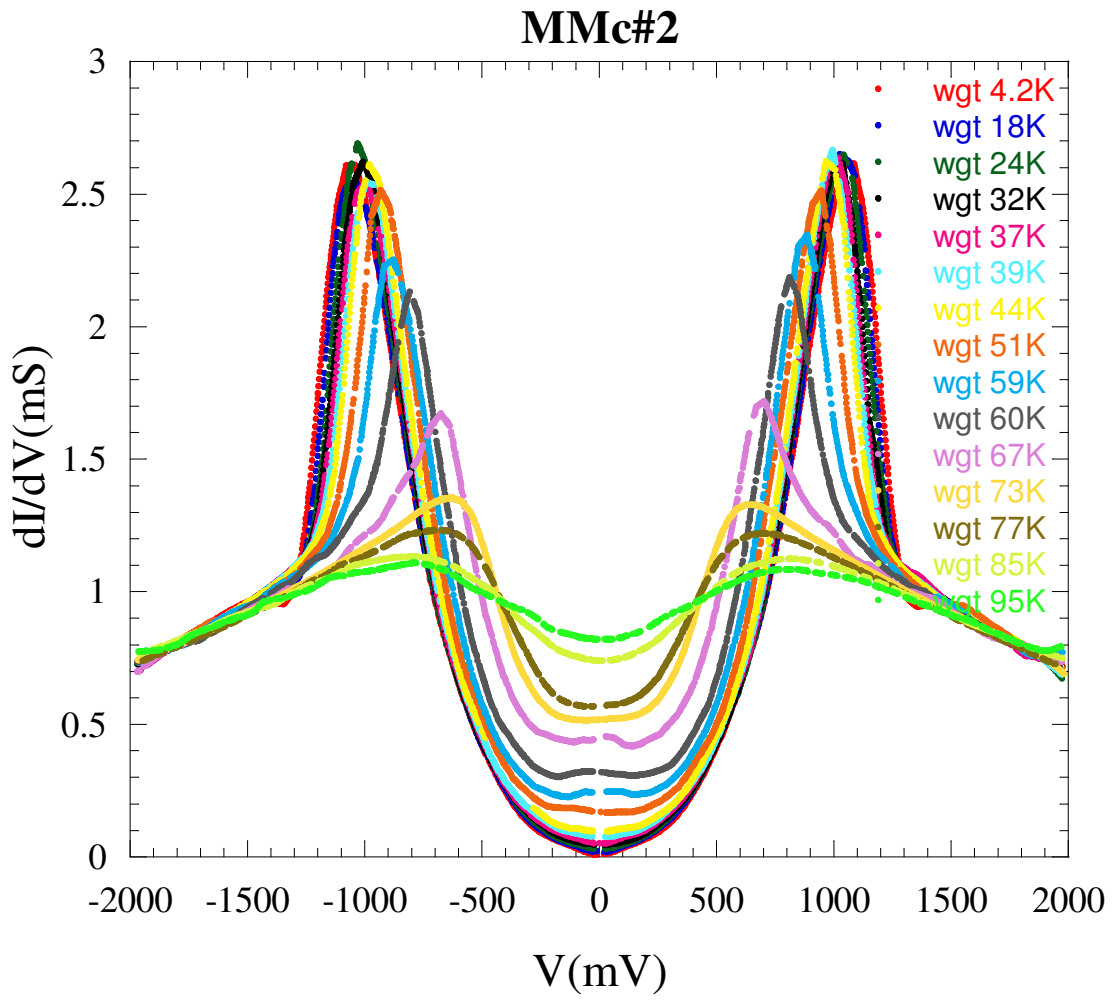
Figure 4.49.Temperature dependence of dI/dV-V characteristic of MMc#2 mesa
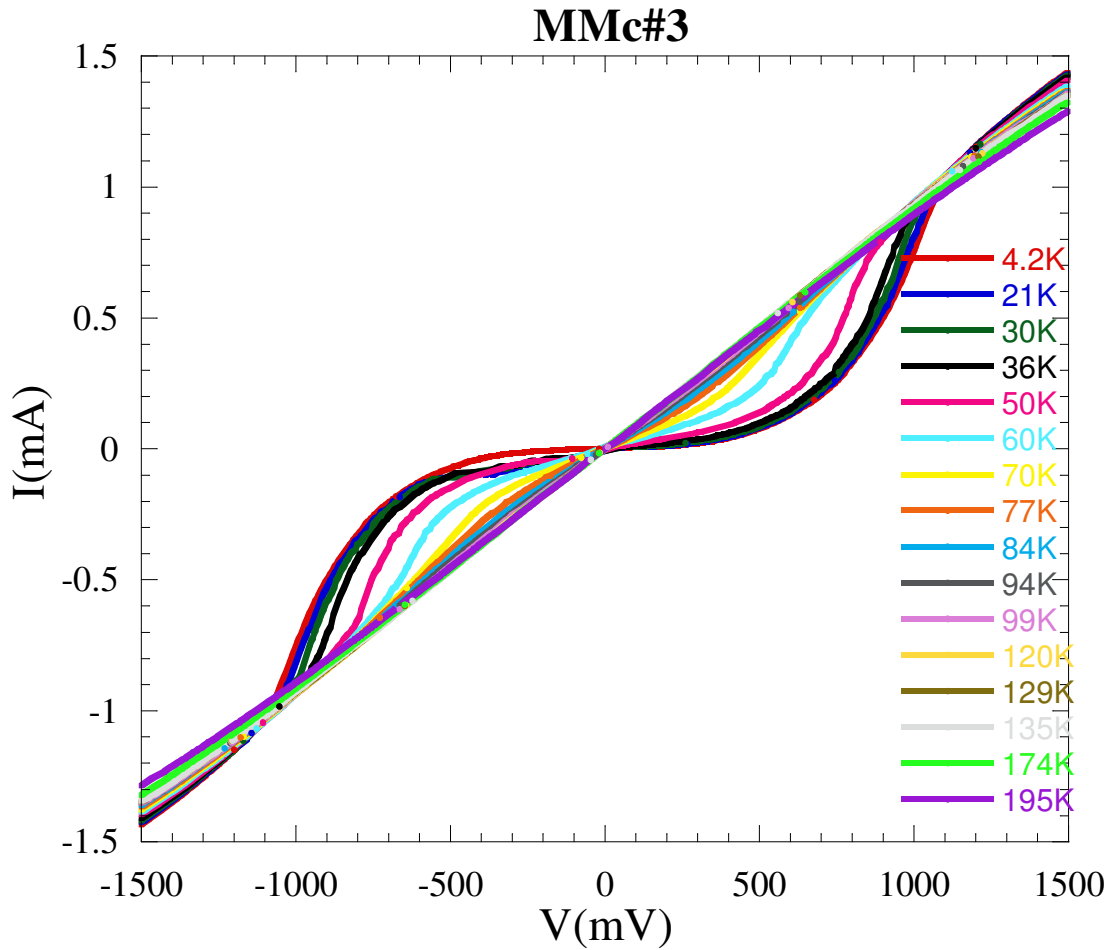
Figure 4.50. Temperature dependence of I-V characteristic of MMc#3 mesa

During the tunneling measurements of the other mesa MMc#3, rapid increase of the temperature was occurred. For these reason the obtained data are not good to investigate the properties of IJJs from this mesa. From the Figure 4.51 it can be seen that there is an asymmetric quasiparticle peaks. Up to 174 K, normal state conductances have a rising tendency but above 174 K curves begin to go down.
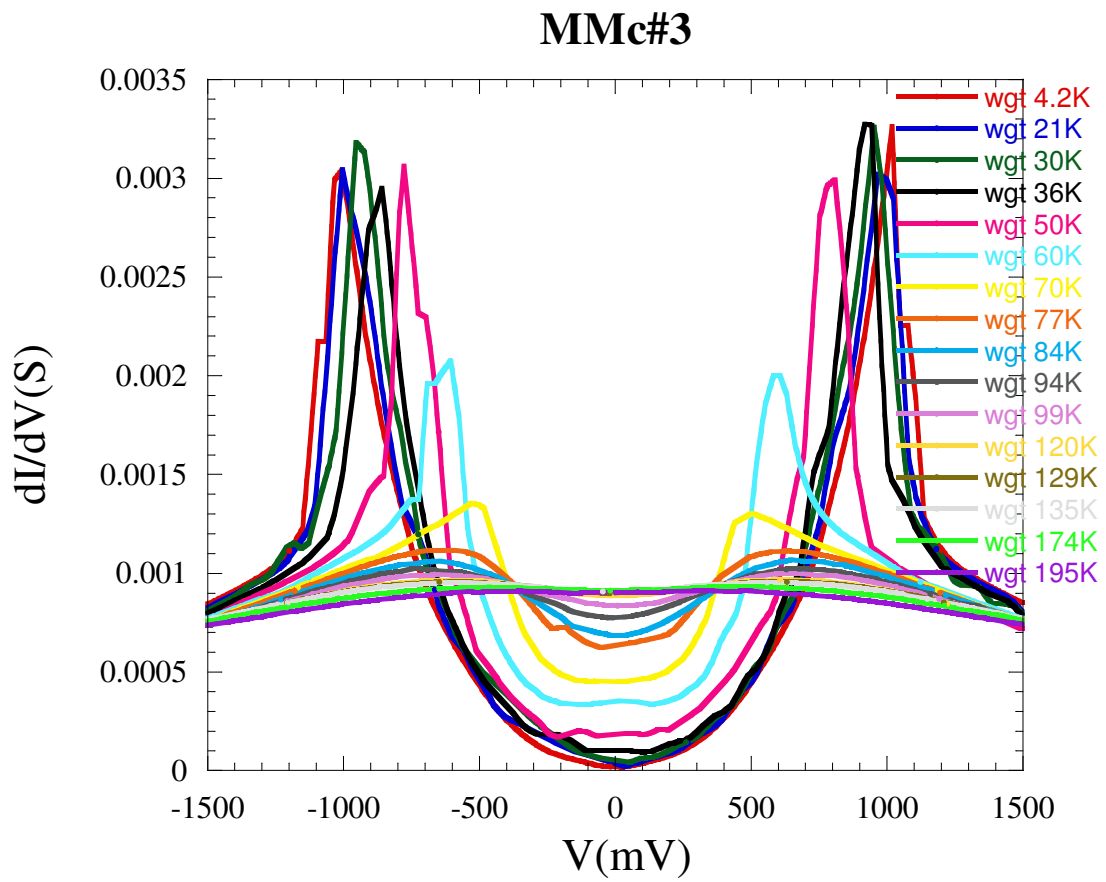
Figure 4.51. Temperature dependence of dI/dV-V characteristic of MMc#3 mesa
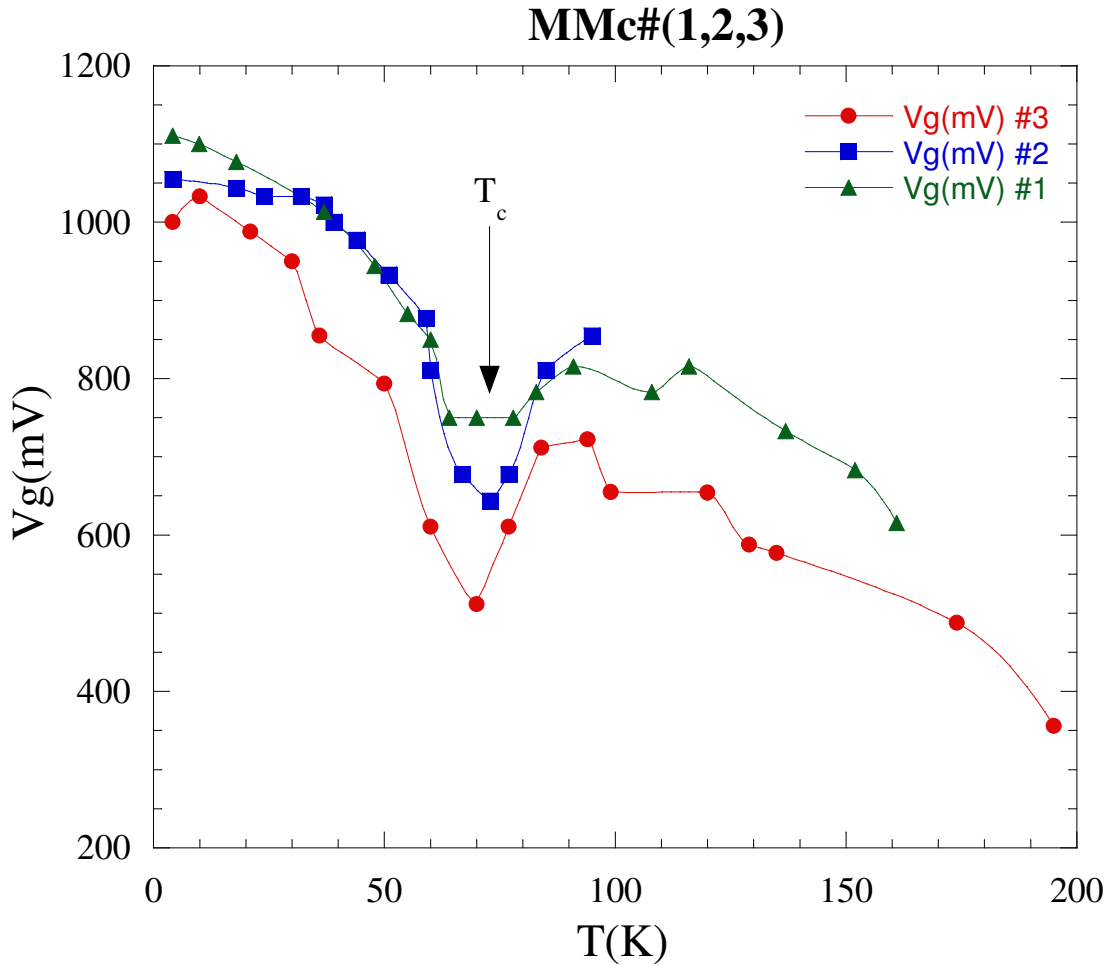
Figure 4.52. Temperature dependence of energy gap of 3 different mesas

Figure 4.52 shows the temperature dependence of the energy gap. According to the BCS theory, when the temperature reach to the critical temperature the energy gap must be totally destroyed. On the other hand from the Figure 4.51 we can understand that energy gap reduces with increasing temperature up to critical temperature but it it can not be zero. Indeed, after the critical temperature it once increases and then again decreases. This indicates the presence of the pseudo gap above the Fermi level.

MMc#(1,2,3)
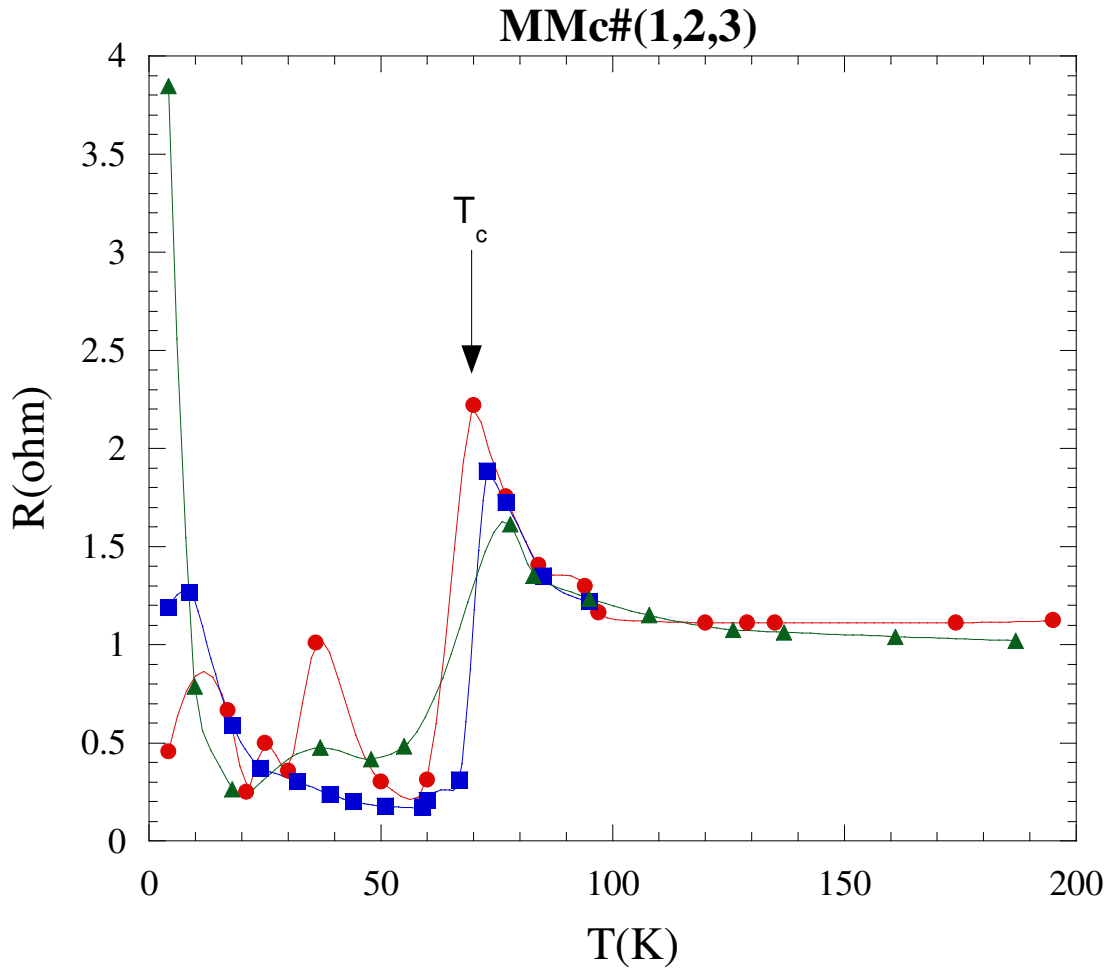
Figure 4.53. Temperature dependence of resistivity of 3 different mesas

When the Figure 4.53 is examined the resistivity difference with temperatures is seen. In our study we used the high temperature superconductor. Bi-2212 with $T_c = 74$ K. Resistivity of all of the superconductors decrease with decreasing temperature and suddenly drops to zero at the critical temperature. But from the Figure we can seen that firstly, the resistivity is constant and beyond the 80 K plot shows the increase after that at the critical temperature it is suddenly drops. HTS has the two fundamental axis, according to the this axis their resistivity show anisotropic behavior. The c-axis resistivity is 100 times than the ab-axis resistivity. c-axis resistivity is shows the this kind of effect which we obtained in Figure 4.53. In our experiment we drive the current along the c-axis so this graph is proof of this feature. Indeed, we can see the resistivity suddenly increased at 4.2 K because this peak shows the resistivity between the first layer and Au film.
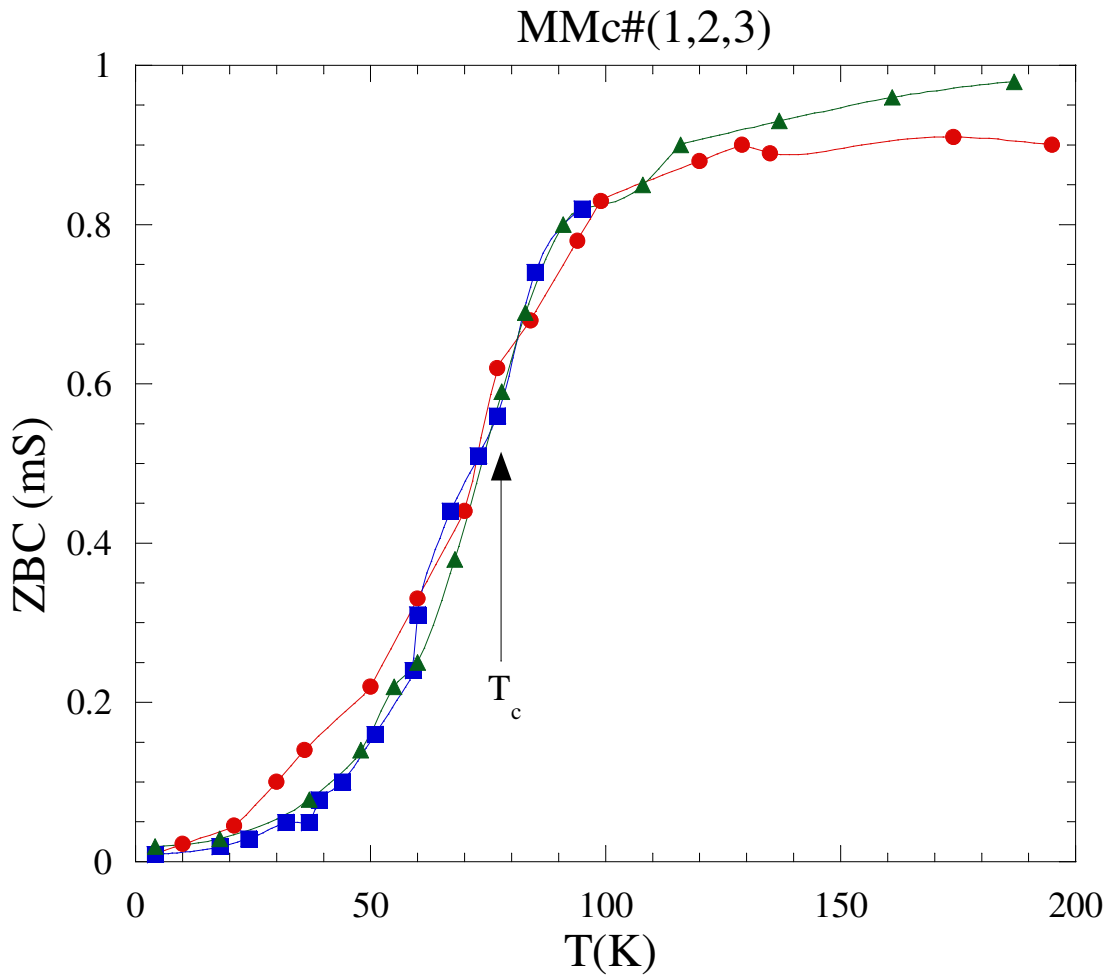
Figure 4.54. Temperature dependence of ZBC of 3 different mesas

Figure 4.54 shows the temperature dependence of ZBC for 3 different mesas. At the dI/dV- V it can be easily seen that, ZBC increase up to critical current and the when the temperature reach to the critical current it must be constant. But we obtained that ZBC still increase after the critical current. This also proof of the pseudo gap at higher temperatures.

BH19a#2 & MMc#3
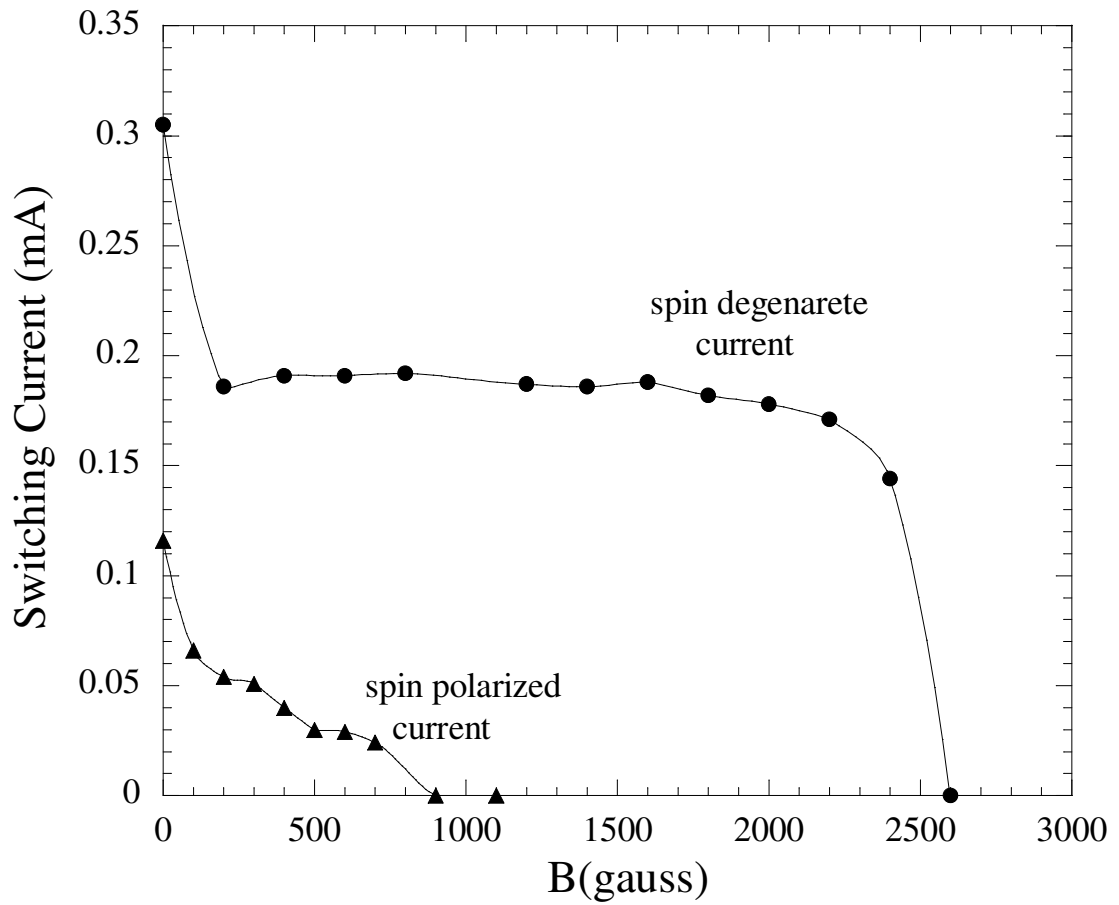
Figure 4.55. Magnetic field dependence of critical Josephson current for both spin polarized current and spin degenerate current

Finally, when we compared the spin polarized tunneling with spin degenerate tunneling, while the switching current of the spin polarized current gradually decrease, that of spin degenerate current suddenly decrease with applied magnetic field because of I mentioned in previous pages.

CHAPTER 5

SUMMARY AND CONCLUSION

We investigated tunneling spectroscopy of IJJs of the intercalated Bi-2212 single crystal with T_c= 74 K using both spin polarized and spin degenerate current. A novel method, PCT is used to get a contact mesa surface and to generate a tunnel junction. Finally, the influence of spin polarized tunneling spectroscopy on IJJs compared with the effect of spin degenerate tunneling spectroscopy on IJJs.

In the first part of this thesis, the single crystal Bi-2212 covered with two different configurations. One set of the single crystal were deposited with ferromagnetic multilayer (Au=15 nm / Co= 80 nm / Au= 156 nm), the others of them were deposited with Au= 70 nm layer using sputter system. 10 x 10 μm^2 mesa arrays have been fabricated using photolithography and Ar ion etching techniques. For pre characterization, Optical microscopy and Atomic Force Microscopy (AFM) were used.

A PCT was used to obtain I-V characteristics of mesa with Au top layer at 4.2 K with and without applied magnetic field. Magnetic field was applied parallel to the c-axis of crystal during the measurements. From the I-V characteristics, it has been understand that, the value of the sumgap voltages does not change with magnetic field application. However, it has been obtained that while the value of switching current is almost same for spin degenerate current without magnetic field, when the magnetic field was applied, the switching current exhibits a gradual distribution. This distinction between them attributed to that the applied magnetic fields penetrate through the first few top layers of mesa and the switching current decreases in these layers. Because CuO_2 layers of mesa close to the bulk of crystal, have larger critical current than the others.

We have also performed PCT measurements on mesa with ferromagnetic Co layer at 4.2 K with and without applied magnetic field. The critical current of quasiparticle branches exhibits the gradual distribution without any applied magnetic field but the reason of such kind of effect has not been found yet. It has attributed to two different mechanisms; one of them is spin polarized current. On the other hand, spin polarized tunneling technique utilizes the excellent lattice math among various perovskite materials for epitaxial film growth of the heterosructures. The other reason of such kind effect is self-field magnetic field of ferromagnetic layer. It can be

penetrate from the superconductor causing the suppression of the superconductivity. After that, magnetic field was applied to the single crystal along the c-axis. The effective magnetic field can be combination of the self–field of ferromagnetic material and applied magnetic field. Depending on the direction of the self field of Co, the magnitude of the effective field can be more or less than applied magnetic filed. This magnetic field increases the polarization of the tunneling current, more polarized current suppress the superconductivity more so the switching current decrease with increasing magnetic field. The reduction of the switching current a none equilibrium bias current is understood in terms of generation of the pancake vortices in the perpendicular magnetic fields. Pancake vortices are in general misaligned along the c-axis direction because of thermal disorder and induce the phase fluctuation between the neighboring CuO_2 layers, thus reducing the Josephson critical current. The switching current is expected to be more reduced with increasing magnetic field and temperature due to the increased interlayer phase disorder.

From the PCT results of the junctions, the energy gap, which is obtained from spin polarized current, is obtained around the 22 meV, this value is very coincidence with the literature. On the other hand, the energy gap is just only 13 meV if spin degenerate tunneling current is referred. The huge difference is due to the heating of the mesa structure during the measurements although we used intercalated samples. And also reason of the reduced energy gap can be high contact resistance between the gold film and Bi-2212 single crystal. Already the I-V characteristics does not show any quasiparticle up to 50 meV, this also show the presence of the high resistance. For this reason the number of IJJs can not be determined exactly.

In order to understand the origin of the quasiparticle excitation gap in HTS, we examined the temperature dependence of the energy gap. The energy gap shows the parallelism with the BCS theory up to critical temperature but above the critical temperature the value of energy gap show the increase with temperature. This phenomenon is the proof of the pseudo gap above the critical temperature.

The temperature dependence of the resistivity shows us that near the critical current resistivity increases and when the temperature reaches to the critical current, it suddenly decreases. This is the proof of that we drove the current along the c-axis during the experiment so driven current along the mentioned axis show this effect.

Finally, the magnetic field dependence of the switching current of spin degenerate current compared with that of spin polarized current. The switching current for spin degenerate current suddenly decrease at certain values while the switching current for spin polarized current gradually decrease.

REFERENCES

Akinobu, I. and Gin-ichiro, O., 2005. "Fabrication of DC SQUIDs Based on $Bi_2Sr_2CaCu_2O_y$ Intrinsic Josephson Junctions." *IEEE Transactions on Applied Superconductivity,* Vol. 15, No. 2, p. 813.

Bae, M., Lee, H., 2005. "Sub-branch splitting in josephson-vortex-flow characteristic of a stack of $Bi_2Sr_2CaCu_2O_{8+x}$ intrinsic josephson junctions" *International Journal of Modern Physics B,* Vol. 19, No. 1, p. 205-208.

Bang, D., Lee, H., Bae, M., Park, W., 2005. "Spin dependence of pair tunneling properties of $Bi_2Sr_2CaCu_2O_{8+x}$ intrinsic josephson junctions." *International Journal of Modern Physics B,* Vol. 19, No. 1, p. 199-203.

Buckel, W., Kleiner, R., "*Superconductivity Fundemental and Applications* ", (Wiley-NCH Verlag GmbH8Co,KgaA, Singapure)

Chu, C. W., 2002. "Materials and Physics of High Temperature Superconductors: A Summary, Two Recent Experiments and a Comment." *Royal Swedish Academy of Sciences,* Vol.102, No.1, p. 40-50.

Cryot, M., Pauna, D., "Introduction to Superconductivity and High-Tc Materials", (World Scientific, Singapure)

Fu, C.-C., Huang, Z., Yeh, N.-C., 2002 "Spin-polarized quasiparticle transport in cuprate superconductors". *Physical Review B*, Vol.65, p.22, No. 224516

Gubbiotti, G., Carlotti, G., Albertini, F., Casoli, F., Bontempi, E., Depero, L. E., Koo, H.,Gomez, R. D., 2003. "Influence of annealing on CoyAu multilayers: a structural and magnetic study." *Thin Solid Films*, Vol. 428, p.102–106.

Ishibashi, T., Sato, K., Yonemitsu, K., Sato, K., 2001. "Spin Tunneling in Co/Au/I/BiSrCaCuO Tunnel Junctions" *Journal of Applied Physics*, Vol. 89, No. 11.

Jiang, Z., Aumentado, J., Belzig, W., Chandrasekhar, V., 2003. "Transport through ferromagnet/superconductor interfaces": Auxiliary Information", cond-mat/0311334

Kashiwaya, S., Tanaka, Y., Yoshida, N., Beasley, M. R**.,** 1999. "Spin current in ferromagnet-insulator-superconductor junctions" *Physical Review B,* Vol.60, No. 5.

Kleiner, R., Steinmeyer, F., Kunkel, G., Müller, P., 1992. "Intrinsic Josephson Effects in $Bi_2Sr_2CaCu_2O_8$" *Physical Review Letters,* Vol. 68, No.15.

Kharmouche, A., Chèrif, S-M., Bourzami, A., Layadi, A., Schmerber, G., 2004. "Structural and magnetic properties of evaporated Co/Si(100) and Co/glass thin films"*Journal of Physics D: Applied Physics.* P.2583-2587.

Kurter, C., Ozyuzer, L., 2005. **"**Fabrication of array of mesas on superconducting $Bi_2Sr_2CaCu_2O_{8+\delta}$. single crystals" *Journal of Optoelectronics and Advanced Materials,* Vol. 7, No. 1, p. 415 – 418.

Mihály, G., Halbritter, A., Mihály, L., Forro, L., 2000. "Search for magnetic field induced gap in a high-*T*c superconductor" *Solid State Communications*, Vol. 116 p.197–200.

Miyakawa, N., Zasadzinski, J. F., Ozyuzer, L., Guptasarma, P., Hinks, D. G., Kendziora, C., Gray, K. E., 1999. "Predominantly Superconducting Origin of Large Energy Gaps in Underdoped $Bi_2Sr_2CaCu_2O_{8+\delta}$. from Tunneling Spectroscopy" *Physical Review Letters,* Vol. 83 No. 5.

Murakami, H., Ogami, T., Qi, Y., Sakai, K., Ito, T., Shigaki, I., Jansen, A. G. M., Wyder, P., 2000. "Problems in point-contact tunneling study on BSCCO" *Physica B,* p. 573-574.

Ozyuzer, L., Zasadzinski, J. F., Gray, K. E., Hinks, D. G., and Miyakawa N., 2003. "Probing the Phase Diagram of $Bi_2Sr_2CaCu_2O_{8+\delta}$ With Tunneling Spectroscopy." *IEEE Transactions on Applied Superconductivity,* Vol.13, No. 2, p.893.

Ozyuzer, L., Kurter, C., Zasadzinski, J. F., Gray, K. E., Hinks D. G., and Miyakawa, N., 2002. "Single Junction and Intrinsic Josephson Junction Tunneling Spectroscopies of $Bi_2Sr_2CaCu_2O_{8+\delta}$." *Journal of Latex Class Files,* Vol. 1, No.11, p.2.

Ozyuzer, L., Yusof, Z., Zasadzinski, J. F., Mogilevsky, R., Hinks, D. G. and Gray, K. E., 1998. "Evidence of d_{x2-y2} symmetry in the tunneling conductance density of states of $Tl_2Ba_2CuO_6$" *Physical Review B,* Vol. 57, No. 6, p. 1-4.

Ozyuzer, L., Zasadzinski, J. F., Kendziora, C., Gray, K. E., 2000. "Quasiparticle and Josephson tunneling of overdoped $Bi_2Sr_2CaCu_2O_{8+\delta}$ single crystals" *Physical Review B,* Vol. 61, No. 5, p. 1-12.

Ozyuzer, L., Zasadzinski, J. F., Kendziora, C., Gray, K. E., 1998. "Point Contact Tunneling Apparattus with Temperature and Magnetic Field Control", *Cryogenics* Vol. 38, No.9, p.911.

Petley, B. W. 1971 "*An Introduction to the Josephson Effects*", edited by J Gordon Cook   (Milles & Boon Limetted, London), pp.13, 75-78

Poole, C.P.,Horacio, A.F., Richard, J.C. 1995. "*Superconductivity*", (Academic Press California)

Shin, H. S., Lee, H. J., 2004. "Depression of the interlayer Josephson coupling in $Bi_2Sr_2CaCu_2O_{8+x}$ single crystals by spin-polarized current injection along the c-axis"   *Physica C,* Vol. 408, No. 410, p. 623–624.

Tinkham, M. 1996. " *Introduction to Superconductivity*", (Mc Graw-Hill, Singapore).

Upadhye, K. V., Kumara, K. G., Purandare, S. C., Pai, S. P., Pinto, R., 2002. "Direct injection of spin-polarized carriers across $YBa_2Cu_3O_{7-\delta}$–$La_{0.3}Ca_{0.7}MnO_3$ interface at 77K"   *Journal of Physics,* Vol. 58, No. 5, pp. 1199–1201.

Wei1, J. Y. T., 2002. "Spin-Injection Quasiparticle Nonequilibrium in Cuprate/Manganite   Heterostructures" *Journal of Superconductivity,* Vol. 15, No. 1.

Wesche, R., 1999 "*High Temperature Superconductors: Materials*, Properties, and Applications",(Kluwer Academic Publishers).

Vas'ko, V. A., Larkin, V. A., Kraus, P. A., Nikolaev, K. R., Grupp, D. E., Nordman, C. A., Goldman, A. M., 1997. "Critical Current Suppression in a Superconductor by Injection of Spin-Polarized Carriers from a Ferromagnet." *Physical Review Letters,* Vol. 78, No.6,.

Yeh, N. C., Wei, J. Y. T., Fu, C. C., Vasquez, R. P., 2000. "Dynamic pair breaking in cuprate superconductors via injection of spin-polarized quasiparticles in perovskite F-I-S heterostructures" *Physica B,* p. 507-508.

Yurgens, A. and Claeson, T., 2001. "Intrinsic Josephson Junctions for Studies of High Tc Superconductors", *Physica C*, Vol. 41

Zasadzinski, J. F., Ozyuzer, L., Miyakawa, N., Gray, K. E., Hinks, D. G., Kendziora, C.,2004. "Correlation of Tunneling Spectra in $Bi_2Sr_2CaCu_2O_{8+\delta}$ with the Resonance Spin Excitation : Auxiliary Information ", cond-mat/0102475